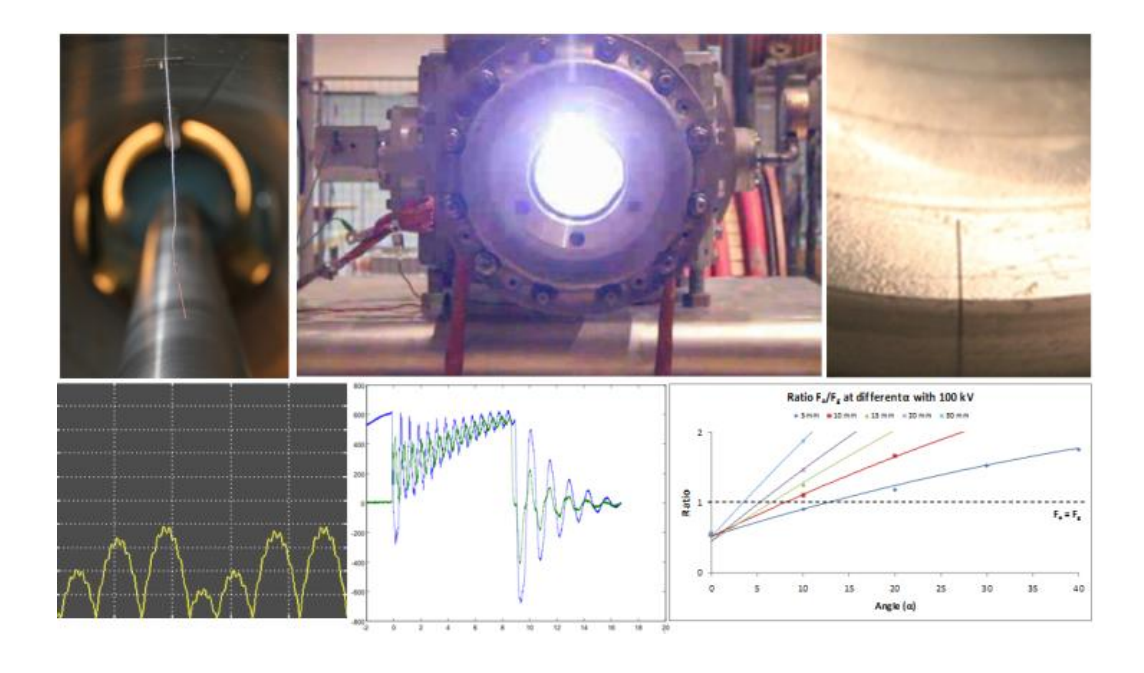
Investigation of Free Moving Particles on theBreakdown Voltage in Gas Insulated Switchgears (GIS) under Different Electrical Stresses

Andreas Putro Purnomoadi Master of Science Thesis





Thesis Committee:

Prof. dr. J.J. Smit

Dr. ir. Sander Meijer

Dr. ir. Madeline Gibescu

Ing. P.V.M.van Nes

MSc. Muhannad Al-Suhaily

Delft University of Technology
Faculty of Electrical Engineering, Mathematics and Computer Science
Department of Electrical Sustainable Energy
High-Voltage Technology and Management Group
June 2012

Abstract

Although the Gas Insulated Switchgear (GIS) reliability has been proven for more than forty years, some failures have been reported. CIGRE report 25/23-01 mentioned the failures caused by free particles and foreign bodies represent 20% of the total distribution of defect type in GIS failures. The presence of these particles results in a local field concentration which influences the insulation medium and can result in breakdown.

Under AC voltage, particles can start "moving" or "jumping" into higher electric field regions. Breakdown may occur if stressing overvoltages, e.g. AC + VFTO, DC + VFTO and AC + LI would occur at the particle get close or attached to the HV conductor

In thesis the influence of free moving particles on the breakdown strength in GIS under different voltage stresses are investigated. For this purpose Different GIS test setups have been used. Particles lengths ranging between 2 to 30 mm have been investigated at 4bar gas pressure.

The results have shown that the particles size of 5 mm and longer can start jumping under AC voltage, while shorter particles were tend to show only a little movements. The visual observations have shown that the particles were moving towards the HV electrode and solid insulators inside the GIS. Therefore the particles as small as 5 mm are considered dangerous to the insulation system under continuous operating AC voltage.

A breakdown area have been distinguished based on the particles length under AC + LI. the particles of 15 mm length and longer are critical under AC + LI. The investigation under AC + VFTO has been performed with the maximum peak 2.1 p.u. At this level, the breakdown has been observed with the 30 mm particle at 90% of the distance gap.

During the experiments partial discharge measurements have been performed by means of:

- the conventional method (IEC 60270)
- the UHF method
- the acoustic method

The PD results have shown that some defects can cause a PD level higher than 10pC. Such PD level gives a good possibility to detect a defect

Table of Content

Abstract

Cha	pter I : Introduction	1
1.1	Gas Insulated Substation	1
1.2	Stressing Voltages and Overvoltages in GIS	2
	Problem Definition	5
1.4	Thesis Objectives	5
1.5	Thesis Layout	5
Cha	pter II : Free Moving Particles in GIS	7
2.1	SF ₆ Breakdown Mechanisms Due to Free Particles	7
2.2	The dynamics of Free Moving Particles under AC Electric Field	13
	2.2.1 Charging Process of Metallic Particles	14
	2.2.2 Lift-Off Electric Field	17
	2.2.3 Motion Equation	18
2.3	Detection of Free Moving Particles	20
2.4	,	
	Insulation Level	22
2.5	Conclusions	23
Cha	pter III : Experimental and Measurement Setup	25
3.1	The GIS Test Setup Used in TU Delft HV Laboratory	25
3.2	The GIS Test Setup Used in Stuttgart University HV Laboratory	26
3.3	The Generation of the AC Voltage in TU Delft HV Laboratory	27
3.4	The Generation of the AC + LI Overvoltages in TU Delft HV Laboratory	27
3.5	The Generation of the AC + VFTO in Stuttgart University HV Laboratory	29
3.6	The Electric Field Distribution in test Setup Used in TU Delft HV Laboratory	30
3.7	The Electric Field Distribution in test Setup Used in Stuttgart University	
	HV Laboratory	31
3.8	The Particles Selection, Shape and Dimension	31
3.9	Detection Techniques	33
	3.9.1 The Acoustic Method	33
	3.9.2 The Conventional PD Detection Method	34
	3.9.3 The UHF/VHF Method	35
3.10) Conclusions	36
Cha	pter IV: The Simulations of the Particles Motion under AC Voltages	37
4.1	The Parameters Used in the Simulations	37
4.2	The Flowchart of the Simulations	38
4.3	Descriptive Statistic Parameters	39
4.4	The Simulation Results	40
	4.4.1 The Particle Maximum Heights and the Distribution of TOF	40
	4.4.2 Key Figures	45
4.5	Analysis	48
4.6	Conclusions	40

Cha	pter V: The Confirmation of Simulation Results by Acoustic Measurements	50		
5.1	5.1 The Definition of Time of Flight (TOF)			
5.2	The Experiment Results	51		
	5.2.1 The Maximum Time of Flights of Different Particles	52		
	5.2.2 Key Figures	53		
5.3	Comparison with The Simulation Results	55		
	5.3.1 The Maximum Jumping Height	55		
	5.3.2 Key Figures	58		
5.4	Analysis	61		
5.5	Conclusions	63		
Cha	pter VI: The Vibration Effects to the Metallic Particles Motion in GIS	64		
6.1	Vibrations in GIS	64		
6.2	Validation of the Mechanical Hit used in the Laboratory	65		
6.3	PD Measurements after the Hit	67		
6.4	Different Situations during the Transition Stage	69		
6.5	Conclusions	73		
Cha	pter VII : Free Moving Particles Detection by Means of Partial Discharge			
	Measurements	74		
7.1	The Acoustic Measurement	75		
	7.1.1 The Effect of Electric Field	75		
	7.1.2 The Effect of Particle Length	78		
	7.1.3 Analysis of the Phase Resolved Signature Patterns	81		
	7.1.4 Analysis of the Amplitude to TOF Patterns	82		
7.2	The PD Measurement based on the IEC 60270 Standard Method	83		
	7.2.1 The Effect of Electric Field	83		
	7.2.2 The Effect of Particle Length	86		
	7.2.3 Analysis	87		
7.3	The PD Measurement by using UHF/VHF Method	88		
	7.3.1 The PRPD Results	88		
	7.3.2 Analysis of PRPD Results	90		
	PD Measurements in GIS	91		
7.5	Conclusions	92		
Cha	pter VIII: Insulation Breakdown of Free Moving Particles under AC +Lightning			
	Impulse Stresses	93		
	The Experiment Results	93		
	The Critical Distance to have a Breakdown	96		
8.3	Conclusions	97		
	pter IX: Investigation of Free Moving Particles under AC + VFTO	98		
	The Test Setup	98		
	The Experiment Results	99		
9.3	The Confirmation of VFTO	101		
	9.3.1 VFTO Simulation in the Test Setup Used in Stuttgart University	101		
	9.3.2 VFTO Rise Time	102		
9.4	Conclusion	102		

Chapter X	: Con	clusions and Recommendations	103
References			105
APPENDIX	В -	Sensitivity Check of the Acoustic Measurement Lift Off Electric Field Investigation Sensitivity Check of PD Measurement by using TE 571	

Acknowledgements

Chapter I

Introduction

1.1 Gas Insulated Substation

The increasing of electricity demand along with the difficulty to find a new space for building a substation are the two important reasons why the development of Gas Insulated Substations (GIS) keeps on growing. Even though the use of SF_6 in GIS has been considered having a potential drawback to the environment, by carefully handling the gas during the GIS operation and maintenance, or, by mixing the SF_6 with less harmful electronegative gasses, the risk can be reduced. figure 1.1 shows an example of a 380 kV Extra High Voltage (EHV) GIS in Meeden, the Netherlands.



Figure 1.1Part of the 380 kV gas-insulated substation in Meeden, the Netherlands

GIS form the nodes in the grid. The electricity distribution as well as the grid protection are the main purposes of GIS. The main structure of GIS consists of gas tight metal enclosures in which the gas is confined. An example of three-phase 145 kV GIS design is given in figure 1.2.

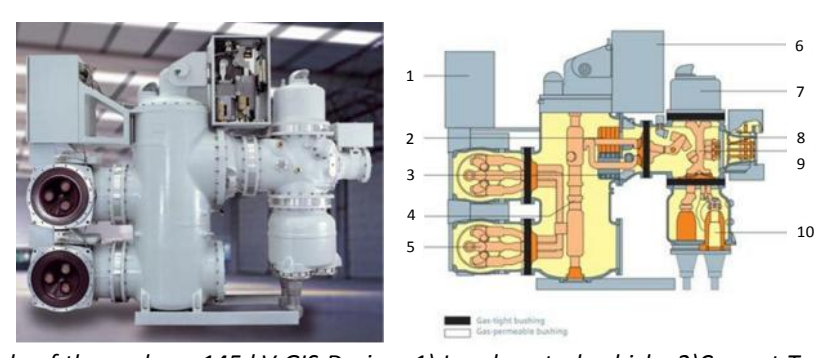


Figure 1.2An example of three-phase 145 kV GIS Design: 1) Local control cubicle, 2)Current Transformer, 3)Busbar II with Disconnector (DS) and Earthing Switch (ES), 4) Circuit Breaker, 5) Busbar I with DS and ES, 6)CB Spring system, 7)Voltage Transformer, 8)High Speed Earthing Switch, 9) Outgoing Feeder, 10)Cable Sealing End (Siemens type 8DN8)

The gas insulation consists of pure SF_6 or a mixture of SF_6 and N_2 . The high-voltage (HV) conductor is placed at the centre of the enclosure by means of epoxy-resin spacers. Beside of the conductor, there are more complex parts like the circuit breakers, disconnector switches and measurement devices.

The GIS has been giving a consistently high performance for years, however some failures have been reported. One of the problems is due to the presence of metallic particles inside of the GIS compartment.

The particle can give rise to field non-uniformities, which can reduce the breakdown strength. The situation becomes even worse when the particle is able to move to the spacers.

CIGRE report 25/23-01 mentioned that the failures caused by free particles and foreign bodies represent 20% of the total distribution of defect type in GIS failures [1]. The origin of the particle is twofold:

- they may remain after GIS erection because they were not detected by onsite tests, or
- they can be produced after the on-site tests, for example by contact wear or by sparking between loose shields.

Based on this situation, the understanding of the insulation breakdown due to the metallic particles is very necessary. It becomes the main subject of this thesis, as well as the detection and diagnostic of the presence of a particle during the GIS operation. Metallic cylindrical particles have been chosen in all of the discussions in this thesis, since this shape has been considered to be the most critical to the insulation [7,15]. The behavior of the particle as well as the insulation breakdown level under different stressing voltages and overvoltages have been investigated. The investigation covered the AC frequency voltages, superimposed of AC + LI, and AC + VFTO overvoltages.

Under stressing AC frequency voltages, the particles motion due to the electrostatic force along with the vibration effects have been measured and simulated. The acoustic measurements using externally mounted acoustic sensor have been used to investigate the height of the particles jump.

The detect ability of the particle existence by means of Partial Discharge (PD) level and Partial Discharge pattern measurements are also discussed. Three different methods have been used, e.g.: the electric measuring systems based on IEC 60270 recommendations, the electric VHF/UHF measuring systems, and also by using the acoustic instrument.

1.2 Stressing Voltages and Overvoltages in GIS

During the GIS operation, different electrical stresses can occur in the system. The possible voltage stresses are the following:

- 1. AC continuous power frequency voltage.
- 2. Temporary overvoltages (TOV) due to the load rejection, earth faults and resonance phenomena.
- 3. Transient overvoltages including the slow-front, fast-front and very fast transient overvoltages.
 - a. Slow-front overvoltages arise from faults, fault clearing as well as from damped lightning strokes on distant overhead lines.
 - b. Fast-front overvoltages which originated from lightning strokes near the GIS. The front-time of the surges is in the range of one to few micro seconds.
 - c. Very fast transient overvoltages (VFTOs) which occur during the switching process of disconnector and circuit breakers. Their front-time is in order of few nanoseconds.
- 4. DC voltage stresses due to trapped charges in some particular GIS segments.

The shapes of the overvoltages curves according to IEC 60071-1 are given in figure 1.3. The amplitudes and the duration according to CIGRE's and TenneT documents are shown in figure 1.4.

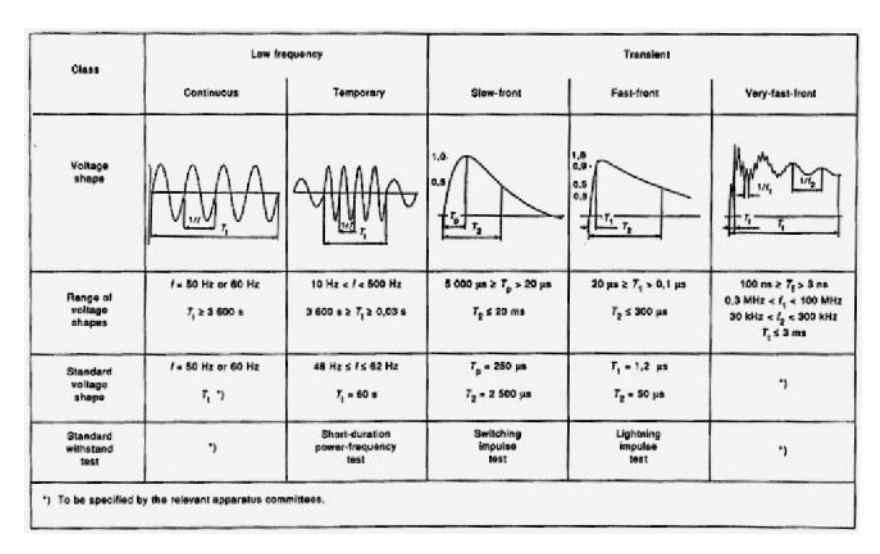


Figure 1.3Classes and shapes of stressing voltages and overvoltages according to IEC 60071-1: Insulation Coordination. DC voltage is not mentioned here. [31]

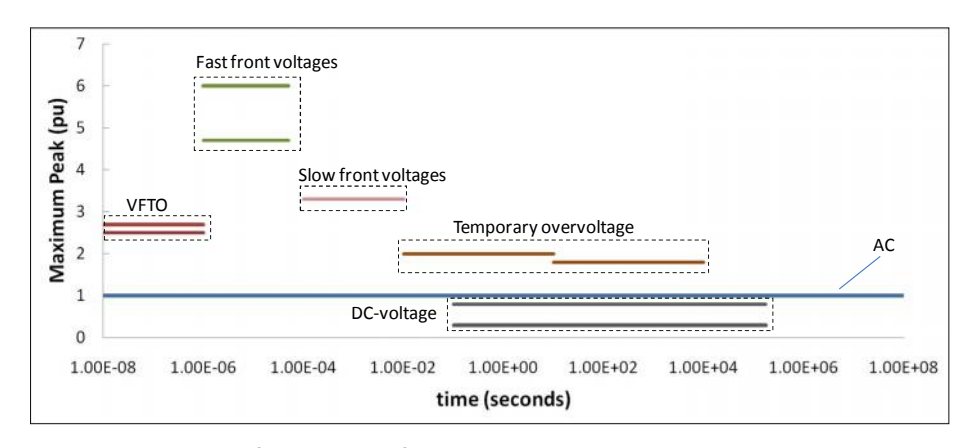


Figure 1.4Representative maximal of amplitude of overvoltages according to their time duration based on CIGRE [2] and TenneT's document [12]

In practice, the stresses can present both as a single voltage level or being superimposed between one and another. They are as follow:

- 1. AC
- 2. AC + LI
- 3. VFTO
- 4. AC + VFTO
- 5. DC
- 6. DC +VFTO

AC voltage stress

With AC voltage stress, as soon as the electrostatic force on the particle overcomes the gravitational force, the particle starts to elevate. In some cases, the vibration which originated from the operation of any switching device can trigger the particle to start moving at lower voltage level. The height of the particle elevation is dependent on the changing electric field as a function of time. Therefore, the possibility of the particles to reach the high voltage conductor is less than with DC voltage.

AC + LI overvoltage stress

When a lightning-stroke is coming into the GIS, a superimposed of AC + LI overvoltage occurs at the conductor. The maximum lightning peak of 4.5 pu can occur [12]. If the GIS is equipped with surge arresters, the maximum peak can be reduced to 2.5 pu. If the surge is superimposed with the AC at maximum peak value at the same polaritywith the lightning, a maximum of AC + LI peak becomes 3.5 pu. However, the occurrence of lightning is different amongst different regions in the world. In the Netherlands for instance, the lightning occurrence is considerably low with less than 5 flashes/km² per year [3].

VFTO and VFTO superimposed overvoltage stress

Another type of electrical stress is the very fast transient overvoltage (VFTO). This stress occurs during the operation of switching devices like CB, ES or DS. The source of the very steep voltage gradient is the reflections and refractions of the travelling wave at the short length of GIS conductors.

Most of the VFTO peaks are below the lightning impulse peak. It does typically not exceed 1.5 pu, but VFTO's with values of 2.7 pu have been reported[4]. About 5% of GIS breakdown was due to the VFTO [5]. VFTO becomes a concern in the system where the ratio between the system voltage and the Lightning Impulse Withstand Voltage (LIWV) is small [51]. The breakdown probability increases when the oscillating frequency increase [2].

DC voltage stress

The DC trapped voltage is originated from the trapped charges that are left at a particular busbar segment after a switching-out process of a disconnector switch. The maximum value of a DC stress depends on the operating speed of the switching device. More charges are trapped with the slower moving disconnector. In general this value is in the range of 0.3 to 0.5 pu, but values as high as 1 pu have also been reported.

The particle movement under DC voltage is more dangerous than with AC voltage. Under DC electric field, as soon the particle is lifted off, the particle is constantly move into the high voltage conductor, since there is no changing direction of the electric field.

However, the duration of trapped charges depends on a constant known as a decay time (τ). The decay time in reality is a function of the trapped charge voltage, and decreases as the trapped charge voltage is increased [2]. The GIS design also influence the decay time. For example, in a single busbar GIS connected to a surge arrester, the value of τ is less than a few seconds, and when an inductive transformer is connected to the busbar, τ can be decreased to less than one cycle [2].

It is now clear that the impact of DC voltage stress is not only influenced by the DC magnitude but also the duration of the decay time. In accordance to this statement, when GIS segments are equipped with circuit transformers, as in the case of Meeden 380 kV GIS, the decay time for the DC trapped charge is very short. In this particular situation, the effect of the DC voltage stress will be less dangerous.

From the previous explanations it can be concluded that the particle behavior as well as the impact of the particle to the insulation system depends on the type of the electrical stresses during the GIS operation. Therefore, the investigation of the free particles needs to be done under different stresses situation. In this thesis, the discussion is limited to: AC, AC + LI and AC + VFTO.

1.3 Problem Definition

The behavior of free moving particles as well as the impact of their presence to the SF_6 gas insulation under different electrical stresses is the main subject of this thesis. In order to investigate this subject, the following questions need to be answered:

- 1. On the investigation with the AC voltage stresses:
 - a. What is the pattern of the particle movement under AC electric field? How high will the particle elevate inside of the compartment?
 - b. During the GIS operation, the vibration which originated from the switching contacts like a circuit breaker cannot be avoided. In reference [6], this kind of vibration might lift-off the particle at lower voltage level. How can this phenomena be explained?
 - c. How can we detect the presence of the particle during the GIS operation? How much will be the Partial Discharge (PD) level and how will be the PD pattern looks like?
- 2. On the investigation with superimposed voltage stresses:

During the particles jump, what will be the critical distance of the particles to the conductor that can create a breakdown when superimposed overvoltages are introduced?

1.4 Thesis Objectives

The objectives of this thesis are the following:

- 1. To estimate the maximum particle jumping height under the influence of an AC electric field by means of simulation and acoustic measurement.
- 2. To define a measureable parameter of a vibration impact to the particle movement inside of the GIS compartment.
- 3. To investigate the PD level and the PD pattern due to the presence of free particles in a GIS.
- 4. To find the breakdown level of the gas insulation under superimposed voltage stresses at different particle distance to the conductor.

1.5 Thesis Layout

The thesis report consists of 10 chapters as the following:

Chapter I: Introduction

In this chapter, the general information of GIS and different voltage and overvoltage stresses are given. The problem definition as well as the thesis objectives are presented in this chapter.

Chapter II: Free Moving Particles in GIS

This chapter consists of theories related to the motion of free particles in AC electric field, as well as some basic explanations on the breakdown mechanism of SF_6 insulation. Different particle detection methods are also explained in this section.

Chapter III: Experimental and Measurement Setups

The descriptions of the test setups are discussed in this chapter. In the beginning, the general GIS compartment setup is given. Later on, the explanations of each test setup of different stress levels are explained in sub chapters. The explanations also include the discussion about the electric field distribution generated in the test setup.

Chapter IV: Simulations of the Particles Motion under AC Voltage

The simulation results of particles motion under AC electric field are reported in this chapter. The simulation is performed by an assumption the particle is jumping in 1 axial direction. The calculation of the net charge is achieved by using the formula given by Felici [26]. The parameters to be investigated are: the maximum particle jumping and the key figures of the time-of-flight distribution.

Chapter V: The Confirmation of Simulation Results by Acoustic Measurements

In this chapter, the acoustic measurements are performed to confirm the simulations. The key figures as well as the maximum jumping height from are compared.

Chapter VI: The Vibration Effects on the Metallic Particles Motion in GIS

In this chapter, the effect of vibrations to start the particles jumping is discussed. PD measurements have been performed to investigate the particle during the transient stage directly after the hit. The simulation by using Finite Element Program has also been performed to calculate the net charge on the particle after the hit

Chapter VII: Free Moving Particles Detection: Partial Discharges Measurements

In this chapter, the PD measurements of three different methods are performed to investigate the detect ability of the particle during GIS operation. The methods are:

- The electric measuring systems based on IEC 60270 recommendations.
- The electric VHF/UHF measuring systems.
- The acoustic measuring systems.

Chapter VIII: Investigation of Free Moving Particles under AC + Lightning Impulse Stresses

The breakdown levels of gas insulation under AC + LI overvoltages due to a free moving particle at different distance from the conductor are reported. The critical distance is obtained from the experiment and compared with the maximum jumping height obtained from the discussion in previous chapters.

Chapter IX: Investigation of Free Moving Particles under AC + VFTO

In this chapter, The breakdown levels of gas insulation under AC + VFTO due to a free moving particle are reported. The experiment has been performed in the High Voltage Laboratory in Universitat of Stuttgart. The confirmation of the VFTO is discussed in this chapter.

Chapter X: Conclusions and Recommendations

Thesis conclusions are given in this chapter as well as the recommendations for future investigations.

Chapter II

Free Moving Particles in GIS

Certain problems are unique to GIS as compared to the conventional air insulated substations. One to be considered is the presence or generation of metallic particle contamination during the process of manufacture, assembly, transportation, erection and operation. Even after a good quality control process during the GIS erection, some particles cannot be avoided due to, for example, mechanical abrasions on the switching contacts and the movement of conductors under load cycling operation.

According to the references [7, 15], the wire-like conducting particles are mostly found in practice and is considered to be the most dangerous to the insulation. Even though non-metallic impurities such as glass and dust have also been observed in the field they only have little or no effect to the breakdown of SF₆ gas. Some impurities like dust may lower the breakdown strength, but the effect is not as significant as the one from free conducting particles [8].

Therefore the dynamics of wire conducting particles in a horizontal coaxial system along with their impact on the dielectric strength of SF_6 insulation becomes the interest of this thesis. This chapter reviews some theoretical backgrounds.

At the beginning of this chapter, different breakdown mechanisms of SF_6 gas are given. Following in section 2.2, the dynamics of free particles under AC electric field will be discussed. Different methods of particles detection during the GIS operation are given in section 2.3. These techniques include the acoustic emission method, the conventional PD measurement based on IEC 60270 and the PD measurement using a VHF/UHF measuring system. The effect of Very Fast Transient Overvoltages (VFTO) to the gas insulation system is given in section 2.4 and conclusions are given in section 2.5.

2.1 SF₆ Breakdown Mechanisms Due to Free Particles

Sulphur Hexaflouride (SF_6) gas is used as an insulation medium in many power system applications, including the circuit breakers, GIS components, transformers and gas insulated cables. Its wide use in power equipment is promoted by its high dielectric strength, its good heat transfer characteristics and its excellent arc-quenching properties. But, the SF_6 gas is a 'brittle' medium, the ionization process is built very rapidly as soon the critical field strength is exceeded. In practice this can happen in the vicinity of any small defects such as free particles. This ionization can grow very fast and possibly trigger a breakdown. To understand the breakdown phenomena in SF_6 , different breakdown mechanisms in gas will be given in the next paragraphs.

There are three mechanisms should be mentioned in the breakdown of insulating gas [16, 17]:

1. Townsend Mechanism

The molecules of electronegative gases like SF_6 have the ability to attach a free electron which is accelerated by the electric field. When the electron collides to a neutral molecule, it may be attached to form a negative ion.

$$SF_6 + e \rightarrow (SF_6)^-$$

This attachment process competes with the collisional ionisation, where an electron with sufficient energy can remove an electron from a neutral molecule to create an additional free electron.

$$SF_6 + e \rightarrow (SF_6)^- + 2e$$

The ionization is a cumulative process. When the rate of ionization is greater than the attachment process, the formation of 'avalanches' of electrons might occur. Such avalanches by itself will not result in a full breakdown of the gas.

Calculation given in reference [15] has shown the critical field strength in SF_6 should be at least 88.8 kV/cm.bar to start the avalanches in uniform field background. This value is useful in estimating the onset voltages in SF_6 insulation. The comparison of the effective ionization coefficient in air and SF_6 is given in figure 2.1.

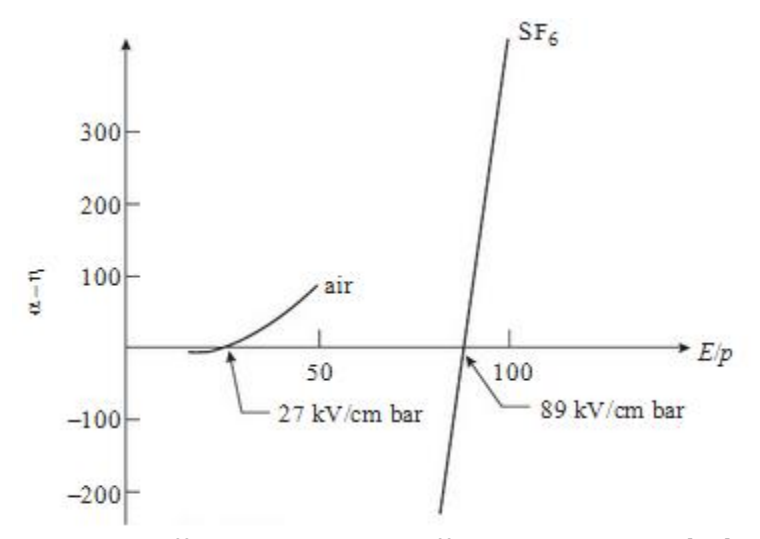


Figure 2.1Effective Ionization Coefficient in air and SF₆ [15]

To create a full breakdown, feed-back processes are necessary to release new start-electrons (secondary electrons). Examples of feed-back processes are: photoelectric emission from the cathode and photo ionization in the gas.

The process described above is called the Townsend mechanism where three stages were necessary to initiate a breakdown [17]:

- 1. The creation of starting electrons by light, or by cosmic irradiation
- 2. The multiplication of electrons leading to an avalanche
- 3. Feedback by a process that releases new electrons from the cathode

The Towsend breakdown criterion can be expressed by:

$$\int_0^x (\alpha - \eta) dx \ge \ln \left(1 + \frac{1}{\Gamma} \right)$$
 ... equation 2.1

here, α represents the ionization coefficient of the gas, η the attachment coefficient of the gas and Γ represents the combined feedback effects. [16, 17]

2. Streamer Mechanism

The Townsend mechanism is only valid if the product of gas pressure and electrode-gap distance is below 5 bar.mm. Beyond this value, the breakdown of the gas can be explained by the streamer theory [17]. This theory states that the space charge formed in the avalanches starts to have effect on the electric field if the avalanche surpasses a critical length. In SF₆, this can be achieved when the number of ions in an avalanche reaches 10⁸ [17].

$$\exp\left[\int_0^x (\alpha - \eta) . dx\right] \ge 10^g$$
... equation 2.2

where α represents the ionization coefficient of the gas and η is the attachment coefficient of the gas.

Streamer mechanism is different to Townsend mechanism in the following situations [17]:

- 1. Time to breakdown is far shorter than Townsend mechanism. The ions cannot move back to the cathode to create secondary electrons
- 2. The breakdown voltage is no longer dependent on the cathode material
- 3. Breakdown channels are sharp and narrow (while in Townsend is diffused)

GIS is designed to have low divergence electric field distribution during the operation. For pressure used in technical specification (p > 1 bar), the streamer process is the accepted breakdown mechanism in SF₆ under relatively uniform field conditions [15].

3. Leader breakdown in SF₆

The leader mechanism occurs at non-uniform gas gaps at higher gas pressure (p > 5 bar) [16,19]. A corona can propagate if the criteria for avalanche ionization and streamer inceptions are fulfilled. It will continuously growing unless the propagation conditions are no longer fulfilled at the streamer tips. According to the references [16, 17,19] there are two types of leader mechanisms can occur:

- Stem mechanism: due to the energy in the streamer channel, expansion of the gas can take
 place, which can results in reduction of the gas density. In this situation the ionization can
 restart and a conducting channel can be created.
- 2. Precursor mechanism: space charge filaments are created by the apart of positive and negative ions. This will locally enhance the field strength and the ionization can again restart.

An example of leader breakdown in case of a protrusion is given in [20]. When a fast-fronted surge takes place at a protrusion, the voltage at the vicinity of the protrusion passes rapidly through the streamer onset level. The initial streamers can be very intense and may lead to the formation of a highly ionized leader channel, before there is time for space charge stabilization of the field at the tip of the protrusion [21]. The leader formation process repeats and results in a stepwise propagation growth of a possible breakdown path as depicted in figure 2.2:

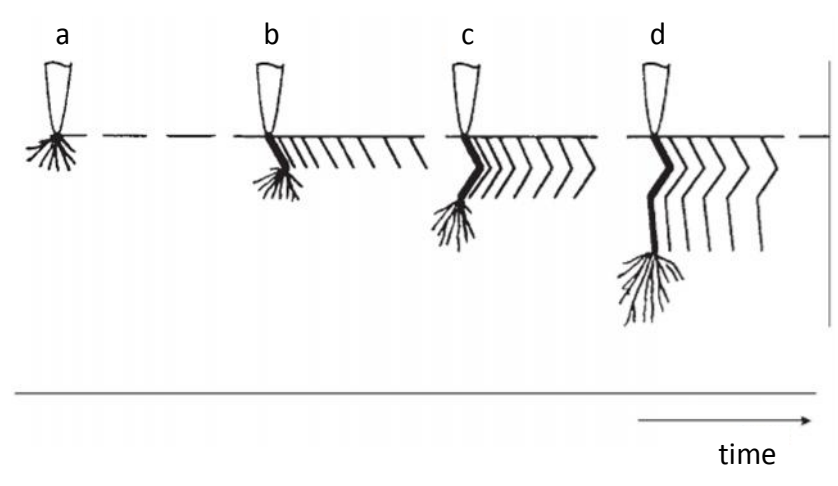


Figure 2.2Schematic of leader development [15]

The explanation of the figure is the following:

- a. From a to b, charge separation the streamer filaments generates an ionizing wave which build-uptheir conductivity. Therefore, one of the streamer filaments is transformed into ahighly conducting leader channel step. This behaves as an extension to the point electrode and new branches of corona burst immediately occurs at its tip b.
- b. The range of this second corona determines the length of the second channel step c.
- c. The leader propagates into the gap in steps typically of a fewmmuntil the streameractivity is too weak for further channel steps to form. If the voltage is high enough, the leader can cross the gap, resulting in breakdown.

To give better picture on different breakdown mechanism, a summarized of Voltage-pressure (V-p) characteristics of different breakdown mechanisms is given in figure 2.3.

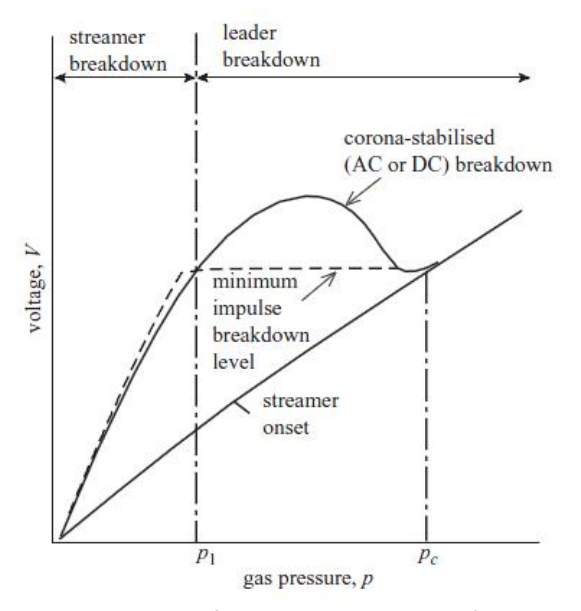


Figure 2.3Idealized V-p characteristics for minimum impulse (direct leader) breakdown and corona stabilized (AC or DC) breakdown in a point-plane gap in SF_6 [22]. p_1 is typically 0.5 bar, the typical GIS pressure is 3-6 bar

Particle Initiated Breakdown

The insulation strength of compressed SF_6 insulation is greatly reduced by the contamination of free conducting particles. The breakdown voltage in particle contaminated SF_6 can be as low as 10% of the value of clean gas. The reduction of the breakdown voltage is governed by some factors such as the particle shape, size, material, location and motion, the gas pressure, and the applied field [8, 12]. The breakdown usually occurs when a particle is close to but not touching the conductor.

Different investigators have proposed mechanisms to explain the particle-initiated breakdown. Cookson et. al. in reference [14] had distinguished the probability of breakdown into 3 different situations:

- 1. The field at the particle may be sufficient, before the lifting field is reached, to initiate breakdown as for a fixed protrusion.
- 2. The particle may be lifted and cross the gap to touch the conductor and initiate breakdown as a fixed protrusion.
- 3. After the charged particle has been elevated, just before it hits the oppositely charged electrode there is a microdischarge which may be sufficient to trigger breakdown.

The first two mechanisms can be explained by the streamer mechanism as mentioned above. When the electrostatic force exceeds the weight of the particle, the particles start to stand up and remain perpendicularly on the electrode surface [11, 13]. This causes field enhancement at their tips and lowers the breakdown voltage of the gas insulation. In some other cases, the particles are able to stand perpendicularly at the conductor after they had travelled through the gap. In this situation, higher field enhancement can occur.

If the particle is fixed to the electrode, there is enough time underAC conditions to guarantee effectivestabilization at each voltage maximum. This is resulting in the typical peaked *V*–*p* characteristic as shown in figure 2.2. But, the situation is different when the particle is just before touching the conductor. Now, a microdischarge is taking place. In this case, when the particle is getting closer to an electrode, the field at the tip is suddenly increased. This is almost as if a short-duration pulsed voltage superimposed with AC is applied to a particle fixed onto an electrode. Under these conditions, the minimumbreakdown voltage is that associated with direct leader breakdown, which is almostindependent of pressure [10, 14, 15].

In reference [27], measurements have been made in 125/250 mm coaxial systems. A good agreement has been shown between the AC breakdown voltage with free particles and the minimum breakdown voltage with 1 μ s rise time impulses applied to a particle fixed to the inner conductor. According to these results, particle initiated breakdown under AC voltage can also be corresponded with the breakdown by leader mechanism, as in the case of fixed point - gap impulse breakdown. This breakdown level is independent with the gas pressure, as shown in figure 2.2.

Breakdown Mechanism at Different Electric Stresses

It has been mentioned in section 1.3, different electric stresses may occur during the GIS operation. Related to these stresses, different breakdown mechanism can be summarized in accordance with the particle existence.

In highly non-uniform field, as in the case of a free particle deposited on the surface of an electrode, two distinct types of breakdown can be mentioned [15]:

1. When the applied voltage is varying relatively slowly, like in AC voltage or switching surges, the corona stabilization process is taking place in the breakdown process [28].

2. If the rise time of the voltage is very steep, like in lightning impulse or fast transients surges, breakdown occurs directly by a stepped leader [20]

AC and DC Voltage Stresses

The effect of corona stabilization process is depicted in figure 2.2 in the region where the breakdown voltage is much higher than the (streamer corona) onset voltage. This can be explained as follow:

In case of positive point, as in the case of particle fixed perpendicularly to the inner conductor with positively half cycle of AC voltage, the electrons generated by the corona are removed immediately from the point, and leave positive space charges behind. This space charge shields the point from the field, the discharge stops, the positive charge drifts into space and the corona discharge reignites [15, 17]. Thus, higher voltage stress is necessary to trigger a breakdown.

If the pressure is increased above the critical value, p_c , the individual streamers become more intense. The corona region is become smaller and the stabilization becomes less effective. Thus, the breakdown voltage is reduced, and its value is moving closer to the onset level. Since the shielding effect is negligible, the streamer which forms at onset is able to initiate discharge which bridges the gap. This discharge has been shown to be identical to the stepped leader discharge [15].

From the given explanations, breakdown mechanism with AC or DC voltage can be summarized as follow:

- 1. When the particle is fixed at the electrode, and the pressure is below the critical value of p_c , a highly voltage stress above the streamer onset level is needed to start the breakdown. Here, both streamer and leader breakdown are possible to occur. But, when the pressure is increased above the p_c , only leader breakdown can occur and the breakdown voltage is close to the streamer onset level.
- 2. If there is a microdischarge during the particle movement, leader mechanism is the breakdown process.

Fast Transients (AC + LI, AC + VFTO, VFTO)

For fast-fronted waves like AC+LI superimposed, AC + VFTO superimposed and VFTO, the electric field is much higher than the minimum onset voltage level. A stepped leader mechanism may be initiated when the streamer corona is large enough.

A summarized of breakdown mechanisms at different electrical stresses due to free particles is given in table 2.1

Stress	Particle	Breakdown		
Type	Situation	Mechanism		
AC	Fixed on the electrode	Streamer or Leader*		
ΑC	Jumping	Leader		
DC	Fixed on the electrode	Streamer or Leader*		
DC	Jumping	Leader		
AC +LI Fixed, Jumping		Leader		
AC +VFTO	Fixed, Jumping	Leader		
VFTO	Fixed, Jumping	Leader		

Table 2.1- Breakdown Mechanisms at different Electrical Stresses

^{*} depends on the pressure. In typical GIS pressure, the breakdown is most likely governed by the conditions of leader propagation in the absence of space charge (see figure 2.2)

2.2 The Dynamics of Free Moving Particles under AC Electric Field

Studies to the dynamics of free moving particles have been developed since the beginning of the development of GIS technology. Lundgaard in 2001 has summarized as the following [23]:

Table 2.2- Studies on The Dynamics of Free Moving Particles with AC Electric Field

No.	Year	Author	Contribution		
1	1972	Cookson et al.	They develop the equation of movement of a particle in an AC stressed gap. The restitution coefficient (CR), which defined the ratio between the velocity of a particle before and after impact on a large body, had shown to be the important factor to the elevation height. The drag force was neglected.		
2	1975	Cookson and Wotton	They further discussed on the equation movement, and calculated and observed distributions of jump heights of moving particles.		
3	1983	Morcos et al.	They developed simulations that cover coaxial gaps and included the drag forces		
4	1987	Morcos, Radwan et al.	They developed computer simulations and discussed the effect of the applied voltage frequency on particle jump heights		
5	1989	Morcos et al.	They have measured and discussed the occurrence of discharges during the flight of elongated particles, and the fields that may occur at the ends of a particle in the proximity of an electrode. They also discussed measurement of discharge onset, rate, and magnitude, for diagnostic purposes.		
6	1987	Leijon et al.	They observed that the ends of an aluminum particle would change shape (i.e. being more rounded shape) during movement. This changing shape distorts the particle movement. They use the average of bounce frequency for discriminating between dangerous and harmless particles.		
7	1990	Lundgaard	He presented the acoustic emission method for GIS diagnostic. He showed some features characterizing the acoustic signals from defects such as discharges from protrusions, bouncing particles and floating shields. The measurement suggested that the acoustic signals from particle impacts were proportional to the square root of the kinetic energy of the particle impact.		
8	1993	Wohlmut	 He presented computer simulations of particle movement and discharges from particle using the charge simulation method. The simulation was verified by an experimental investigation. He showed that the dielectrophoretic forces are ~10% of the Coulomb forces for a 10 r long particle. This indicates the error from assuming a point charge in simplified simulation. He also introduced scheme for risk evaluation based on PD 		
		Holmberg	He used distribution of elevation time (time of flight, TOF) to compare measurement and simulation. He used this for estimation of particle characteristics.		
		Runde et al.	They have founded that amplitude to elevation time has a very characteristic pattern correlated to particle length, and the maximum measured amplitude was proposed as descriptor.		
9	1997	Schlemper	He made the amplitude to elevation-time plots which are showing the significance of the charge to mass ratio on the elevation time. He also concluded that the signal amplitudes following particle impacts were proportional to the momentum of the particle		
		Lundgaard et al.	They have proposed a scheme based on an energy approach for explaining particle movement and for estimating particle characteristics from acoustic measurement alone		
		Lundgaard & Holmberg	They both discussed about microdischarges just before and after impact during the particle movement and their impacts to the particle movement		

According to these histories, some points can be noted:

- 1. Elongated particles have been studied for years. Simulations and experiments have been done by different researchers. At the beginning of investigation, the parameters of Coefficient Restitution (CR) and drag forces had been considered to be responsible to the elevation height. Later, microdischarges were found to be another important factor that influences the particle movement. In the last situation, an energy based model has been developed to simulate the dynamics of the particles, mainly with the influence of AC electric field.
- 2. The amplitude of acoustic signals, and the elevation time have a very characteristic pattern that can be used both in the detection and diagnostic of the particles. Lundgaard has developed many efforts on this subject.

In the following paragraphs, the charging process as well as different forces acting on the particle will be describe to give a better understanding on the dynamic of particle behavior in AC electric field.

2.2.1 Charging Process of Metallic Particles [11, 24, 25]

When a metallic particle is rest at a grounded electrode, it has no charge density distribution on its surface. But, as soon as the particle experiences an electric field, a surface charge distribution will be developed. The electrons inside the particle will move in such a way to oppose the external electric field.

If there is no microdischarge during the particle excursions, the net charge remains constant. The particle gains new charge as soon it has connection to an electrode. The situation is illustrated in figure 2.3. Charges are flowing between the particle and the grounded electrode, so that the particle becomes zero potential and the particle will gain a net charge.

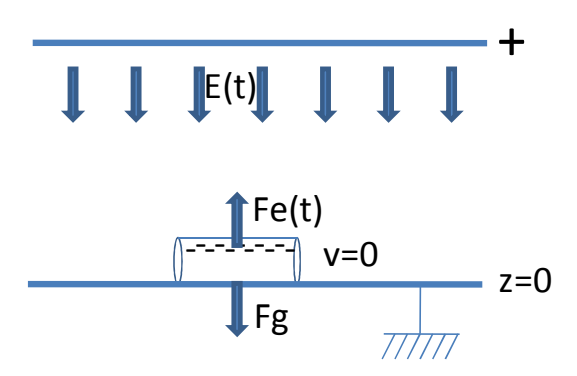


Figure 2.4An illustration of charging process in a particle with the influence of electric field [11]

The negative charge distribution on the particle surface is proportional to the applied electric field. If the applied field is increasing, then the negative charge distribution will also be increased. The electrostatic force (F_e) which is defined as the charge times electric field will increase and at the moment its value is higher than the gravitational force (F_g) , the particle start to lift-off.

The particle is moving in the direction of the electric field. In case of an AC electric field, the direction is changing every half of a cycle period. If the particle reaches the upper electrode, it will gain a new net charge which also makes the particle to change its direction.

Due to the polarity changing of the electric field, the particle motion in AC will be random-like. The new net charge after each consecutive impact of the particle to the bottom electrode will most likely be different. The situation is different under DC electric field where as soon the particle starts to lift-off the particle will constantly move towards the upper electrode.

The mobility of the particle is also influenced by its shape. An elongated particle is more mobile than a sphere [11]. This is due to the charge-to-mass ratio, which for an elongated particle is greater than for a sphere. Leijon in 1987 had observed that the tip of the particle can change its shape after several bouncing processes. This condition also influences the particle motion.

For the purpose of particle net charge calculation in a GIS, the formulation by Felici [26] has widely been used. In his equations, the time needed to rearrange the charges on the particle surface is negligible. The formulas are valid as long the particle is in good contact with the electrode.

For a wire-like particle the formulas for horizontal and vertical positions are the following:

Q =
$$2.\pi.\epsilon_0$$
. r. ℓ . E ... horizontal position, equation 2.3, [11]

$$Q = \frac{\pi \cdot \varepsilon_0 \cdot \ell^2 \cdot \mathbf{E}}{\ln\left(\frac{2\ell}{r}\right) - \mathbf{1}}$$
... vertical position, equation 2.4, [11]

where r and \P are the radius and the length of the cylinder. ε_0 is the permittivity constant and E is the applied electric field. It should be noted that in the vertical formulation, the particle is assumed has a semi-ellipsoid shape.

The validity of these formulas has been checked using a finite element program (FE), COMSOL Multiphysics 3.4. In the finite element method, triangular elements are used to divide the area between electrodes. Better approximation of curved boundaries can be obtained through these meshes of triangular elements [17]. The fine mesh is only needed in the vicinity of the sharpest electrode as it has shown in figure 2.4.

With the finite element program, the net charge on a closed surface S on the particle is calculated by the integration of the surface charge density, where the surface charge density is equal to the permittivity times the normal electric field (ϵ . ϵ _n):

$$q = s(\epsilon, E_n) dS$$
 ... equation 2.5, [11]

In the simulation of the vertical position, two dimensional (2D) geometries with rotational symmetries have been used, while for the horizontal position, the calculation was done in three dimensions (3D). The rotational symmetry is only valid for the vertical position.

To check the validity of the formulas, particles with three different lengths were subjected with homogeneous field of 5 kV/cm and 10 kV/cm. The charges derived from the Felici-formula are compared with the results from the FE program. The results from FE program using the maximum number of mesh elements are chosen as the "correct" reference results since the more fine the meshes means the more precise the calculation

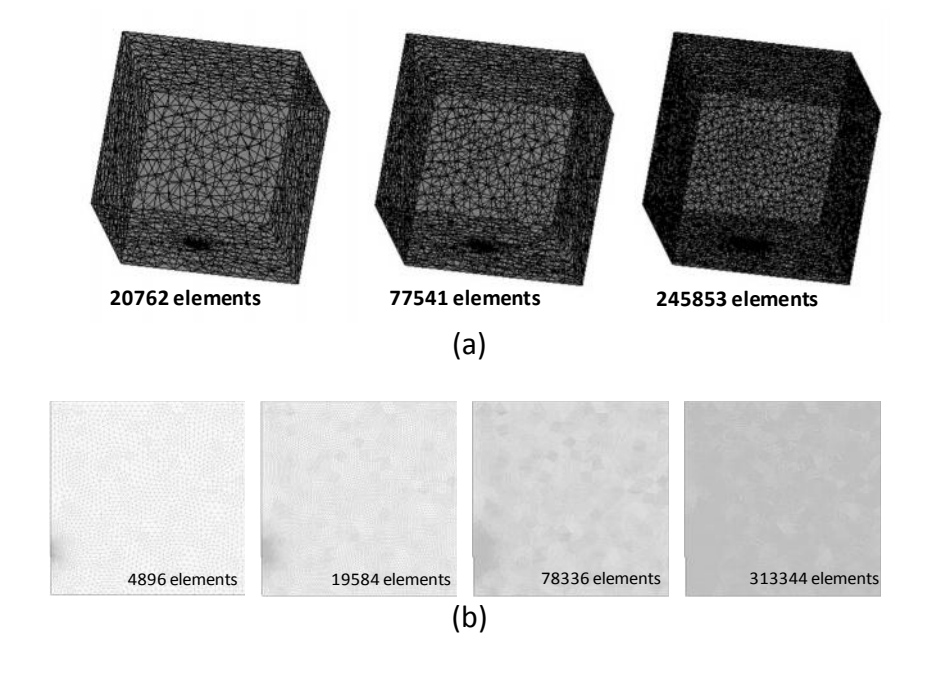


Figure 2.5Mesh Elements at different intensities. Particle in horizontal position modeled in 3D model (a)

Particle in vertical position modeled in 2D rotational model (b).

Table 2.3 - Comparison of The Net Charge Calculation According to Felici's and FE Solver for the horizontal cylindrical particle

particle radius/length	Electric Field		charge	(in nC)	
(mm)	(kV/mm)	Felici	~20000	~75000	~240000
		horizontal	elements	elements	elements
0.25/5	5	0.035	0.034	0.035	0.035
0.25/10	5	0.07	0.07	0.07	0.07
0.25/20	5	0.14	0.13	0.13	0.14
0.25/5	10	0.07	0.07	0.07	0.07
0.25/10	10	0.14	0.13	0.13	0.14
0.25/20	10	0.28	0.21	0.27	0.27

Table 2.4 - Comparison of The Net Charge Calculation According to Felici's and FE Solver for the vertical cylindrical particle

particle radius/length	Electric Field			charge	e (in nC)		
(mm)	(kV/mm)	Felici vertical	~1200 elements	~4800 elements	~19000 elements	~75000 elements	~300000 elements
0.25/5	5	0.13	0.14	0.15	0.16	0.16	0.16
0.25/10	5	0.41	0.39	0.44	0.47	0.49	0.49
0.25/20	5	1.36	1.08	1.31	1.46	1.54	1.58
0.25/5	10	0.26	0.27	0.3	0.31	0.32	0.32
0.25/10	10	0.82	0.77	0.88	0.94	0.97	0.98
0.25/20	10	2.73	2.16	2.62	2.93	3.09	3.16

There are some points that can be concluded from the results:

- 1. With the horizontal particle position, the Felici-formula has shown a good conformity with the results from FE 3D solver. About 20000 mesh elements are sufficient to give satisfying results in 3D simulation of a horizontal particle. The results are showing that the Felici's results are having better conformity with the results from FE solver at higher number of mesh elements.
- 2. With the vertical particle position, the results derived from Felici Formula are diverging to the FE results at lower number of mesh elements (< 5000 elements). But, when the number of mesh elements is increased, the difference between both results is increased. A difference of ~20% has been observed at ~300000 elements. It should be noted that Felici derived his formula based on a semi-ellipsoid shape of vertical particle, not a fully cylindrical shape particle.
- 3. The elements number is different between the 2D and the 3D models. In the program, the number of meshes is coming in stages. At the first stage of the simulation, for example, the simulation with the 2D model is coming with ~ 1200 elements while in 3D model is about 20000 elements. By increasing the stages, the number of elements is increasing and the more fine meshes are involved. It also should be noted that the simulation with the 3D models are occupying more memory of the computer than the 2D models, even at merely the same elements number.

Even though in vertical calculation, the Felici formula gave a significant difference from the FE solver, still the Formula is valid, amongst other simplifications, to simulate the particle motion. This will be discussed in sub chapter 2.2.3.

2.2.2 Lift-Off Electric Field [11, 13]

When a wire-like particle is lying at the bottom of a grounded electrode, as soon as the electric field is above the level of the lifting field, the particle will suddenly raise to a vertical position [13]. So, at the beginning, the particle was charged according to equation 2.3 and then immediately charged according to equation 2.4. At the same electric field value, equation 2.4 results in a higher charge value.

Holmberg in reference [11] mentioned that when a particle is in contact or very close to an electrode, it senses an attractive force due to image charges in the electrode. The attractive force decreases quickly as soon as the particle leaves the electrode. Due to this situation, a correction factor k_a is needed to calculate the electric field required to lift a particle off. The modified electrostatic force thus becomes:

$$F_e = k_a$$
. Q. E, where $(0 < k_a < 1)$... equation 2.6

In the same reference, it is mentioned that the constant k_a varies from about 0.71 for a horizontal cylinder to almost unity for vertical cylinder particle. However this value is dependent with many parameter of the test setup, including the dimension, material, etc. The calculated electric field lift off of aluminum particle with different particle diameter and at different value of constant k_a is given in the figure 2.5. It should be noted that for a cylindrical particle, at the similar constant k_a , the lift off electric field is independent with the particle length.

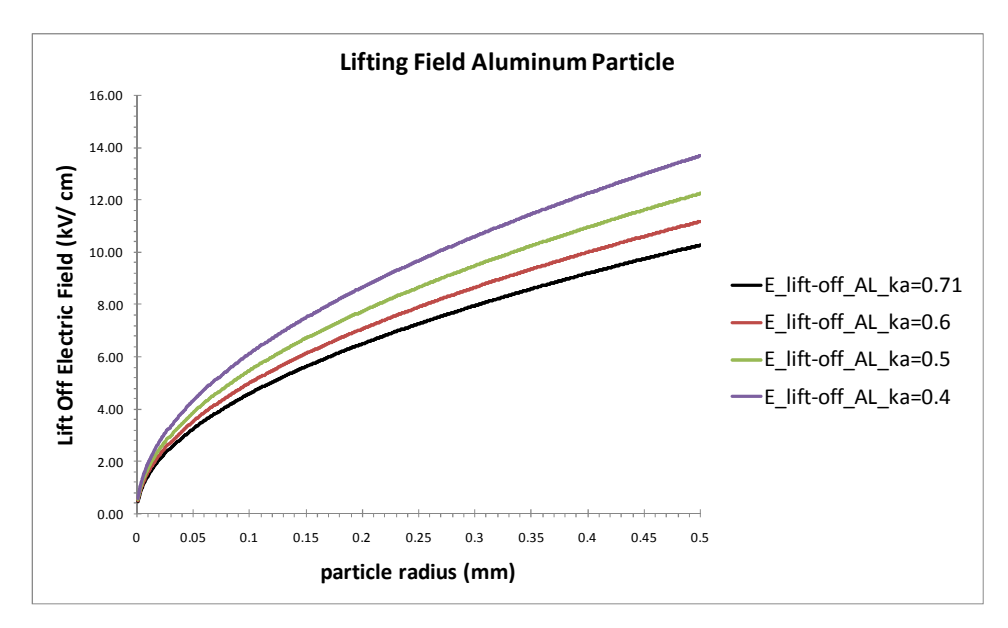


Figure 2.6Lifting Field of Aluminum Particle at different radius and with different constant k_a

It has been shown that the lift off electric field is increasing as the correction factor, k_a , decreased. The value of k_a is important during the particle simulation especially for the initial jumping condition when the particle position is changing immediately from horizontal to vertical position.

2.2.3 Motion Equation [11, 24]

Cookson et al. in reference [24] gives the force equation for a particle subjected with an electric field:

$$m \cdot \vec{a} + k_a \cdot Q \cdot \vec{E} + m \cdot \vec{g} + \overrightarrow{F_d} = 0$$
 ... equation 2.7

The first part is the first Newton equation of force with m is the particle mass and \vec{d} is a vector of particle acceleration. The second part of the equation is the electrostatic force (F_e) which has been previously described. The gravitational force, F_g, and the drag force, F_d, are sequentially the next parts of the equation. Each force will be discussed in the next paragraphs.

1. Electrostatic Force

The electrostatic force is calculated by multiplying the net charge on the particle with the value of the electric field.

$$F_e = k_a$$
. Q. $E_{[t, y(t)]}$... equation 2.8, [11]

where y(t) is the distance of the particle from the bottom electrode. In case of a GIS bus, y(t) is the distance from the outer electrode.

The electric field distribution in a coaxial configuration such in a GIS bus can be expressed as:

$$\frac{\hat{V}\sin \omega \mathbf{t}}{[ro - y(t)].\ln \left[\frac{r_o}{r_i}\right]}$$
... equation 2.9

where \vec{V} is the peak value of applied voltage on the inner conductor, r_i and r_o are consecutively the inner and the outer radii of the electrodes.

2. Gravitational Force

Since the gravitation acceleration inside the GIS bus is considered to be constant, the gravitation force is also a constant. For a cylinder shape particle with radius of r and the length of ℓ , the expression of gravitation force is:

$$F_g = m. g = \rho . V . g = \rho . (\pi.r^2.\ell) . g$$
 ... equation 2.10

where ρ is the density of the particle.

3. Drag force

The drag force will act in the opposite direction of the motion. It originates from the skin friction along the surface of the particle and also due to energy dissipation in the shock wave in front of the particle [11].

Holmberg's divided the drag force into two components. The one that appears around the hemispherical ends of the particle which is due to shock and skin friction (F_{d1}), and the other drag force which occurs along the sides of the particle due to the skin friction component (F_{d2}). The expression of both components is given below:

$$F_{d1} = 6 \cdot \pi \cdot \mu \cdot r \cdot \bar{y} \cdot k_d(\bar{y})$$
 ... equation 2.11 (Stoke's equation), [11]

where: μ is the viscosity of the gas

 \bar{y} = dy/dt is the velocity of the particle

 $k_d(\bar{\mathcal{I}})$ is a dimensionless drag coefficient which depends on the Reynolds number, R_e , which is a number that characterizes the degree of turbulence behind the moving particle.

$$\begin{split} k_d(\ddot{\mathcal{Y}}) &= \text{exp} \; [0.1142 + 0.00543 \; \text{ln} \; [R_e] + 0.0516 \; (\text{ln} \; [R_e])^2], \\ &\quad \text{with} \; R_e = 2.r. \; \rho_g. \; \ddot{\mathcal{Y}} \; / \; \mu \\ &\quad \text{and} \\ &\quad \text{the gas density,} \; \rho_g = 7.118 + 6.332.P + 0.2032.P^2 \; \text{with} \; 1 < P < 10 \; (\text{Bar}), \; [11] \\ &\quad F_{d2} = 1.328 \; . \; (2\pi r) \; . \; [\mu. \; \rho_g \; . \; \ell]^{0.5} \; . \; \ddot{\mathcal{Y}}^{1.5} \qquad ... \; equation \; 2.12, \; [11] \end{split}$$

The total equation for the drag force then become:

$$F_d = F_{d1} + F_{d2} = \bar{y}$$
. π .r { 6 . μ . k_d (\bar{y}) + 2.656 [μ . ρ_g . ℓ . \bar{y}]^{0.5}} ... equation 2.13, [11]

With consideration of these forces, the motion equation expressed in equation 2.7 can also be expressed as:

$$m.\ddot{y}(t) = F_e - F_g - F_d$$

$$m.\ddot{y} = \frac{\pi.\varepsilon_{o}.\ell^{2}.E(t_{o})}{\ln\left(\frac{2\ell}{r}\right) - 1} \left(\frac{\hat{V}.\sin\omega t}{[r_{o} - z(t)].\ln\left(\frac{r_{o}}{r_{i}}\right)}\right) - m.g - \dot{y}(t).\pi.r.\left(6\mu k_{d}(\dot{z}) + 2.656\left[\mu.\rho_{g}.\ \dot{z}(t)\right]^{0.5}\right)$$
... equation 2.14, [11]

By solving this equation, the particle trajectory can be derived.

2.3 Detection of Free Moving Particles in GIS

The detection of particles during the GIS operation is necessary to prevent failures. Besides, since the decision to overhaul of a GIS is cost full and time consuming, the detection should be able to demonstrate a sufficient high sensitivity to distinguish between the harmful and the harmless particles.

In general, defects in GIS generate Partial Discharge (PD) activity before the complete breakdown. This is also the case with the free particles. The PD has many effects, such as light which is originated from the emission of excited molecules, chemical decomposition products like SF_4 , thionylflouride (SO_2F_2) and sulfurlyflouride (SO_2F_2), mechanical pulses and electrical signals. Only the last two are considerably suitable for the diagnostics of free particles in GIS [29].

Electrical signals are originated from the corona discharges. For the free particles, corona discharges are produced during the particles flight. At the moment the particles are striking the electrode surface, it generates not only the contact discharges but also mechanical pulses.

The most promising diagnostic methods on free particles are [30]:

1. The acoustic method (with the frequency range of 5-1000 kHz)

The acoustic PD measurement technique is based on the acquisition of sound waves in the GIS compartment by using ultrasonic sensors such as accelerometers and resonant transducers or acoustic emission sensors. This method is able to detect signals emitted from mechanical impacts of a particle on the enclosure, and the joule heating of the gas in corona discharges. The sensitivity of this method

is good. External noise is rarely a problem, as the signals from the particle have a bandwidth of several MHz, while the environmental noise is below 100 kHz [8, 30]. Thus, the signal to noise ratio is high.

2. The conventional electrical PD detection technique (with the applied frequency range of some 10 kHz and 1 MHz)

This method measures the apparent charge from corona and contact discharges using a coupling capacitor and a measuring impedance according to IEC 60270. The measuring circuit is shown in figure 2.6.

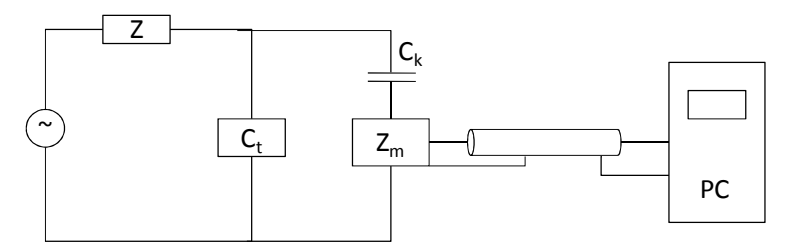


Figure 2.7Test setup according to IEC 60270 [8]

The test object in the figure is shown by C_t , in this case is a GIS. A PD produces an impulse travelling which can be detected by the coupling capacitor, C_k , and the measuring impedance Z_m . The current flowing through Z_m , is proportional to the discharge current at the test object.

The relation between the two currents cannot be determined due to the unknown capacitance configuration at the discharge location. The detected charge through Z_m is known as the apparent charge [8]. The magnitude of the measured apparent charge depends on the radial position of the discharge [29, 32]. To avoid integration of errors, the detection circuit should have as low a cut-off frequency as possible. [29, 33].

This method is less used in field since the external noise may disturb the measurements.

3. Very High Frequency (VHF: 30 - 300 MHz) and Ultra High Frequency (UHF: 300 - 3000 MHz) methods.

The current that coming with PD path rises in a very short of time (~ 1ns) and contains electromagnetic waves with frequency in the range of 0 to 3000 MHz [8]. These excited electromagnetic waves propagate in the insulation system along its coaxial structure. The signals are transmitted as Transverse Electromagnetic wave (TEM), Transverse Electric wave (TE) or Transverse Magnetic (TM) waves.

TEM propagation mode occurs at low (power) frequency conditions, where the wavelength is long compared to the diameter of the structure [16]. Here, both the magnetic and the electric fields are transverse to the direction of transmission, and without any field in the direction of the transmission. These waves cannot pass the switching components since both inner and conductor are necessary to be present.

The TE- and TM-modes occur at higher frequencies. In these modes, the magnetic field has both longitudinal and transverse field components, and the transverse electric wave has a transverse electric field component. Different with the previous TEM, TE and TM modes can propagate through the opened contacts of the switching components [16].

Since the common signals used are above 100 MHz, the external noise from air corona is strongly suppressed [29, 34]. Thus, this method is commonly used in online diagnostic of GIS. Several sensors are installed at different places of GIS segments.

The measurement parameters

As it has been mentioned in the beginning, it is expected that the parameters derived from the measured signals can describe the characteristics of the particles. These include, for example, the particle behavior and the particle location. The scalar parameters, like signal level and its repetition rate, and the apparent charge are used as the basis for the characterization and risk assessment. The most commonly used parameters are [29]:

- 1. rms of signal amplitudes;
- 2. peak signal amplitudes;
- 3. repetition rate in pulses per second or the time between impacts (example: time of flight in acoustic measurement);
- 4. periodicity of signal groups with respect to the power frequency,
- 5. phase angle of individual PD pulses with respect to the power frequency.

The phase resolved partial discharge (PRPD) pattern has been introduced to analyze these parameters [35]. This technique can be implemented to all the above diagnostic methods. Regarding to the particle existence, another voltage-dependent parameters can be mentioned:

- 1. PD inception and extinction voltage,
- 2. Stand-up, lift-off and fall-down voltage of free particles.

This information derived from these parameters can be very useful, for example in the estimation of the particle size inside of the GIS compartment.

2.4 The Effect of Very Fast Transient Overvoltages (VFTO) to the Withstand Insulation Level

Two main sources of VFTO in a GIS are: the switching of disconnector switches and the earth faults [8]. During the operation of switching contacts, like circuit breakers or disconnector switches, an overvoltage with a very steep front-rise time in the order of few nano second can be rised. This can be happen due to a number of internal reflections and refractions of travelling wave, at a short length of GIS conductors, which superimposed each others and can give rise to the VFTO.

In a defect free GIS, the VFTO is considered not to be dangerous to the insulation. This is due to the fact that the typical magnitude of VFTO is rarely exceed 70% of the Basic Insulation Level (BIL).

In the presence of protrusion, the withstand voltages for both the lightning impulse (LI) and VFTO are drastically reduced. However, according to the reference [8], the minimum withstand voltage with the existence of a protrusion is in the range of the lightning impulse time to peak. This is shown in the following figure:

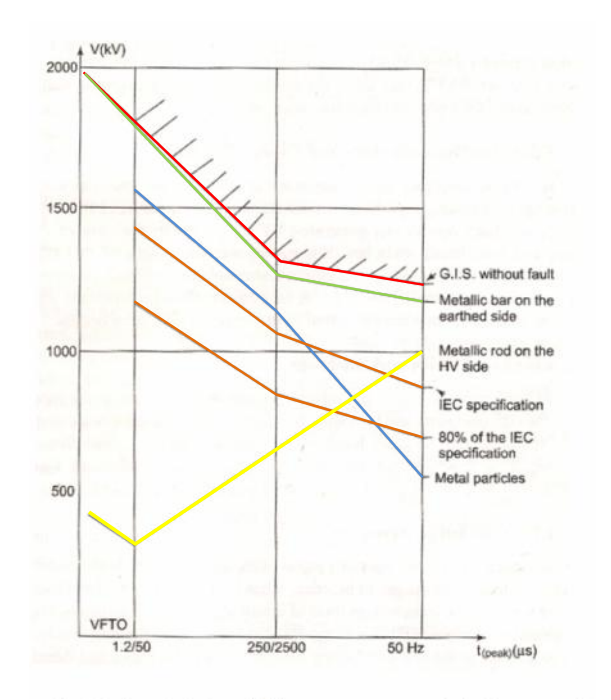


Figure 2.8Voltage-time curve of 420 kV GIS for different types of defects. Withstand voltage versus time to peak of the applied voltage, from VFTO domain up to power frequency domain [8]

From this figure, three conclusions can be derived:

- 1. In GIS without any fault or defect, the VFTO withstand voltage is higher than the other voltage stresses.
- 2. The same situation is also applied when a metallic bar is placed on the earthed side.
- 3. When there is a protrusion, the VFTO withstand voltage is still higher than the LI withstand voltage. The minimum withstand voltage is given at the point of LI impulse stress.

The withstand level with the free particles is still not yet drawn in the graph as well as the VFTO withstand level for the IEC standard. The line in the graph is showing a tendency to keep increasing to the upper left direction, which means the withstand level with the VFTO will be higher than the others. If the particle is welded to the electrode, the situation will be the same as in the case with protrusion.

2.5 Conclusions

- 1. Different breakdown mechanisms of insulating gas have been discussed. In SF₆ gas with particle impurities, with typical GIS pressure, the breakdown mechanisms are governed by the streamer or the leader mechanisms. With the influence of fast transient voltage stress, leader mechanism is most likely to occur. While, under AC or DC voltage stress, it depends with the particle situation in between the electrode gap, both streamer or leader mechanisms are possible to occur.
- During the simulation of the particle movement, different forces should be considered:
 The electrostatic force, the gravitation force and the drag force. The particle trajectory can be derived by solving the motion equation.

- 3. PD activity occurs prior to a complete breakdown. Among different signals originated from the PD activity, mechanical pulses and electrical signals are suitable for the detection of free moving particles. The acoustic and the unconventional PD measurement with VHF/ UHF methods are more persistent to the external noise than the conventional PD method according to the IEC 60270 standard. Thus, these methods are suitable for on field PD detection and for on-line continuous PD monitoring in GIS. While the conventional PD detection, is commonly used in high voltage tests after manufacturer process, during the erection of GIS or after an overhaul work.
- 4. The effect of VFTO in a sound GIS is negligible. But, in the presence of a protrusion, the withstand level is decreased. The withstand level with the free particle is not yet concluded, except when the particle is fixed to the electrode and become a protrusion and this implies the importance of this thesis work.

Chapter III

Experimental and Measurement Setups

In general, three different setups have been used in this thesis work to investigate the impact of the particle on the GIS insulation under the following (over) voltages:

- AC voltage
- 2. AC + LI overvoltage
- 3. AC + VFT overvoltage

The first two test setups are built in the HV laboratory of Delft University of Technology while the investigation involved the AC + VFTO is performed by using the GIS test setup in the High Voltage Laboratory of Stuttgart University of Technology. This is because they have the ability to generate the VFTO and the required measuring devices.

In this chapter:

- 1. The GIS test setups used to investigate the impact of the particle movement under AC, AC+LI and VFTO are explained
- 2. The generation of different voltage types is discussed in sections 3.3 to 3.5.
- 3. The electric field distribution in the test setup is shown in sections 3.6 to 3.7.
- 4. The particles used in the experiments are discussed in section 3.8.
- 5. Finally, different detection techniques used to detect the particles are discussed in section 3.9 to 3.11 respectively. The detections include:
 - a. The acoustic method
 - b. The conventional method based on the IEC 60270 standard
 - c. The unconventional method by using the UHF/VHF sensor

3.1 The GIS Test Setup Used in TU Delft HV Laboratory

This test setup has been used to investigate the impact of the free moving particles on the GIS insulation under AC and AC + LI. This test setup has been built of used parts which are originated from 380kV single-phase GIS compartment manufacturer by Siemens. The outer/ inner conductors are made of aluminum and have radius of 150/35 mm, see figure 3.1. The inner electrode is connected to the voltage source via a gas filled (Nitrogen at 2 bar) bushing.

The inner surface of the outer electrode was coated with a thin antioxidant-layer. The enclosure is equipped with an internal UHF sensor to allow the partial discharge measurements and a small window which has been used for measurements and observation purposes. The test setup is grounded via a copper strip.

A camera connected to a video display is placed in front-of the window to observe the particle movement during the investigation under AC Electric Field. Sulphur Hexaflouride gas (SF₆) at 4 bar is used to insulate the high voltage conductor. The 4 bar gas pressure is selected to simulate the lowest gas pressure in the 380 kV GIS installation located in Meeden.

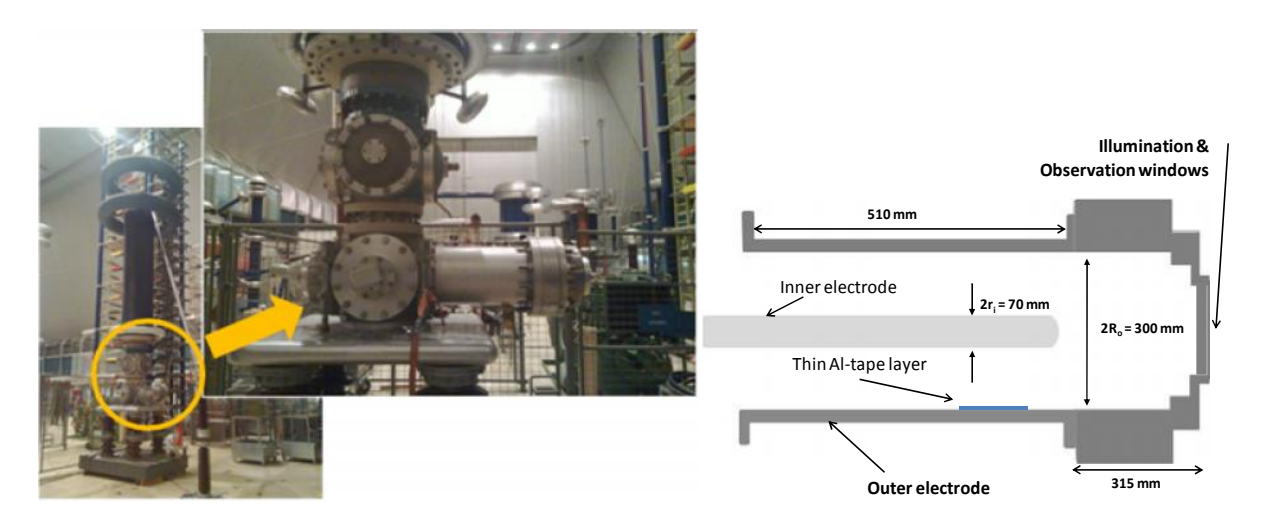


Figure 3.1 Picture of GIS bus used in the experiments with AC and AC + LI electric field (left). Dimensions, illumination window are shown in the right figure.

3.2 The GIS Test Setup used in Stuttgart University HV Laboratory

The investigation involved the AC+VFTO is taking place in Stuttgart University of Technology in Germany. The compartment is an ABB type ELK-3 of 550 kV GIS with the ratio of outer/inner diameter of 250/80 mm. The center conductor is made of aluminum, except at the sparking gap, two copper sphere electrodes are used with adjustable distance gap.

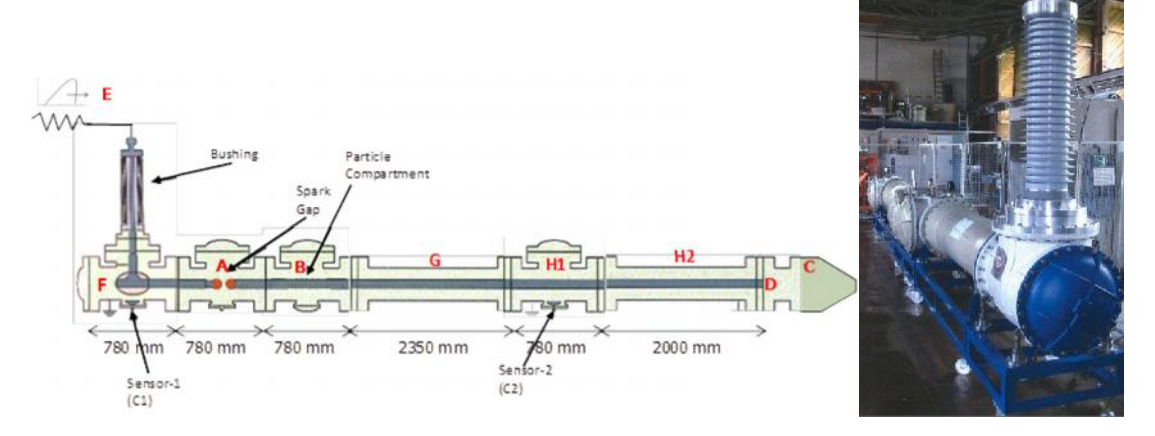


Figure 3.2 Schematic diagram (left) and the GIS compartment used in the investigation of VFTO (right)(courtesy of Stuttgart University of Technology, High Voltage Laboratory)

Observation windows are placed at the top of the spark-gap and the particle compartments. The total length of the test setup is about 7.5 m, the length of the individual compartment is depicted in figure 3.2.

Some of the test setup compartments are filled with the SF_6 , see compartments F, A and B in the figure, the remaining compartments are filled with air. The pressure in compartment A is adjusted between 1 and 5 bar to obtain the desired VFTO peak, while the pressure in compartment B is adjusted 3 – 4 bar during the experiment. The other compartments are filled with air at 5 bar pressure. There are capacitive sensors placed in compartment F and H1 which are used to measure the VFTO signals. In order to obtain the VFTO, an impulse generator is used to provide the surge voltage.

The required (over)voltages used in TU Delft and TU Stuttgart are explained and discussed in the following sub chapters.

3.3 The Generation of the AC Voltage in TU Delft HV Laboratory

The AC voltage is provided by a power transformer that can deliver voltage up to 200 kV rms. The voltage regulation is done by using an auxiliary regulator installed in parallel at the low voltage side of the transformer. Due to some limitation at the auxiliary regulator, the maximum voltage that can be delivered by the transformer is reduced to 145 kV rms.

The main voltage supply to the transformer is taken from the system grid, i.e. 220 V, 50 Hz. By using the voltage regulator, the voltage amplitude is regulated in a range of 0 - 550 V. A current limiter is installed to protect the auxiliary systems (shown by number 3 in figure 3.3).

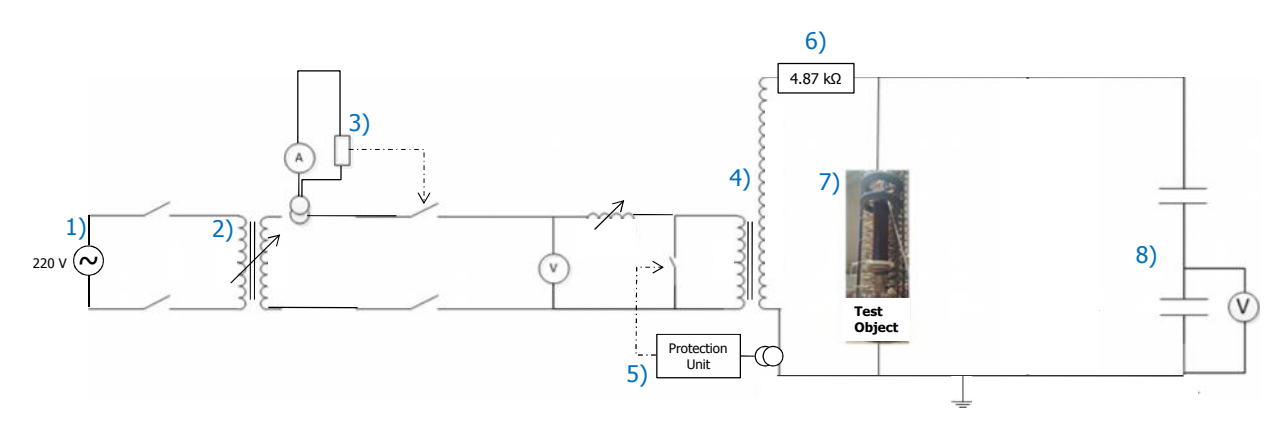


Figure 3.3 The schematic diagram of the generation AC Voltage in TU Delft HV Laboratory

The low and high voltage sides of the transformer are marked by number (4) in the figure. It is a single phase oil power transformer. The maximum capacity of the transformer is 200 kVA.

At the ground point of the power transformer, another protection unit (5) is installed to protect the transformer whenever a breakdown occurs in the test object. The protection is connected to the relaying systems using an optic cable to assure the high speed of the tripping circuit.

A resistor of 4.87 kV is placed in between the power transformer and the test object (6). This resistor has the purpose to limit the fault current. However, after few measurements, the resistor was degraded and it was disturbing the PD measurements (as shown in Chapter VII). Therefore, it has been removed afterward.

A voltage divider, marked with number 8 in the figure, connected to a display is used to measure and view the amplitude of the applied voltage during the experiments, a voltage level of 1 p.u. is equal to 120 kV (rms). With this value, the distribution of the electric field generated in the test set up is comparable to the field distribution in the 380 kV GIS substation located in Meeden (the distribution of the electric field will be discussed in sub section 3.6).

3.4 The Generation of the AC + LI Overvoltage in TU Delft HV Laboratory

A superimposed of AC + LI can occur in GIS and reaches as high as 3.5 p.u, see section 1.2. The objective of the experiment under this superimposed voltage is to investigate whether there is a breakdown can occur in the presence of a free moving particle especially when a particle is jumping. The worst situation occurs when the lightning impulse at the moment when the particle is close or attached

to the high voltage electrode and the lightning impulse superimposed exactly at the peak of the ac voltage and both have the same polarity.

To achieve this situation in the laboratory, the experiment should be performed first under AC voltage and later after the particle starts jumping, the LI is given into the test object. However, it is difficult to observe the height of the particle jumping at the moment the lightning is given. Therefore the test is only running with the lightning impulse. This is valid since the duration of the LI is much shorter than the duration of the AC voltage. The particle distance to the inner conductor is adjusted by hanging the particle by using a cotton thread. The particle setup will be discussed in section 3.8

The lightning impulse used during the experiments is in accordance to the IEC standard. It has a front time of 1.2 μ s and a tail (time to half-value) of 50 μ s, as shown in figure 3.4. The complete test setup is given in figure 3.4:

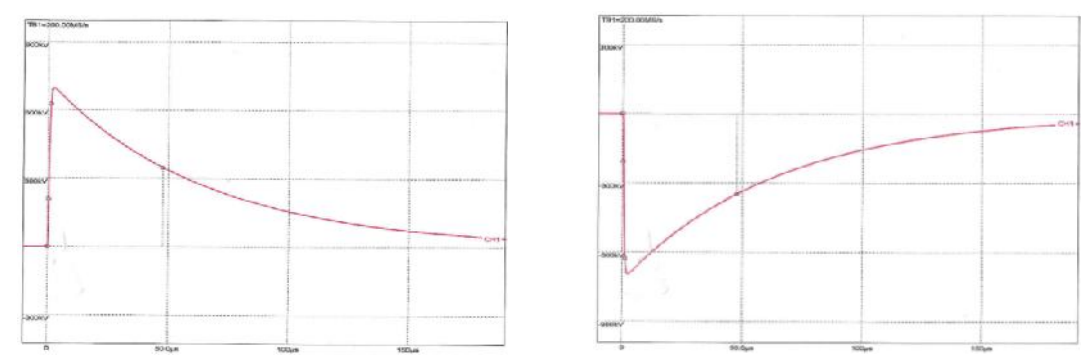


Figure 3.4 Standard Lightning Impulse according to IEC 60071-1, positive polarity (left) and negative polarity (right)

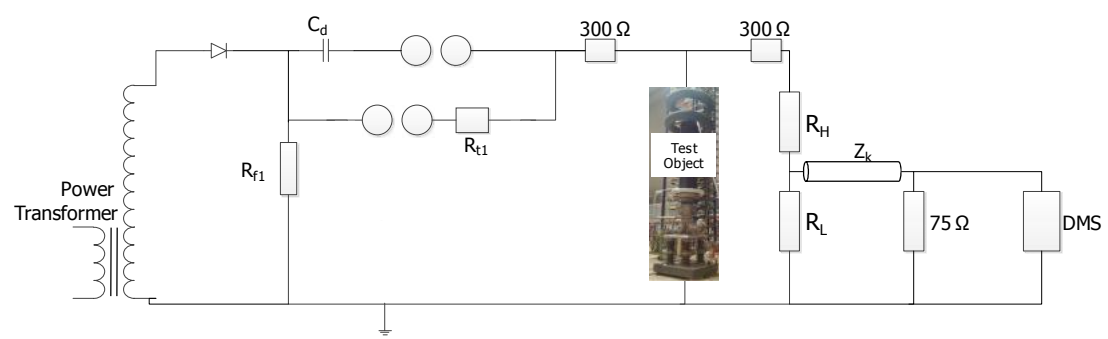


Figure 3.5 The schematic diagram of the generation Lightning Impulse in TU Delft HV Laboratory

The energy of the impulse generator is supplied by the power transformer as shown at the left side. The energy is stored inside the discharge capacitor, C_d . The discharge capacitance should always be larger than the load to maintain the high efficiency of the generator [11]. The high voltages can be generated by charging the discharge capacitors, C_d , in parallel and discharging them in series.

The shaping of the impulse is governed by the front resistance, R_{f1} , which determines the front rise time; and the tail resistance, R_{t1} , which controls the time to half-value. The value of R_{f1} and R_{t1} respectively are 925 Ω and 140 Ω .

To the right hand side of the test object, a voltage divider is placed. The ratio between R_H/R_L represents the voltage ratio between the high voltage side (lightning impulse side) and the voltage at the measuring circuit. Therefore, the value is much higher for R_H , which is in the order of 12 k Ω , while only about 200 Ω for the R_L . The voltage information is sent into the Digital Monitoring Systems (DMS) via a

coaxial cable with impedance, Z_k ,of 75 Ω . Another 75 Ω impedance is placed in parallel to the DMS system.

3.5 The generation of the AC + VFTO in Stuttgart University HV Laboratory

The test setup used to generate the VFTO is shown in figure 3.6:

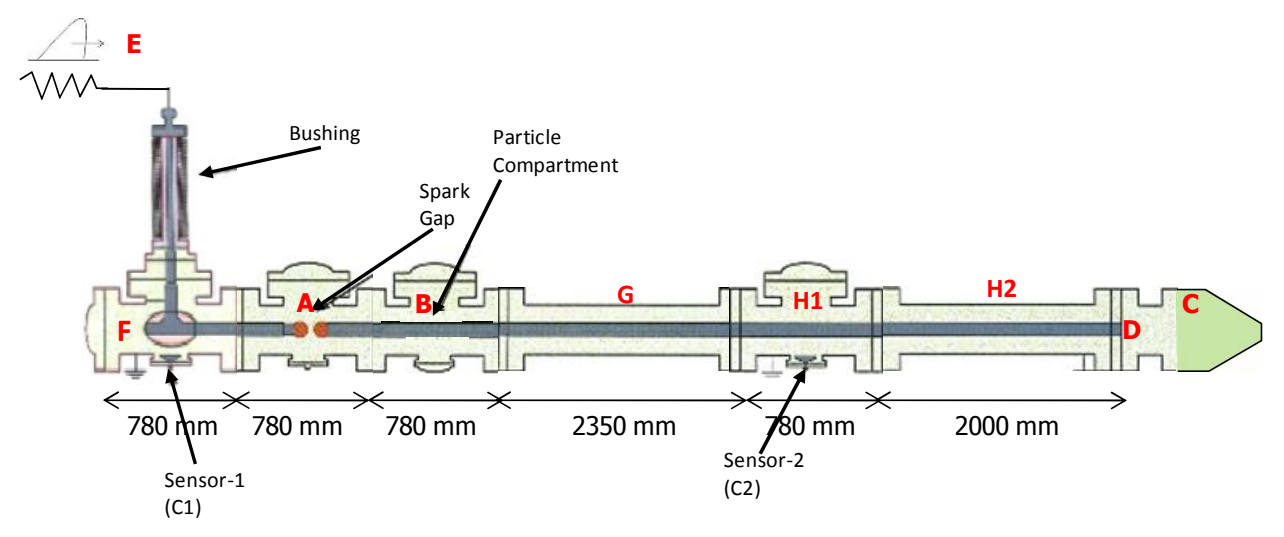


Figure 3.6Scheme diagram of the test setup used in Stuttgart

The VFTO is generated by using the combination of a lighting impulse and sphere gaps instead of using an actual switching device. A surge is generated from the impulse generator, when the surge level is higher than the breakdown voltage of the spark gap, a sparkover occurs between the gaps and initiates the VFTO.



Figure 3.7 The spark gap used in generating the VFTO (on behalf of the Stuttgart University)

The peak of the VFTO can be adjusted by changing the value of the gas pressure or by changing the distance of the spark gap. The polarity of the VFTO can be adjusted by changing the termination connection at the end of the GIS [41]. If the termination is open, the travelling waves are reflected by a positive factor close to +1. Meanwhile, the termination connected to the ground, the travelling waves are reflected by a negative factor close to-1.

3.6 The Electric Field Distribution in the Test Setup Used in TU Delft HV Laboratory

In Chapter I it has been mentioned that this thesis work is taking a study case of the 380 kV GIS Substation located in Meeden. In Meeden, the ratio of the outer/inner electrodes is 277/65 mm while in the laboratory is 150/35 mm. The electric field distribution in both compartments is calculated by using the formula given in equation 2.9 which is rewritten below:

$$E(t) = \frac{\hat{V} \sin \omega t}{[ro - y(t)] \cdot \ln \left[\frac{r_o}{r_i}\right]}$$

Bychoosing the 1 p.u. = 120 kV rms in the laboratory, the comparison of the maximum and the minimum electric field in both setups are given in table 3.1. The maximum and the minimum electric field in both setups are similar.

Table 3.1The Calculated Maximum and the Minimum Electric Field In Meeden 380 kV GIS and TU Delft HV Laboratory Test Setup

	Electric Field Calculated (in V/m)		
	Meeden	Lab	
MAX	2.33E+06	2.36E+06	
MIN	5.46E+05	5.50E+05	

The electric field ratio which determines the ratio between the electric field at a particular position to the maximum electric field in both setups are shown in the following figure:

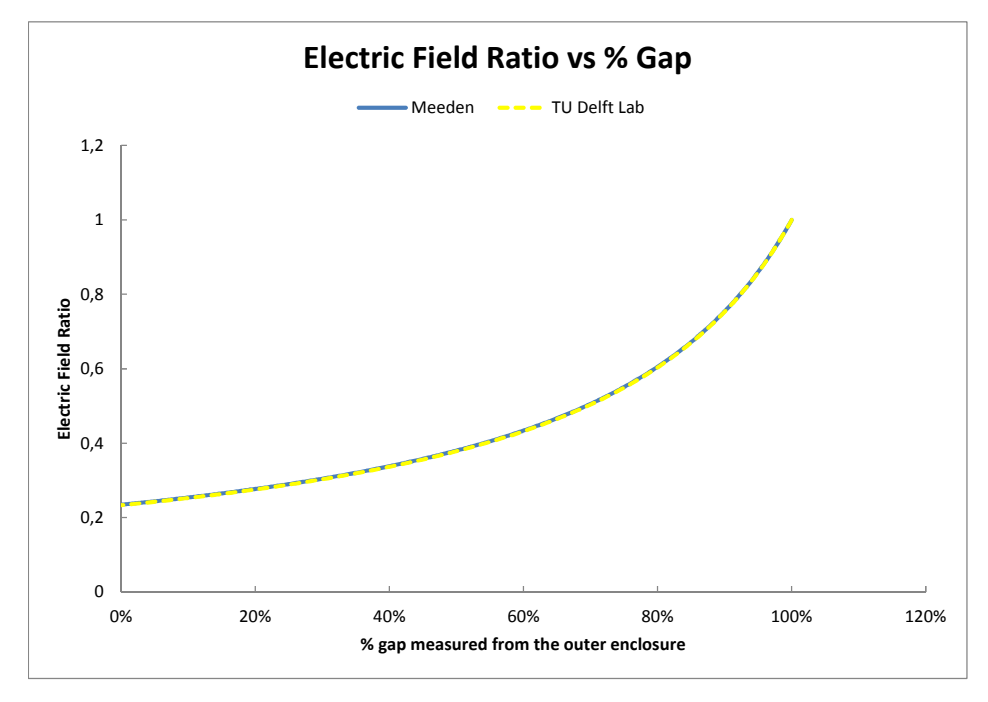


Figure 3.8 The electric field ratio vs. percentage of the distance gap for the GIS compartment in Meeden and the test setup used in TU Delft HV Laboratory

According to the results, the electric field in both setups is comparable. However, the rate of the electric field changing along the gap is higher in the laboratory setup.

3.7 The Electric Field Distribution in the Test Setup Used in Stuttgart University HV Laboratory

The electric field distribution in the test setup used in Stuttgart has been analyzed to investigate whether it is comparable to the electric field distribution in the test setup used in Delft. The electric filed distribution has been calculated by using the formula used in section 3.6.

The comparison of the electric field distribution between in Stuttgart and TU Deflt is presented in Figure 3.9. Since the particle can jump close into the inner conductor, the maximum electric field in the test setup in Stuttgart is adjusted to be similar with the electric field in TU Delft test setup. The maximum difference in both setup is 28% at the bottom electrode. However, during the experiment the particle is placed 80% - 90% of the gap, where the difference of the electric field ratio at that distance is in the range of 10%.

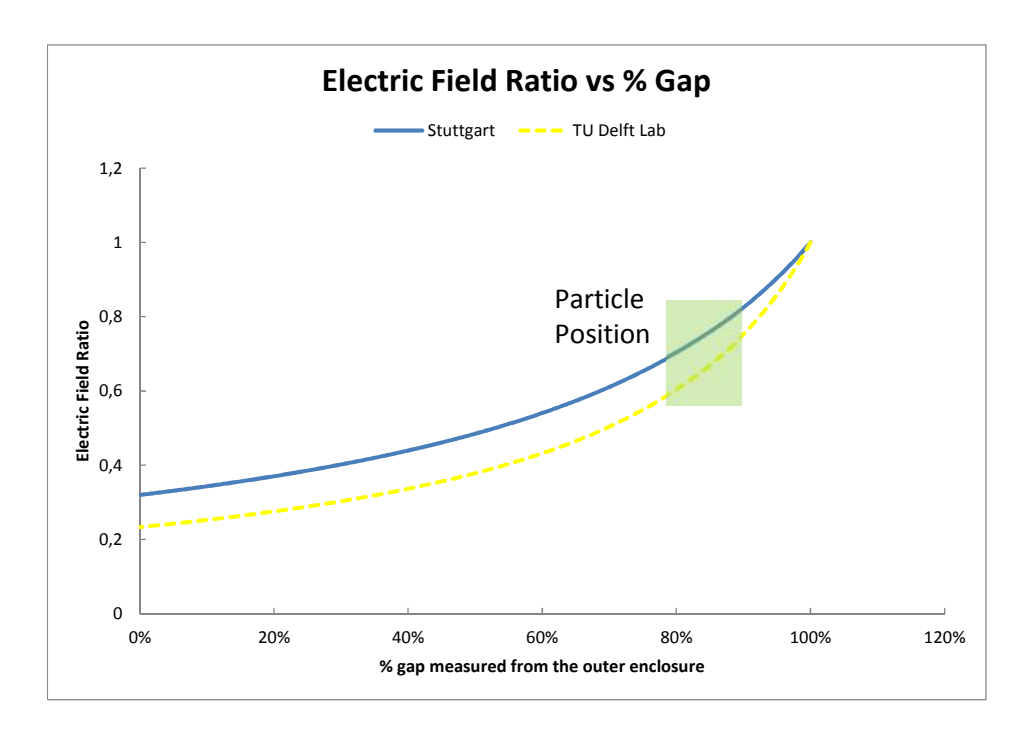


Figure 3.9 The electric field ratio vs. percentage of the distance gap for the test setup used in Stuttgart and the test setup used in TU Delft HV Laboratory. The green area shown in the picture is showing the distance where the particle is placed during the experiment with AC + VFTO

3.8 The Particles Selection, Shape and Dimension

The free moving particles are originated from different sources. The particles do not have a certain shape, and their material depends on their origin. The particles originated from moving contacts, for example, have tungsten as material, while the debris after an overhaul work probably contain of aluminum, steel or copper particle.

During the experiments elongated cylindrical particles of 2-30 mm length are used. The reasons are the following:

1. The cylindrical metallic shape is the most founded particles in practice [7,15]

- 2. The cylindrical metallic shape is considered to be the most dangerous to the insulation system [7,15]
- 3. The particle as small as 2 mm can be detected by the PD activity under normal operating stress [54]. The length of particle to be tested is limited to 30 mm for a safety reason.

During the investigation under AC voltage, the aluminum particle is used due to its low material density. The aluminum particle is easier to start jumping, hence can be consider more critical comparable to other materials. An example of 10 mm aluminum particle is given in figure 3.10. The initial position of the particle is lying horizontally at the bottom of the enclosure.



Figure 3.10 An example of aluminum particle used during the investigation under AC Voltage.

In the investigation under AC + LI overvoltage and under AC + VFTO, the copper particle is used. There is no specific reason in choosing copper instead of aluminum. Besides, the breakdown either by the streamer or leader mechanism is independent of the electrode material [11]. During these experiments, the particle is hanging at the outer electrode as shown in figure 3.11.

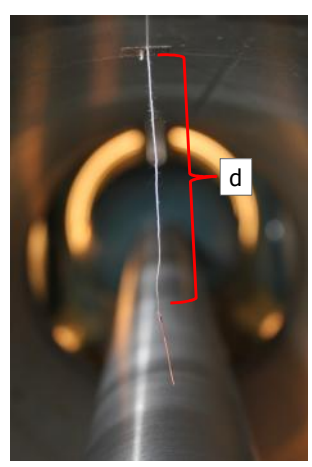


Figure 3.11 The hanging particle to represent the height of the particle jumping. The distance, d, determines the distance in % of the gap.

The length of the thread represents the height of the particle jumps (d).

It should be mentioned that the experiments may deviate from the actual situation due to the following:

- 1. In actual situations, the particle is charged during its motion. This charge may results into field enhancement at the tips of the particle which has a positive influence on the breakdown strength. Due to the fact that the particle has been hanged by using a cotton thread, it was not charged.
- 2. Once the breakdown occurs, the sample should be replaced since it is degraded.

3.9 Detection Techniques

Particle inside of GIS can be detected by different PD detection methods. In the following sections, three methods are discussed namely:

- 1. The acoustic method
- 2. The conventional method
- 3. The UHF method

3.9.1 The Acoustic Method

The acoustic method is based on the detection of the sound signals transmitted by the particles inside the GIS. The acoustic signal itself is a pressure wave which basically originated from two main sources:

- 1. from the partial discharges (PD) inside the GIS, and
- 2. from the mechanical impact of the bouncing particle to the bottom electrode

At the moment that the particle hit the enclosure, PD signals are generated, their amplitude is much smaller than the mechanical signals generated by the particle[29].

During the experiments, a commercial Acoustic Insulation Analyzer (AIA) manufactured by TransinorAS has been used to measure the acoustic signals. The signal is received by a piezoelectric sensor which attached at the external part of the GIS enclosure. The acoustic signal is converted into the electric signal by means of a PAC 1220A converter. The signal is then amplified by the pre-amplifier before they received by the AIA processor. An oscilloscope is connected to the output port of the AIA to view signals. This is schematically is shown in figure 3.12

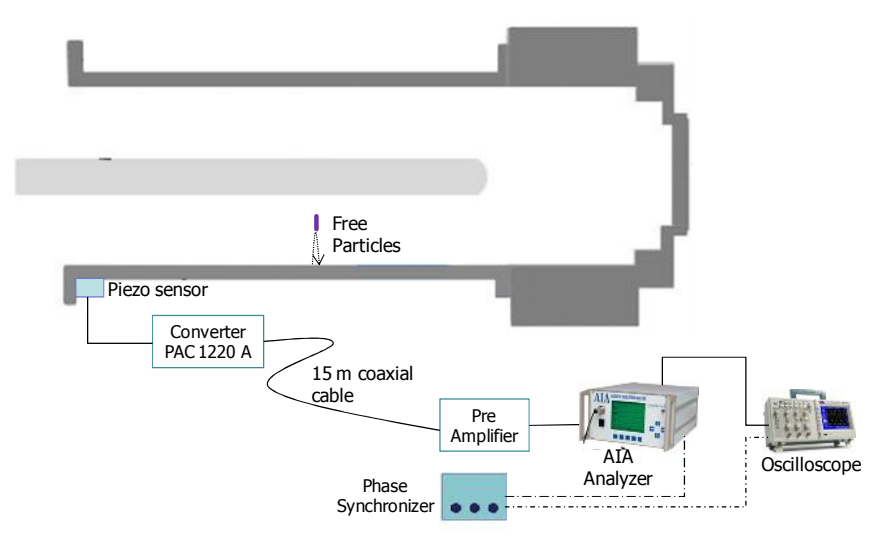


Figure 3.12 The setup diagram of the acoustic measurement

A set of parameters are necessary to get the best acoustic signal out of the AIA instrument are discussed below:

1. Gain

The gain parameter has a function to amplify the signal. It is possible to select among the following amplification ratios 1x, 3x, 10x, 30x, 100x, 300x, 1000x, 3000x

During the experiments, the gain is set between 1x and 3x. These values are sufficient to get the best signal without overflowing the measuring system.

2. Lower rolloff frequency

This parameter has a function to limit the low frequency noise. In [38] it has been described that the best selection is between 10-20 kHz as the lower rolloff frequency. This value should be selected carefully to match the PD signals frequency range which is 20 - 80 kHz. If the lower rolloff frequency is too high, the PD will possibly be undetected. During the experiments the rolloff frequency is set to 10 kHz.

3. Upper rolloff frequency

This parameter has a function to limit the high frequency noise without affecting the original signal. The available steps for this parameter are: 20 kHz, 50 kHz, 100 kHz, 200 kHz, and 500 kHz. The default for the upper rolloff frequency is 100 kHz. However, during the experiment in the laboratory, an upper rolloff frequency of 500 kHz gives a good result; this can be related to the low noise level at the laboratory.

4. Trigger reference level

This parameter should be low enough to trigger on weak particle impact, and high enough to avoid unwanted triggering the noise signal. The default of this parameter is 68 mV. The trigger reference level may be set in the following steps:

0, 10mV, 15mV, 22mV, 33mV, 47mV, 68mV, 100mV, 150mV,

220mV, 330mV, 470mV, 560mV, 680mV, 1V, 1,5V, 2.2V, 3.3V, 4.7V

During the investigation, the trigger reference level is set at 47 mV and 68 mV. This level is sufficient to get the signals from the bouncing particles.

The use of the acoustic measurements has two purposes:

- 1. To calculate the maximum jumping height of a particle inside the GIS the Time-of-Flight (TOF) (which represents the duration of the particle levitate is derived from the measurement) is determined
- 2. To obtain the Phase Resolved Signature pattern. The Phase Resolved Signature is achieved by analyzing the amplitude signal (in mV) as a function of the voltage phase

Voltage phase shifting between the grid and the test object may occur. This is due to the non-linear components in the voltage regulation process. Therefore, a phase synchronizer is connected to the instrument as shown in the figure above.

3.9.2 The Conventional PD Detection Method

The conventional PD detection is a standardized method for partial discharge measurement according to the IEC 60270. The explanation of this measurement has been given in section 2.3 and the measurement setup is given in figure 2.7.

In the laboratory, this method has been applied by using the Haefely TE 571 PD Detector and the Haefely PD Detector type 560. The parameters that can be measured using these instruments are:

- 1. PD Inception Voltage (PDIV)
- 2. Apparent PD Level in pC at different voltage level
- 3. PD pattern (PRPD)

During the experiments, each measurement has been run for 2 minutes. During the PD measurements, the following parameters are measured:

- 1.the maximum of PD magnitudes,
- 2.the average of PD magnitudes
- 3. and the number of PD pulses [39]

These three parameters are plotted as a function of phase angle of AC voltage.

Before starting the PD measurements it is required to perform a calibration process. The calibration of the measuring setup is performed as following, see figure 3.13:

- 1. the calibrator is connected to the terminals of the test object, a)
- 2. Signals of standard charges are injected between the test setup and the ground [40].
- 3. Signal are received and the setting of the PD detector are adjusted according to the amplitude of the signals have been received.

Thus, the overall relation between the discharges (in pico Coulomb, pC) and the output of the detector is known. This relation is independent of impedance, bandwidth, and etc. [40].

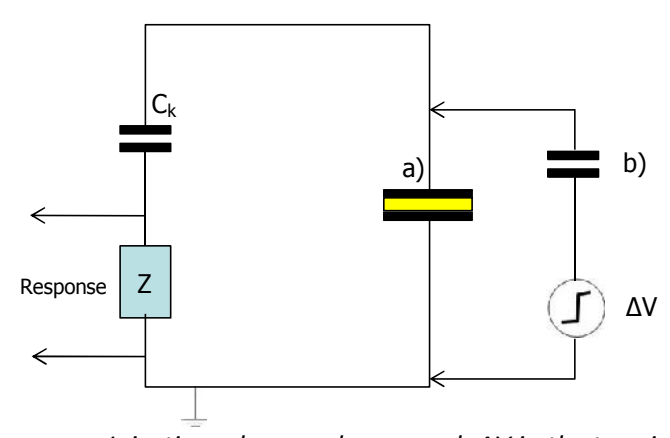


Figure 3.13 Calibration process. Injecting a known charge $q = b.\Delta V$ in the terminals of test object, a. The response is adjusted to a required value. [40]

The purpose of the measurement by using this method is to find the characteristic of PD pattern due to the free particles and to find the relation between the PD magnitude and the size of the particle. The measurements results are shown in Chapter VII.

3.9.3 The UHF/ VHF Method

The previous conventional method has a certain limitation due to its sensitivity to the ambient noise [29], therefore it is difficult to implement it for the onsite work since a lot of noise are generated in the field.

Another possible method is by the detection of UHF/VHF electromagnetic waves exited by the PD pulses. In section 2.3, it has been explained that electromagnetic waves in a range of 0 to 1000 MHz are generated during the PD occurrence. To pick up these waves, either internal or external UHF couplers are used.

During the experiments an internal UHF coupler is used, and the frequencies which have been measured are in the range of 100 - 900 MHz [16]. The experiment in the laboratory has shown that the frequencies outside this range contain more noise rather than PD.

The measurement setup is basically consists of: the sensor mounted inside the GIS compartment (internal UHF coupler), pre-amplifier, spectrum analyzer, phase synchronizer and a computer equipped

with PD software analysis. The function of the phase synchronizer is similar to the previous measurement with the acoustic method. The setup diagram is depicted in the following figure:

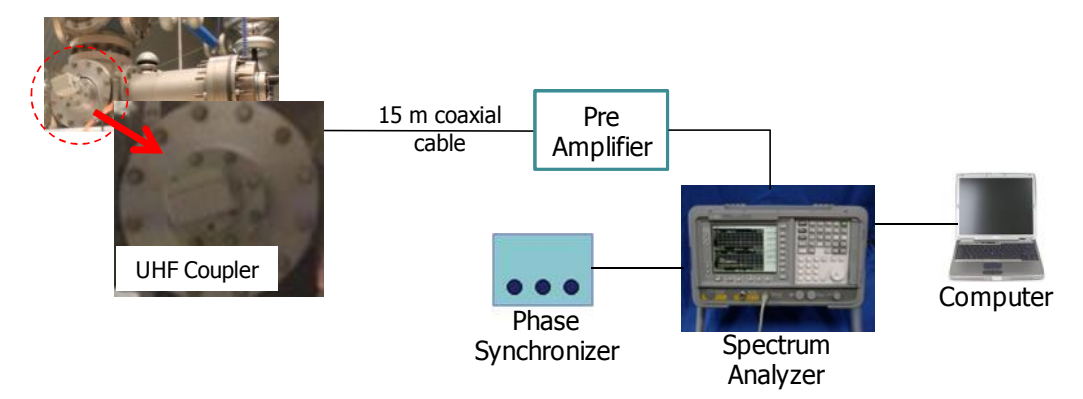


Figure 3.14 The UHF/VHF PD Detection Measuring Systems

The signals from the coupler are amplified by a 30 dB amplifier and measured using a spectrum analyzer. A computer aided with software analysis is connected to the Spectrum Analyzer (SA) to produce the Phase-Resolved PD pattern.

For a proper use of SA, the input signal has to be stable in magnitude, pulse shape, etc. However, the PD pulse is not stable, therefore the optimization of the SA setting is important. The settings include: the sweep time, total time of a measurement and acquisition mode [55]. The previous study in reference [16] concluded the minimum sweep time has to be at least 5 seconds and the measurement consisting 20 sweeps of 5s is sufficient to observe the PD.

A frequency well above the noise level in spectrum frequency can be selected for the PRPD Analysis. The SA is used to demodulate the "suspected" frequency into the range of few MHz in the following way: [16]

- 1. The center frequency, f_c , of the SA is set to the selected measuring frequency,
- 2. The measured span is set to zero,
- 3. The sweep time is set to 20 ms in order to obtain PD patterns that correlated to the 50 Hz sine wave.

The detection of the free particles by using this method is also discussed in Chapter VII.

3.10 Conclusions

- 1. The electric field distribution in the test setup in TU Delft HV Laboratory is comparable to the field distribution in the 380 kV GIS located in Meeden. To perform this 120 kV-rms has been used during the experiment under AC voltage.
- 2. In general, the field distribution in the test setup in Stuttgart University deviates from the electric field distribution in TU Delft HV Laboratory with maximum value of 28%. However, during the experiment with VFTO, the particle is placed at 80%-90% of the gap distance which implies a deviation of about 10% only, and therefore at this location it is comparable to the electric field distribution in Delft.To have this field distribution in Stuttgart, 215kV (rms) was required.

Chapter IV

The Simulation of the Particles Motion under AC Voltage

The particles motion under AC voltage has been discussed earlier in Chapter II. At a certain levels of the electric field, the particles may start jumping due to the electric forces. The height of their jumping can be calculated by solving equation 2.14, as depicted below:

$$m.\ddot{y} = \frac{n.\varepsilon_o.\ell^2.E(t_o)}{\ln\left(\frac{2\ell}{r}\right) - 1} \left(\frac{\hat{V}.\sin\omega t}{\left[r_o - z(t)\right].\ln\left(\frac{r_o}{r_i}\right)}\right) - m.g - \dot{y}(t).\pi.r.\left(6\mu k_d(\dot{z}) + 2.656\left[\mu.\rho_g.\ell\dot{z}(t)\right]^{0.5}\right)$$

...equation 2.14

By knowing the distance to the inner conductor, the possibility to have a breakdown due to the particles can be investigated.

In this chapter, the particles motions are simulated and discussed. The simulation work is based on the equation given above. Aluminum cylindrical particles are used of 0.25 mm radii and 2-30mm length, see section 3.8. It has been assumed that the particles start with a vertical position.

The simulation has to give the following results:

- 1. The pattern of the particles motions vs. time
- 2. The maximum height of the particles jump
- 3. The distribution of the time-of-flights (TOFs) by means of using the descriptive statistics parameters, e.g.: the average, the variance, the skewness and the kurtosis. The time-of-flight is the duration of the particles during their airborne with the influence of AC electric field. It is calculated by measuring the time elapsed between two successive impacts resulting from attaching the particles to the bottom electrode.

4.1 The Parameters Used in the Simulations

The parameters used in the simulation are the following:

1. GIS parameters:

- Outer radii = 150 mm - Inner radii = 35 mm

Gas pressure = 4 bar (absolute)
 The SF₆ viscosity (μ) = 15.5e⁻⁶ kg/ms

2. Particle parameters:

- length = 5 mm, 10 mm, 15 mm, 20 mm, 30 mm

- radius $= 0.25 \, \text{mm}$

- particle density = 2700 kg/m³ (Aluminum)

3. Other parameters:

Restitution factor = 0.4, 0.5 and 0.6
 Gravitation constant = 9.81 m/s²

4. Constant $k_a = 1$ (vertical position).

4.2 The Flowchart of the Simulations

The general steps for the simulation are shown in the flowchart shown in figure 4.1:

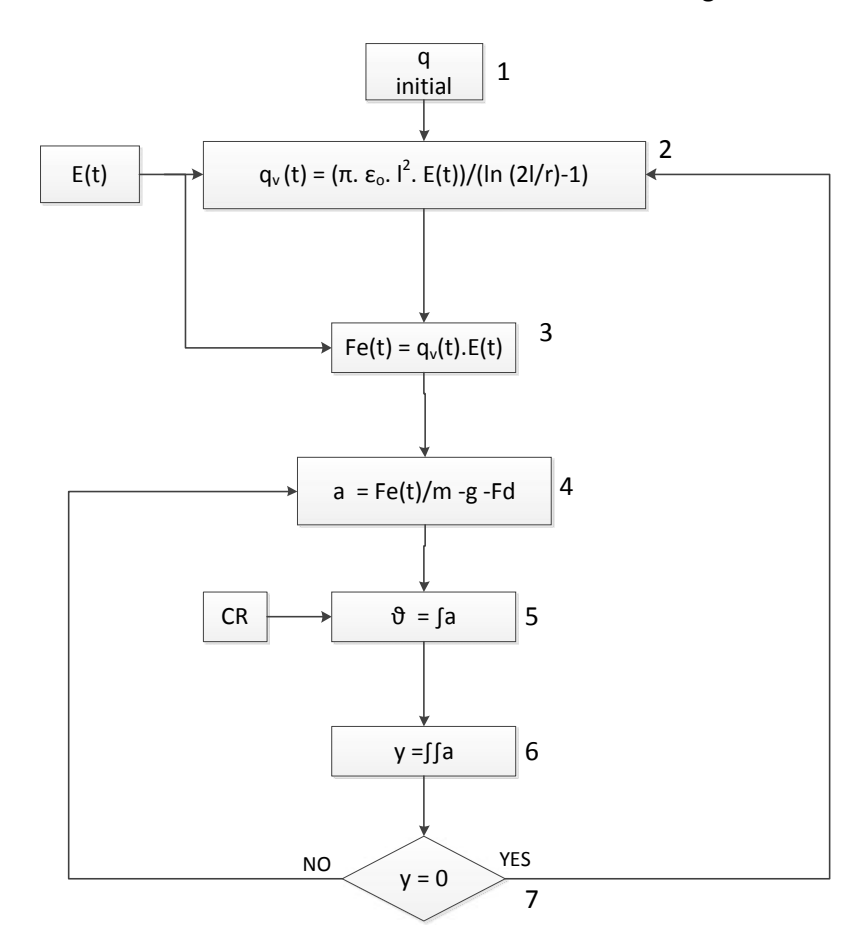


Figure 4.1The Flowchart Diagram of the Simulations

The simulation steps are:

- 1. Initial position: It has been assumed that the defects lay vertically on the GIS tank. Thus, the net charge on the particle surface is calculated by *equation 2.4*.
 - The initial charge: The initial charge is the lowest possible charge that makes the electrostatic force slightly above the gravitation force.
- 2-3. The net charge and the electrostatic force are calculated by Equations 2.4 and 2.6 respectively. It should be noted that at the starting position i.e. the vertical position, the constant k_a is equal to 1.
- 4-6. The equation of motion is solved in steps
 - a. The acceleration "a" is calculated by solving equation 2.7.
 - b. The first integration of the acceleration is the particle velocity (v). The restitution coefficient (CR) is inserted in this process to simulate the bouncing effect of the particles when they are hitting back the bottom electrode. The CR value is a coefficient which defined the ratio between the velocity of a particle before and after an impact on a large body.
 - The integration is done with the time steps of 1.e⁻⁵ seconds to give sufficient calculation accuracy. In reference [23], the restitution coefficients of a wire-shaped aluminum and copper

particles are approximately 0.5 and tend to decrease below 0.4 when the mass of the particle is less than 2 mg.

During the experiments, the lowest mass is 2.7 mg (for 5 mm particle) and the maximum mass is 15.9 mg (for 30 mm defect). Therefore, different CR values are used during the simulation works, these are 0.4, 0.5 and 0.6.

The next integration results to the height of the particle from the bottom electrode, y (t).

The equation of motion is simulated until the particle is hitting back the bottom electrode, e.g. at y(t) = 0. When the particle hits the bottom electrode, it gained a new net charge. This is shown in the flow chart by the loop line going in step 2.

To be comparable with the results from the acoustic measurements which will be discussed in Chapter V, each of the simulations is run for 30 seconds.

4.3 Descriptive Statistic Parameters

Descriptive statistic parameters have been used to determine the distribution of time of flight (TOF). As mentioned earlier, the TOF is calculated by measuring the delta time between two consecutive impacts when the particle hit back the bottom electrode. The information of the TOF is plotted in histograms and characterized by the following key figures:

1. The Average (\overline{X}) , which is defined as:

$$ar{X} = rac{\sum_{j=1}^{N} X_j}{N}$$
 ... equation 4.1

Where X_j denotes any of the N time of flight from X_1 to X_N .

2. <u>The variance</u> of a set of data is defined as the square of the standard deviation and is a measure of the *width of the data* in the distributions.

Variance =
$$\frac{\sum_{j=1}^{N} (X_j - \bar{X})^2}{N}$$
 ... equation 4.2

3. The Skewness represents the degree of asymmetry of a distribution and the value is defined as

$$Skewness = \sqrt{N} \cdot \frac{\sum_{j=1}^{N} (X_{j} - \bar{X})^{3}}{\left[\sum_{j=1}^{N} (X_{j} - \bar{X})^{2}\right]^{3/2}} \dots equation 4.3$$

The positive and the negative Skewness are illustrated in figure 4.2

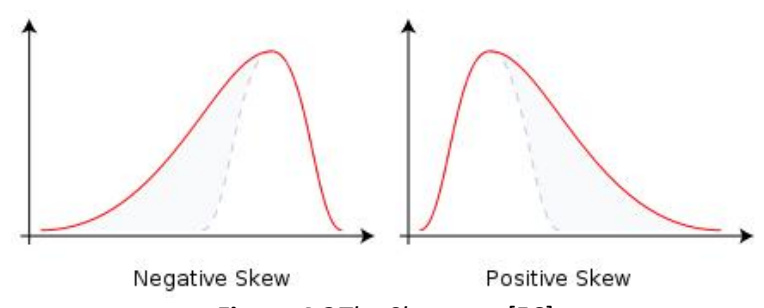


Figure 4.2The Skewness [56]

4. <u>The Kurtosis</u> represents the degree of peakedness of a distribution, usually relative to the normal distribution. It also used as a measure of the concentration of data around the mean. The Kurtosis is formulated as follow:

$$Kurtosis = N \cdot \frac{\sum_{j=1}^{N} (X_j - \bar{X})^4}{\left[\sum_{j=1}^{N} (X_j - \bar{X})^2\right]^2} \qquad \dots equation 4.4$$

These key figures are used in the following section.

4.4 The Simulation Results

The aluminum particles of 0.25mm radii and lengths of 5, 10, 15, 20, and 30 mm have been simulated. The voltage has been increased in steps of 20 kV from 80 kV up to 140 kV. The following figure shows an example of a part 15 mm particle motion at 120 kV. The abscissa represents the time and the ordinate represents the height of the particle jumping. This is a part from larger data array.

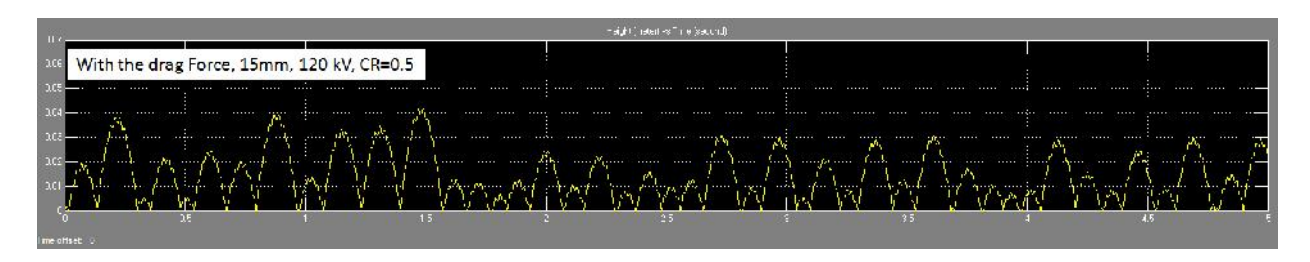


Figure 4.3An example of motion pattern from the 15 mm particle under 120 kV ac voltage

From the simulations on different particles at different voltages, some points are derived:

- 1. The ripple on the particle motion shows the influence of the 50 Hz frequency voltage.
- 2. The longer the particle is, the higher the altitude it can reach
- 3. The height of the particle jump increases as the restitution coefficient increases.
- 4. The jumping height increases with the voltage increase.

4.4.1 The Particle Maximum Heights and the Distribution of TOF

The maximum heights of different particles are given in figure 4.5:

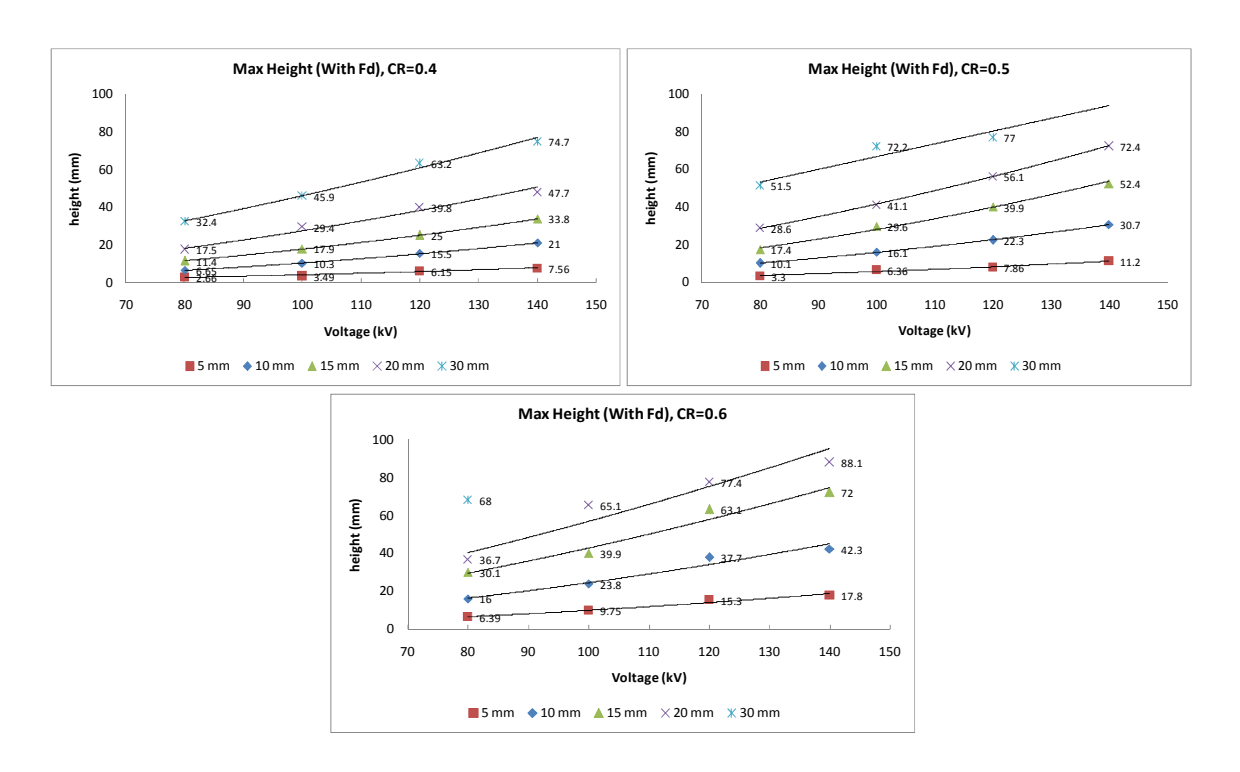


Figure 4.4The maximum heights at different voltages with various CR coefficients

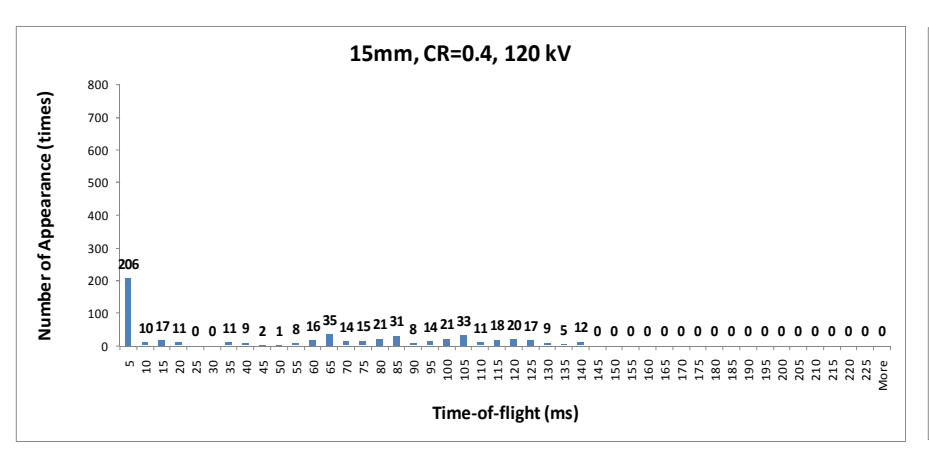
From figure 4.4 it can be observed:

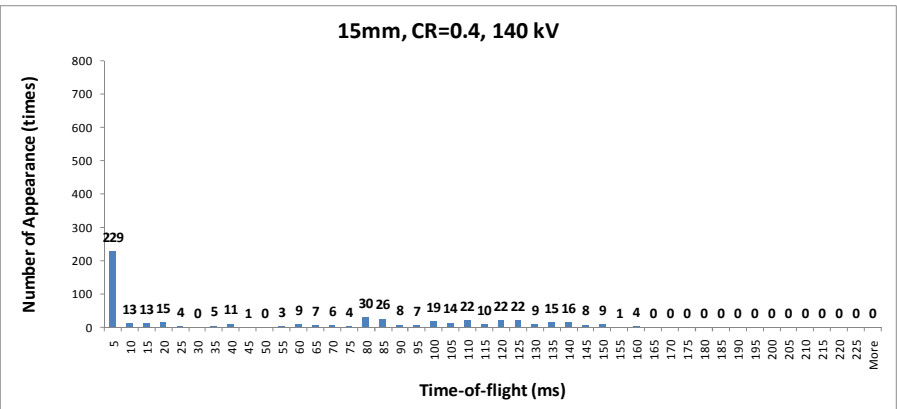
- 1. The maximum jump height increases with the voltage.
- 2. As the voltage increases, the height differences amongst different particles also increase. Not all particles were continuously jumping during the simulations, especially with the 5 mm particle at the lower voltage level with CR < 0.5.
- 3. In general, the maximum heights at 140 kV are about 2.5 3.5 times than the heights at 80 kV.
- 4. Some results with the 30 mm particle with the voltages 100 kV and above are not put into the graphs since the particle reaches the inner conductor.

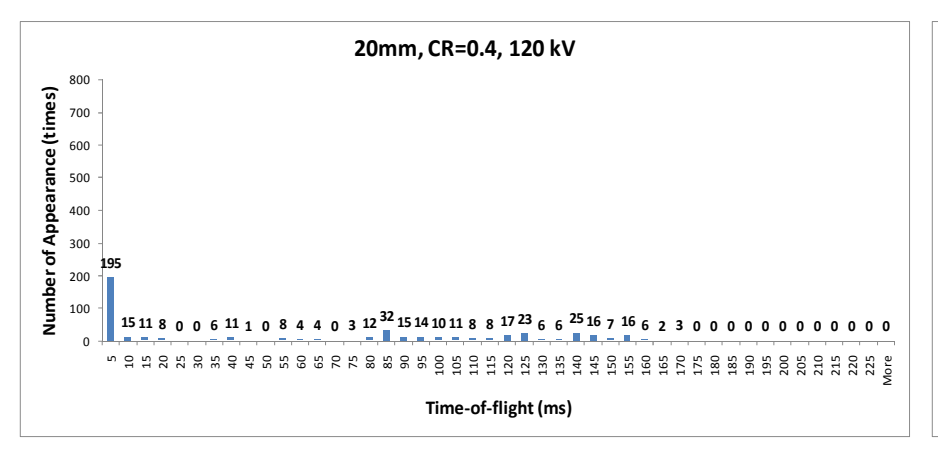
Not all particles were continuously jumping during the 30 seconds of the simulations, especially with the 5 mm particle at lower voltage level. At the beginning of the simulation, the initial charge to run the simulation is sufficient to lift-off the particle. But if the electric field at the moment the particle hits back the bottom electrode is not sufficient to lift off the particle, the integration of the distance result into zero (see steps 4-6 in figure 4.1), and also with the followed integrations also result zero since the block set is a looping process.

Later in Chapter V, it has been observed from the experiment, the 5 mm particle only jump for few seconds, before it back into the rest. This condition is similar to the simulation.

The distributions of the time-of-flights (TOF) have been derived for all of the particles. Some examples, the TOF distributions from the simulations with the 15 mm and 20 mm aluminum particles with different CR factors are given in figures 4.5-4.7:







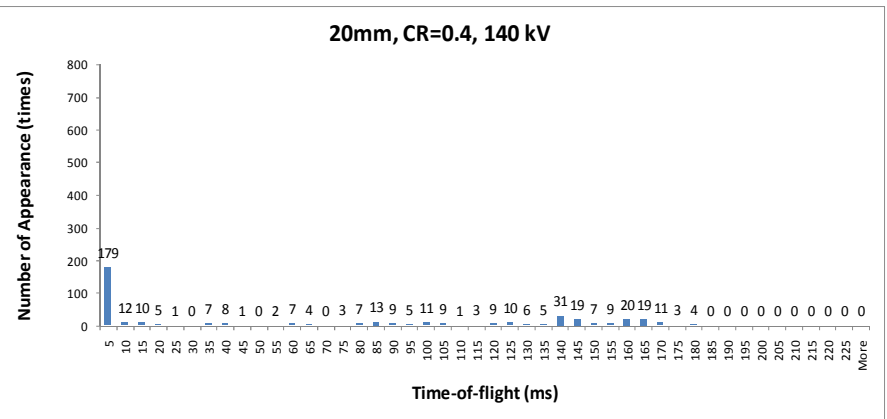
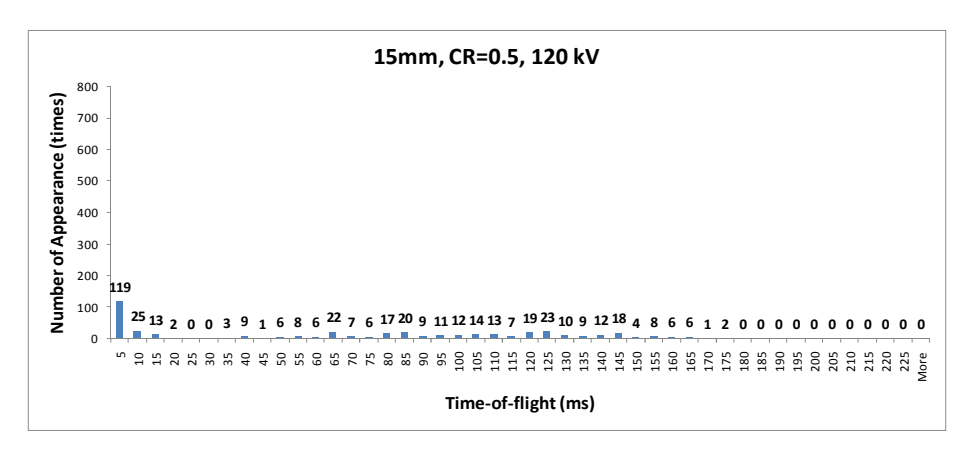
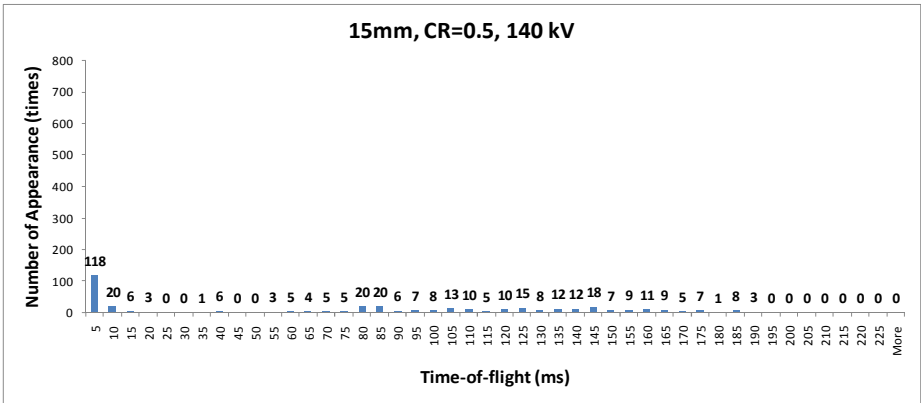
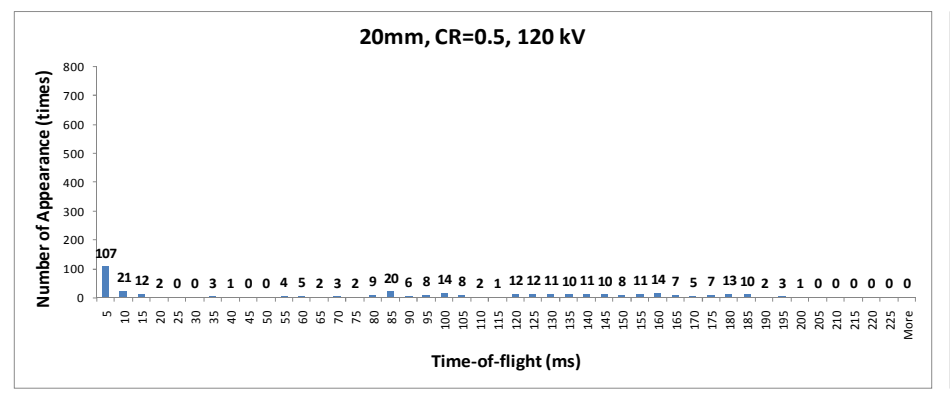


Figure 4.5The TOF Distributions for 15 mm and 20 mm Aluminum Particles with CR=0.4 at 120 kV and 140 kV







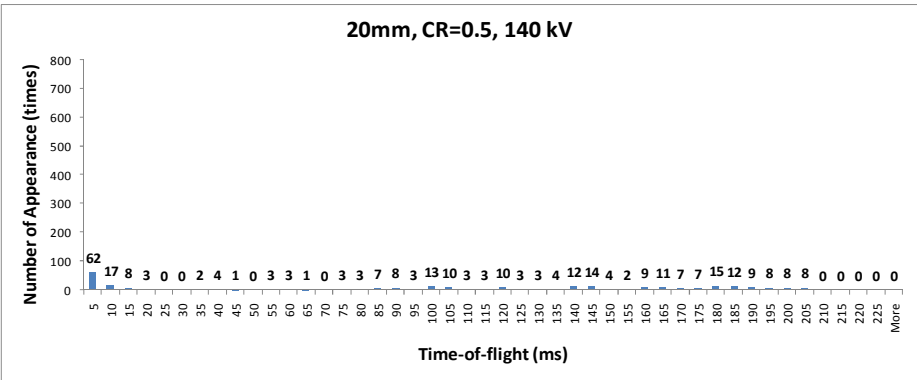
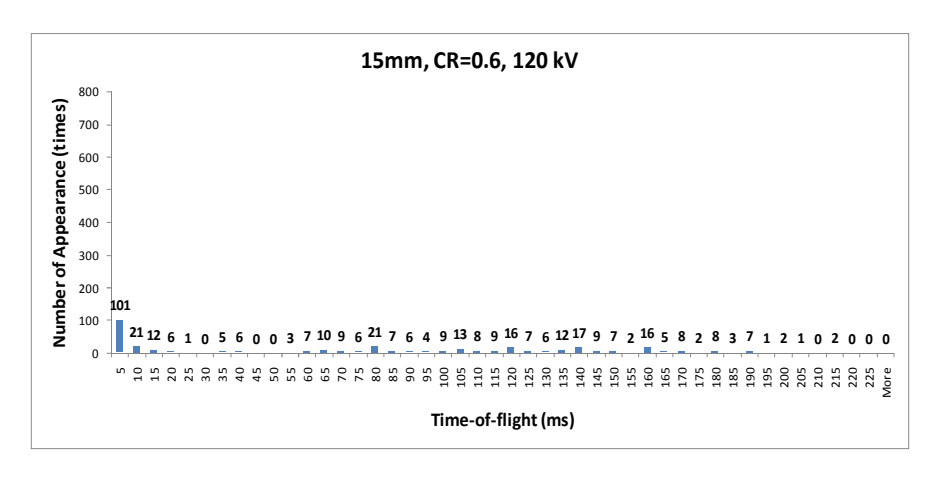
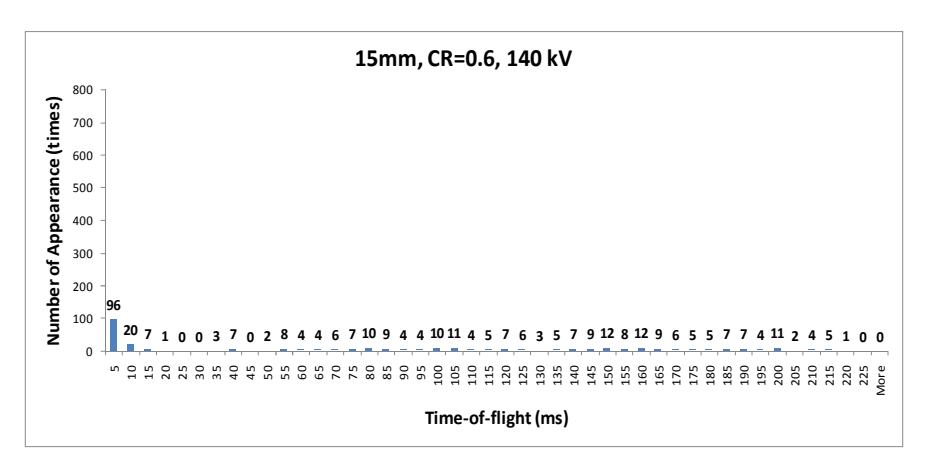
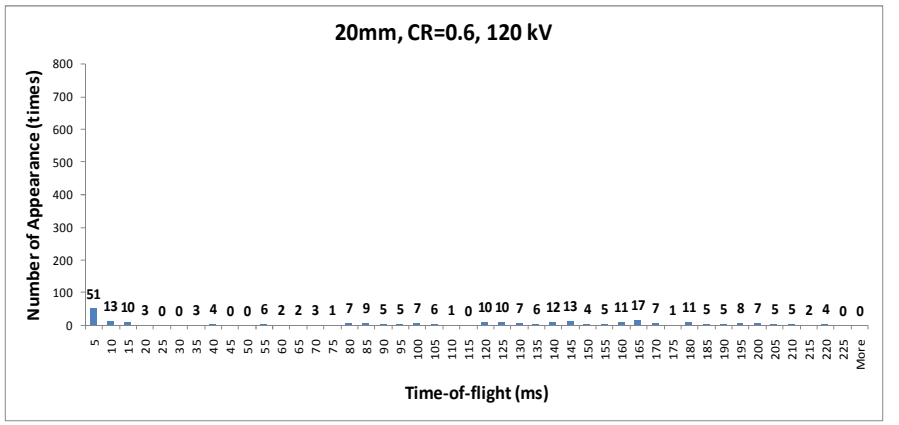


Figure 4.6The TOF Distributions for 15 mm and 20 mm Aluminum Particles with CR=0.5 at 120 kV and 140 kV







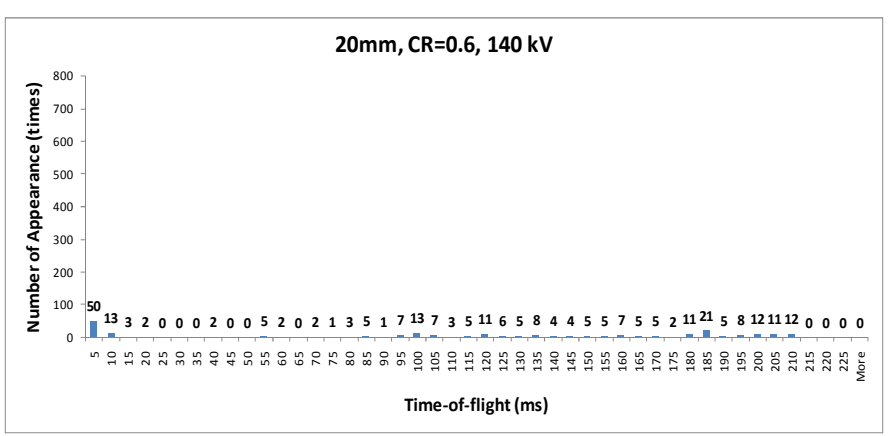


Figure 4.7The TOF Distributions for 15 mm and 20 mm Aluminum Particles with CR=0.6 at 120 kV and 140 kV

- Some points can be summarized according to these distributions from the simulations of all samples:
- 1. About 40% of the total distributions are placed in the range of 0 5 ms when CR has a value of 0.4
- 2. By increasing the CR values, the distributions are more equally distributed to the right side. And the peaks observed in the range of 0 5 ms are decreased.
- 3. Increasing the voltage shifts the distributions to the right side. The higher TOF values have also been observed at the higher voltage levels.
- 4. Shorter particles shows a higher distributions at the low range between 0 5 ms.

4.4.2 Key Figures

The key figures are summarized in figures 4.8 - 4.11:

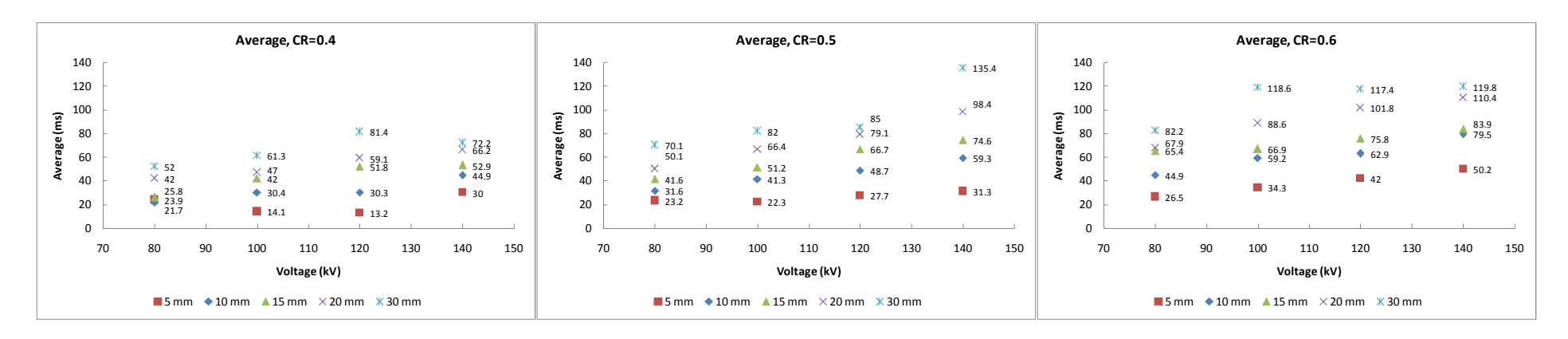


Figure 4.8 The Average of the time-of-flights distributions according to the simulations with the drag force

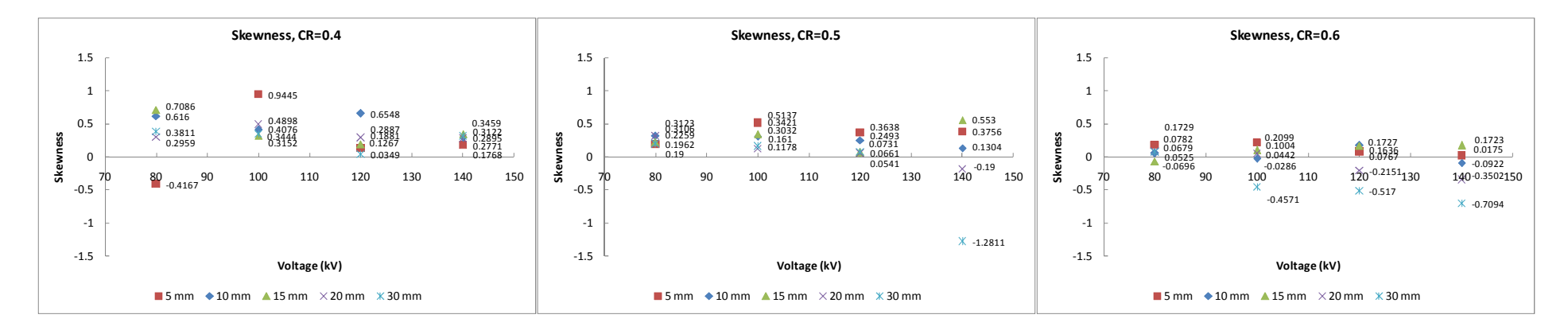


Figure 4.9 The Skewness of the time-of-flights distributions according to the simulations with the drag force

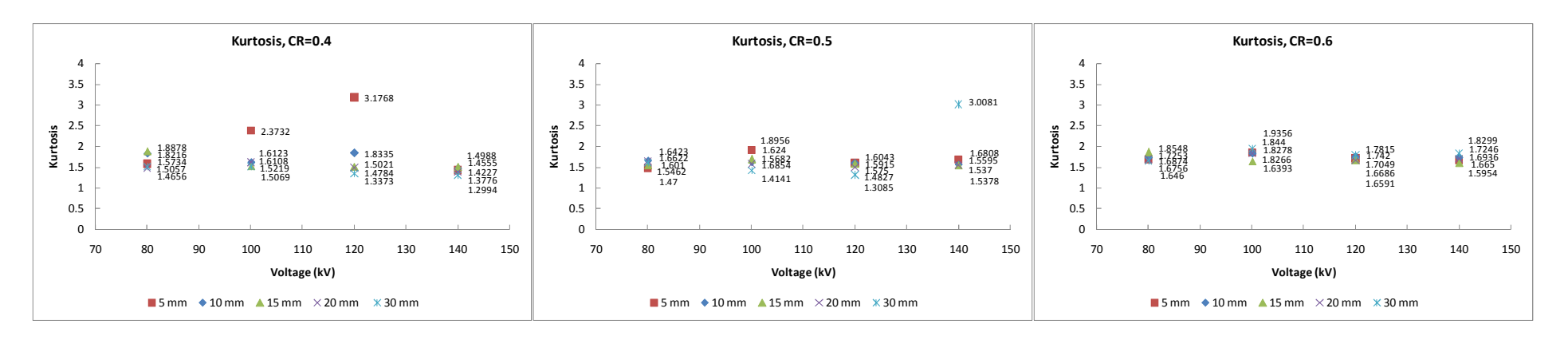


Figure 4.10 The Kurtosis of the time-of-flights distributions according to the simulations with the drag force

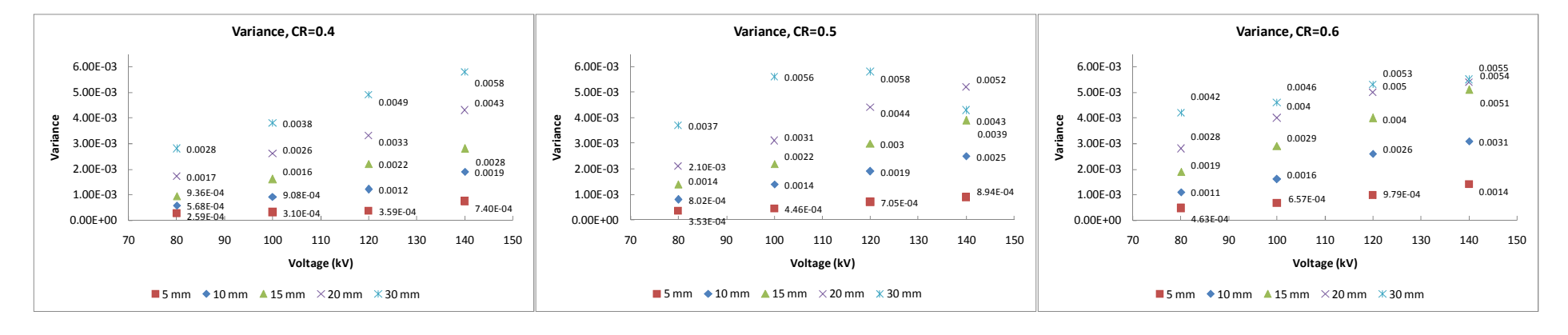


Figure 4.11The Variance of the time-of-flights distributions according to the simulations with the drag force

Based on these key figures, the following can be summarized:

- 1. The average TOF increases with the voltage and CR value.
- 2. Most of the skewness is positive, which means the concentrations of the TOF distributions are at the lower time distributions. Some negative skewness has also been observed, especially for the particles size of 20 mm and 30 mm with CR > 0.4. The skewness tends to move from the positive to the negative, as the voltage is increased. This movement is more obvious at the higher CR factor.
- 3. The kurtosis is mostly distributed below 2, with few exceptions for the 5 mm and 30 mm particles.
- 4. The variance increases as the voltage and the size of the particles increased. The values are more spread at the higher CR factor.

These key figures expressed the distribution of the TOF from the simulations. Later in Chapter V, these parameters are compared with the results from the acoustic measurements to see whether the simulation is comparable to the real situation.

4.5 Analysis

- 1. The simulation results of the Aluminum particles have been reported. In the simulations, the maximum heights as well as the average time-of-flights are found to be increased with the voltage. This can be explained by the following mathematical approach:
 - a. By neglecting the drag force in *equation 2.7*, the force can be simplified as: $m.a_{(t)} = q.E_{(t)}$ -m.g, which can be rewritten as:

$$a_{(t)} = (q.E_{(t)}/m)-g$$

since $q :: E$ and $E :: V$, then $a :: E^2$ or $a :: V^2$... equation 4.5

- b. Double integration of the acceleration results into the height of the particle jumps. since $\iint a = y$, then $y :: V^2$... equation 4.6
- c. To prove this relation, the simulation result of 15 mm Aluminum particles is given in the table 4.1as an example:

Table 4.1 The Maximum Heights Ratio as compared with the square of the Voltage Ratio

15 mm	Maximum Heights (mm)			Height Ratio		(Voltage Ratio)^2				
CR=0.5	80 kV	100 kV	120 kV	140 kV	100/80	120/80	140/80	100/80	120/80	140/80
No Fd	17.8	30.1	41.3	54.2	1.69	2.32	3.04	1.56	2.25	3.06
With Fd	17.4	29.6	39.9	52.4	1.70	2.29	3.01	1.56	2.25	3.06

According to the results in table 4.1, the relation in equation 4.6 is valid, with errors below 10%

- 2. The influence of the CR factor is summarized as the following:
 - a. The maximum heights are increasing as the CR factor is increased.
 - b. The distributions of the TOF in the lower range (0-5 ms for example) are decreasing as the CR factor is increased. The distributions are moving into the higher TOF values. This can also be observed from the Skewness key figures.
 - c. The higher the CR factor is, the higher the maximum TOFs observed.
 - d. The variance of the TOF distributions is also increasing as the CR is increased.
- 3. If the CR is increasing, the impulse (p=m.v) experienced by the particle at the moment hitting back the bottom electrode also increase. And this makes the particles tend to jump higher with a higher CR coefficient. The ratio of the maximum heights at different CR factors can be summarized as follow:

a. CR=0.6/CR=0.5 :: 1.2 - 2 b. CR=0.6/CR=0.4 :: 1.7 - 2.8 c. CR=0.5/CR=0.4 :: 1.2 - 1.9

- 4. In the simulation, the TOF distributions are moving into the right as the particle size is increased. It means the longer particle will experience the jumping longer.
- 5. As explained earlier, the longer the particle is, the more net force attached on the particle that makes the particle accelerates faster in the opposite direction of the gravitation force. This relation will continuously maintain as long as the electrostatic force is higher than the gravitation force.

4.6 Conclusions

In this chapter, the motion of Aluminum particles of 5, 10, 15, 20 and 30 mm length have been simulated. The simulation results have shown:

- 1. During its travel, the particle makes an oscillatory movement which is in-phase with the applied AC voltage.
- 2. The maximum height of the particles under AC voltage has been simulated. The results under 1 p.u. are presented in Table 4.2

Table 4.2 The Maximum Particle Jump at 1 p.u. based on the simulation work

Particle Size	Maximum Height (% of gap distance)			
2 mm	0%			
5 mm	5% - 14%			
10 mm	14% - 35%			
15 mm	22% - 57%			
20 mm	35% - 69%			
30 mm	55% - 100%			

the height a particle can jump increases with the particle length under the same electric field.

Chapter V

The Confirmation of Simulation Results by Acoustic Measurements

The motion of free moving particles in GIS is simulated, the results have shown that the height a particle can jump is linearly proportional to the following parameters:

- 1. The length of the particles.
- 2. The voltage level.
- 3. The specific CR coefficient.

A complete overview of the simulation results is:

Tab	le 5.1	The sumn	iary oj	the	Simul	ation	Results	at 1	p.u.
-----	--------	----------	---------	-----	-------	-------	---------	------	------

Particle Size	Maximum Height (% of gap distance)			
2 mm	0%			
5 mm	5% - 14%			
10 mm	14% - 35%			
15 mm	22% - 57%			
20 mm	35% - 69%			
30 mm	55% - 100%			

However, to confirm the simulation results the acoustic measurements have been carried out. The test setup of this measurement has been presented in sub section 3.9.1 (See figure 3.12). The particles of sized: 5 mm, 10 mm, 15 mm, 20 mm and 30 mm are tested, an example of these particles is given in figure 3.10.

In this chapter, the Acoustic Insulation Analyzer (AIA) has been used to measure the time-of-flight (TOF) of the free moving particles. The TOF distributions are then analyzed and the results are compared with the simulation

5.1 The Definition of Time of Flight (TOF)

Under the influence of the AC electric field, a metallic particle can get lifted and moves up towards the inner conductor. As the voltage decreases the defect de-accelerates and therefore it gets attached or bounced on the low voltage electrode, as a result sound waves are transmitted. The origin of these sound waves is, firstly the partial discharges resulting between the defect itself and the low voltage electrode, and secondly the sound results from the mechanical impact of the defect on the low voltage electrode. These sound waves are received by the acoustic sensor placed on the GIS enclosure as shown in figure 3.12.

The PAC converter transforms these sound waves into electric pulses before they processed by the AIA processor.

The time of flight is the time distance between the two consecutive sound signals as illustrated in figure 5.1:

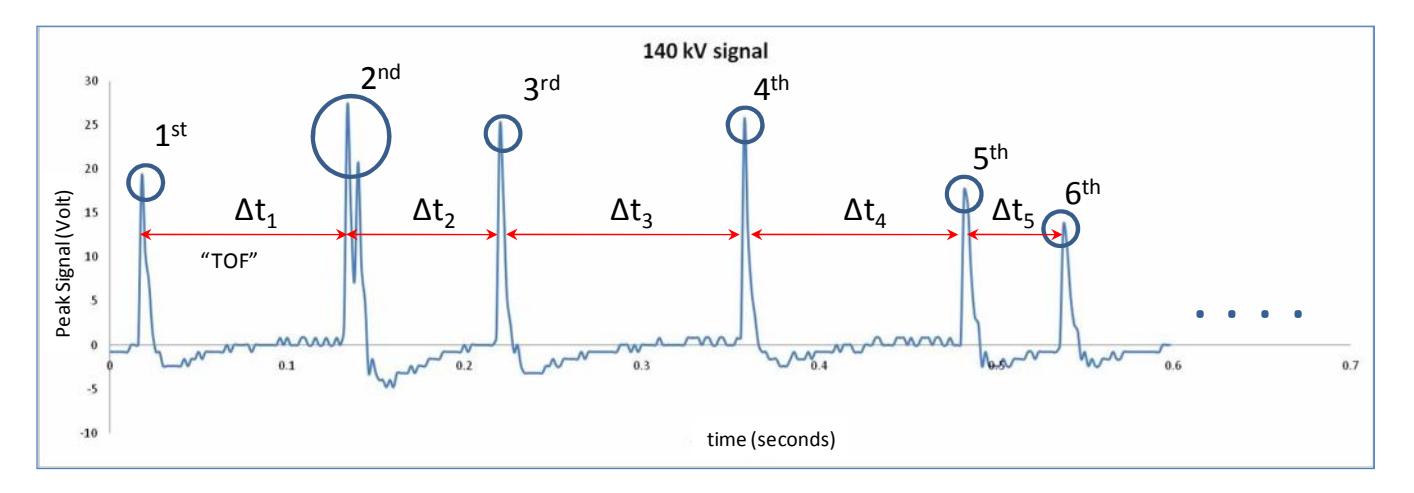


Figure 5.1 The acoustic signals from the bouncing particle

The signals in the figure are originated from the measurement of 15 mm particle at 140 kV. Each of the peaks determines the moment when the particle is hitting the bottom electrode.6 peaks can be observed. The TOF is calculated by measuring the time elapsed between these signals as shown by Δt in the figure.

Before running the experiment, the sensitivity check has been performed with this instrument by comparing the results with the reading from an accelerometer. The results are comparable with accuracy 99%. The complete report of sensitivity check is presented in *Appendix A*.

5.2 The Experiment Results

By using the AIA, two modes of measurements are possible [38]:

- 1. The phase measurement mode: In the phase measurement mode, the signals are plotted as a function of the voltage phase. Therefore, the phase synchronizer is necessary in this measurement. The information about where on the voltage cycle the discharges or particle impacts happen can be obtained. This mode is usually used during the investigation of the partial discharges and the corona, thus, it will not be discussed in this chapter.
- 2. The pulse measurement mode: In the pulse measurement mode, the signals are plotted as a function of the elevation time (TOF). An example of this plot on the free particle is shown in figure 5.2. This pattern is characteristic for different particles and it changes with the voltages.

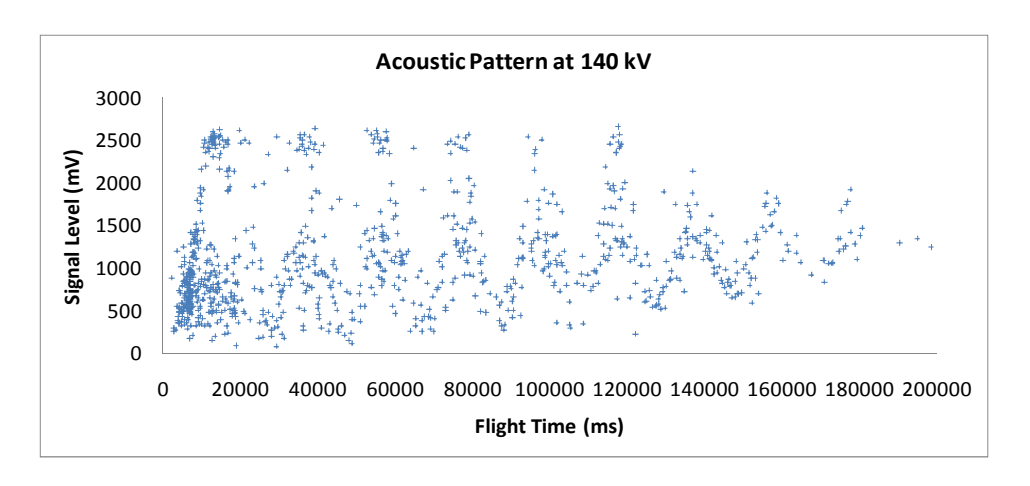


Figure 5.2 The signal levels plotted as a function of the TOF

During the measurements with the AIA, the signals are recorded in a group of 1000 points data.

5.2.1 The Maximum Time of Flights of Different Particles

The acoustic measurements have been performed with the 5, 10, 15, 20 and 30 mm particles. The results are summarized in table 5.2:

Table 5.2 - The Summary of the Experiment with the Acoustic Measurements

Particle	Voltage when the p	particle start jumping	Recorded	Remarks	
Size	Without	With	TOF		
	Mechanical Hit	Mechanical Hit			
2 mm	Not Jump	Not Jump	-		
5 mm	Not Jump	120 kV	the particle only jumping for 15 seconds	The particle is jumping for a few seconds and then welded vertically at 120 kV	
10 mm	Not Jump	80 kV 130 kV	TOF at 130 kV	After jumping for minutes, the particle is welded at 80 kV	
15 mm	Not Jump	130 kV	TOF at 70 kV, 80 kV, 100 kV, 130 kV	After jumping for minutes, the particle is welded at 60 kV	
20 mm	Not lump	80 kV	TOF at 80 kV, 100 kV,		
20 mm	Not Jump	100 kV	120 kV		
30 mm	Not Jump	120 kV	TOF at 120 kV		

The summary of the maximum TOF of different particles are shown in figure 5.3:

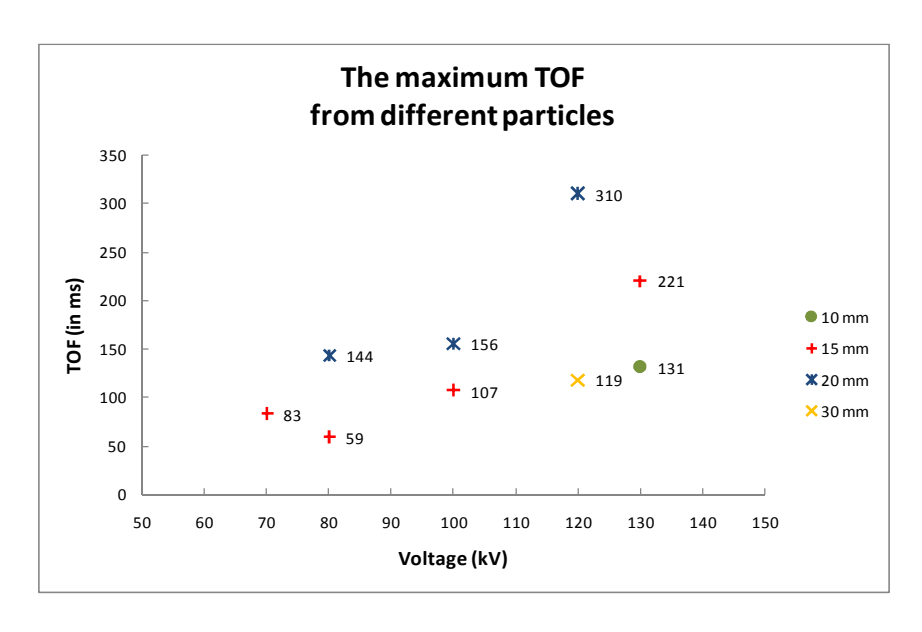


Figure 5.3 The maximum TOF of Different Particles at Different Voltages

The longer particles in general jump higher than the shorter particle, except for the 30 mm. A steep increase has been observed from the experiments with the 15 mm and 20 mm particles when the voltage is raised above 110 kV.

5.2.2 Key Figures

The key figures are summarized figure 5.4 - 5.7:

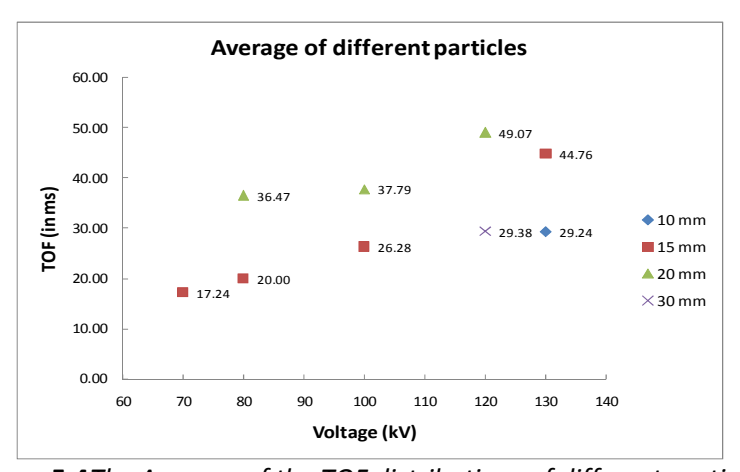


Figure 5.4The Average of the TOF distributions of different particles

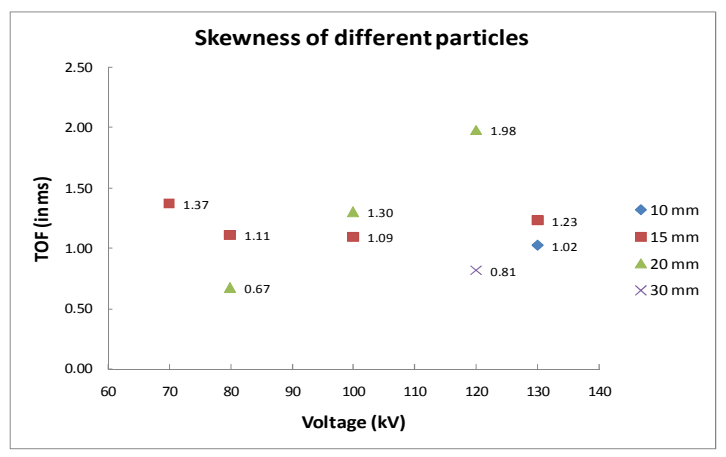


Figure 5.5 The Skewness of the TOF distributions of different particles

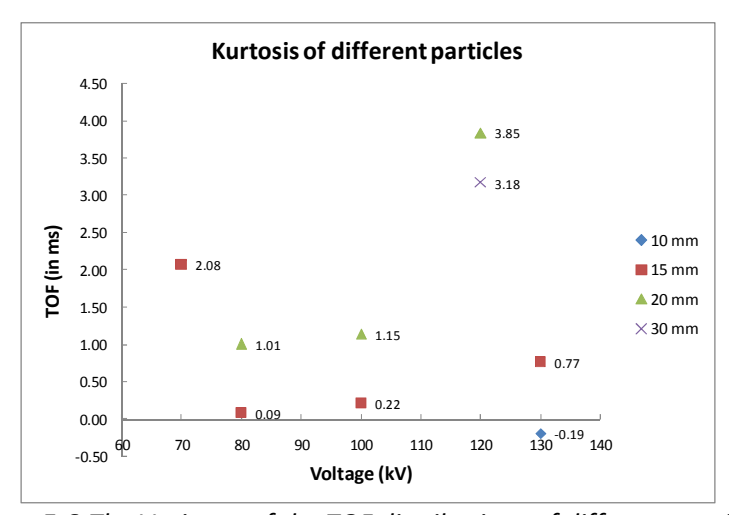


Figure 5.6 The Variance of the TOF distributions of different particles

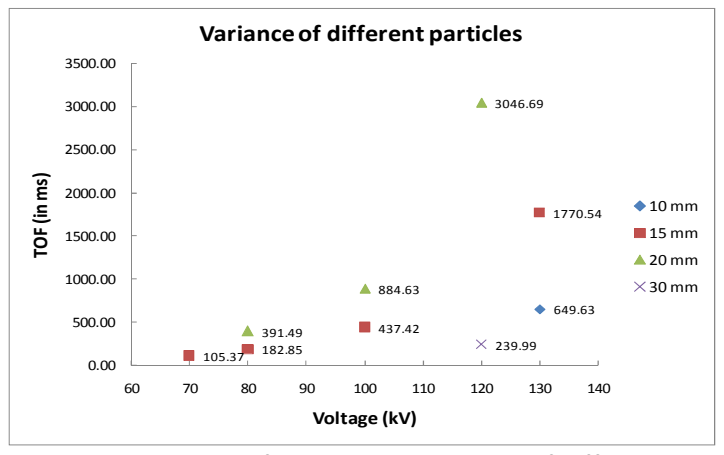


Figure 5.7 The Variance of the TOF distributions of different particles

From figure 5.4 - 5.7, the following can be summarized:

- 1. The average of the distributions, in general, increases as the particle size increases. An exception is observed with the 30 mm particle. Its distribution is lower than the 20 mm particle length at a similar voltage level.
 - It is expected that the longer particle will gain more charges rather than the shorter particles. According to the formula given in the equation 4.1, the net force on the 30 mm particle should be the highest compared to the other particles which lead into the highest jumping.
 - The decrease in the particles jump can be due to the discharges that occur during the travel of the particle, which is also known as the micro discharges [8, 11]. Lundgaard [23] explained that the longer particle has the higher probability to experience the micro discharges. The discharges reduce the net charge on the particle and consequently reduce the acceleration of the particle during its excursion. This have been discussed in details in the analysis part.
- 2. The skewness and the kurtosis of the 20 mm particle distributions increase as the voltage increases. All the skewness are positive, which implies that most of the distributions occur at the lower time range.
- 3. In general, the variance increases as the voltage increases. The highest variance is observed at the 20 mm particle length at 120 kV. An increased variance with the voltage indicates that the particle jumps higher at higher voltage level, however small jumps at lower TOFs are also occurred.

5.3 Comparison with the Simulation Results

In this section, the experiments and the simulations results are compared In the term of the maximum TOF and the key figures.

5.3.1 The Maximum Jumping Height

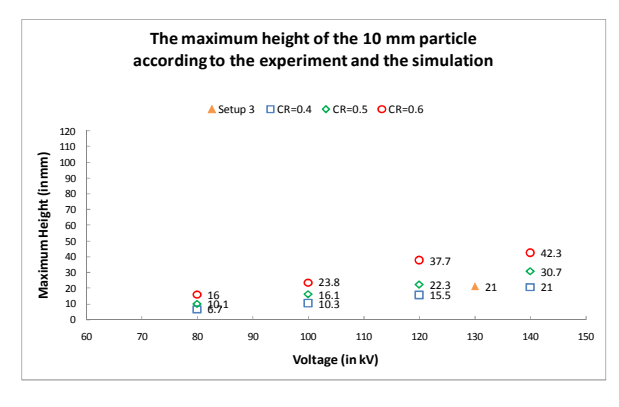
The maximum TOF from the experiments are translated into the distance (in mm) by assuming that the particle moves in a parabolic trajectory and by disregarding the oscillations during its travel, the highest point in the trajectory, h_{max}, has been calculated by:

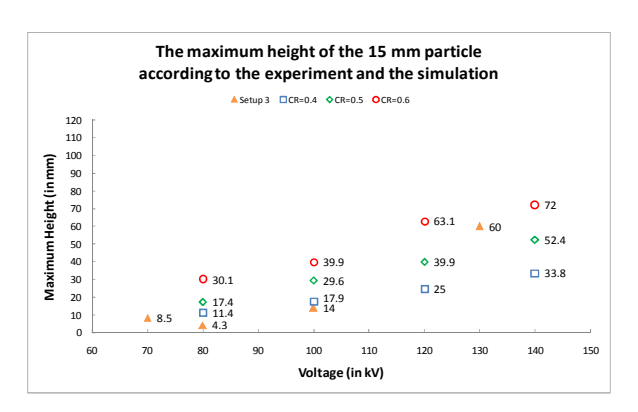
$$h_{max} = \frac{1}{2}.g.\left(\frac{t_{max}}{2}\right)^2$$
,... equation 5.1,[23]

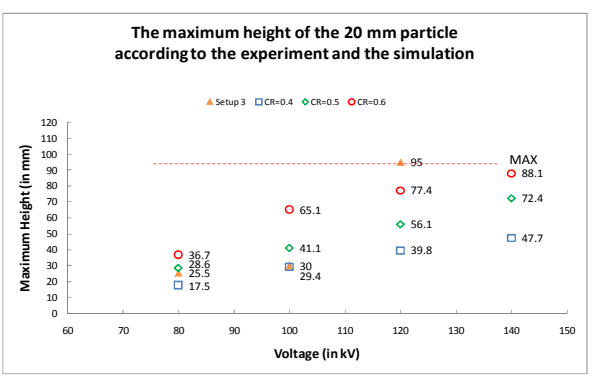
where:

 $g = 9.81 \text{ m/s}^2$, the gravitation constant $t_{max} = \text{the maximum time of flight in seconds}$

The results are presented in the following figures:







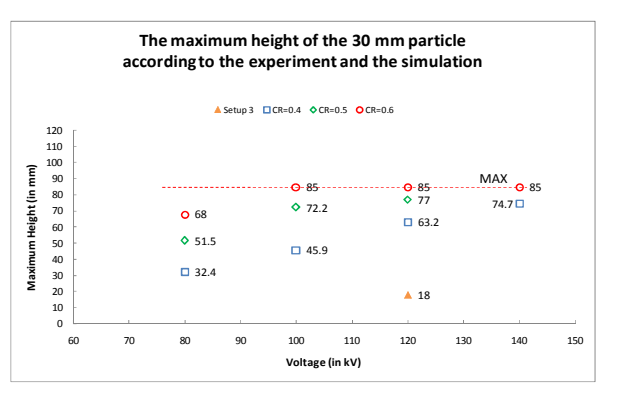


Figure 5.8 The maximum height of different particles according to the simulations and the experiment results.

The difference between the simulations and the measurements have been analyzed by the calculation of the distance between the points measured from the acoustic and the simulations trending lines. The trending lines are using the power relation, since the jumping height, y, is proportional to V^2 as shown by the *equation 4.3*. The results are shown in figure 5.9 - 5.12:

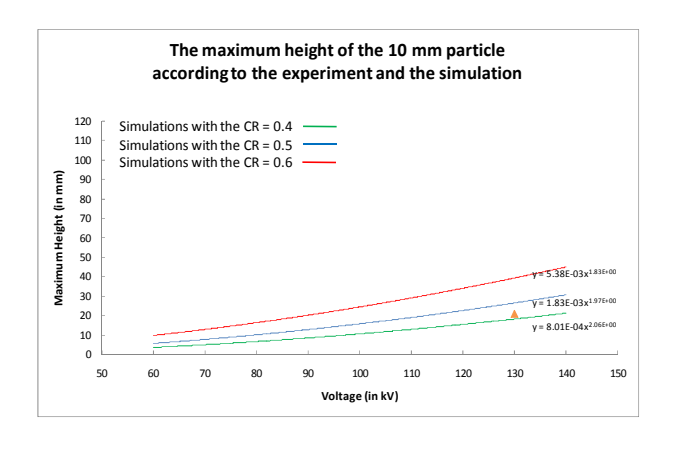


Figure 5.9.The simulations trending lines vs. the points from the acoustic measurement. Particle size = 10 mm.

The errors of the simulations as compared to the measurement at 130 kV: (in % of distance gap)

- vs. Simulation with CR=0.4: 2%
- vs. Simulation with CR=0.5: 5%
- vs. Simulation with CR=0.6: 16%

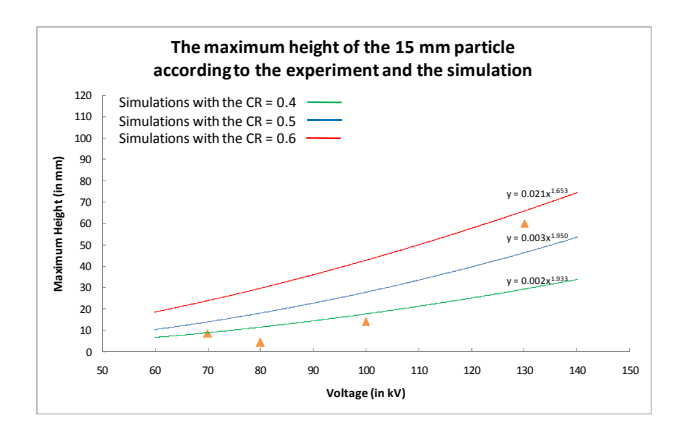


Figure 5.10. The simulations trending lines vs. the points from the acoustic measurement. Particle size = 15 mm.

The errors are the following: (in % of distance gap)

	Voltages (kV)					
	70	80	100	130		
vs. CR=0.4	1%	5%	1%	31%		
vs. CR=0.5	3%	10%	9%	18%		
vs. CR=0.6	13%	22%	25%	5%		

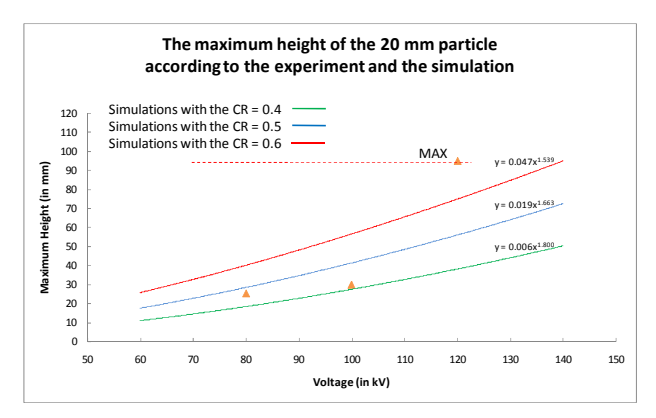


Figure 5.11.The simulations trending lines vs. the points from the acoustic measurement. Particle size = 20 mm.

The errors to the distance gap are the following: (in % of distance gap)

	Voltages (kV)				
	80	100	120		
vs. CR=0.4	8%	5%	54%		
vs. CR=0.5	2%	9%	35%		
vs. CR=0.6	13%	23%	18%		

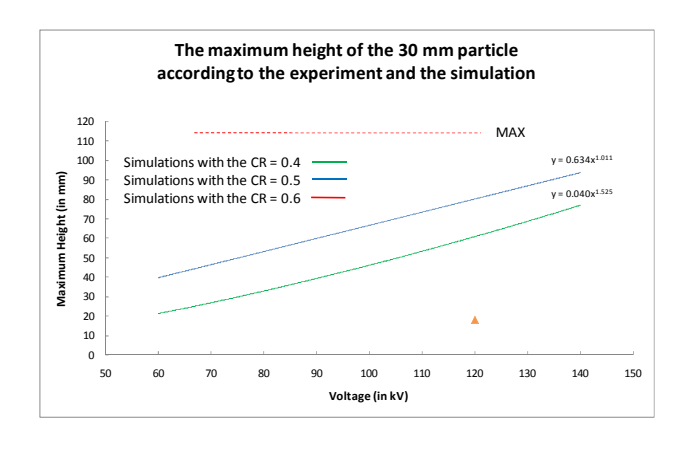


Figure 5.12.The simulations trending lines vs. the points from the acoustic measurement. Particle size = 30 mm..

The errors of the simulations as compared to the measurement at 120 kV: (in % of distance gap):

- vs. Simulation with CR=0.4: 36%
- vs. Simulation with CR=0.5: 54%
- vs. Simulation with CR=0.6: >54%

Based on these results, some points can be drawn:

- 1. With the voltages below 120 kV, the maximum height is best estimated with the simulation using CR = 0.4. At the 10 mm particle, even the simulation is still valid with the voltage = 130 kV. They are both coming with the maximum error of 5% distance gap. The errors with the 30 mm particle is unknown.
- 2. When the voltage increases from 120 kV and above, the maximum height is best estimated by the simulation using higher CR values, except for the 30 mm particles as shown in the figure 5.12.

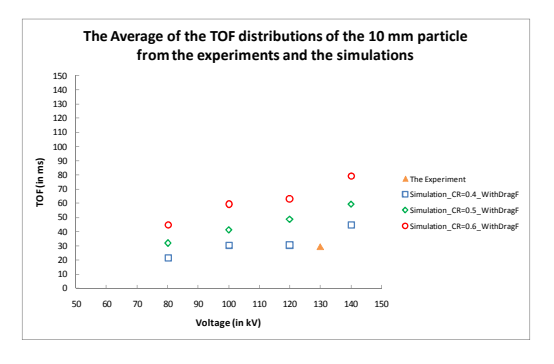
The best general estimation for this simulation is by using CR = 0.4 for the simulation with the voltages up to 120 kV, and CR = 0.5 for the voltages beyond 120 kV. With this approach, the maximum

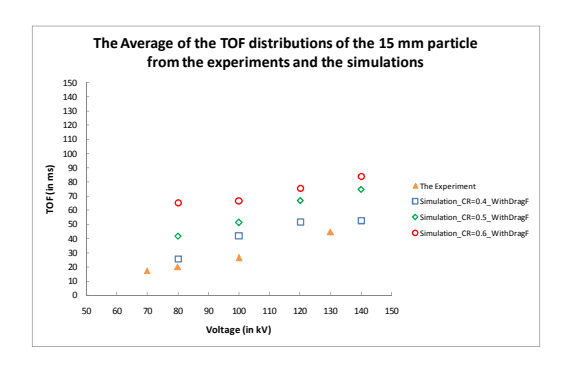
error of 5% distance gap can be achieved for the voltage below 120 kV, and the maximum error increases up to 54% for the voltage higher than 120 kV.

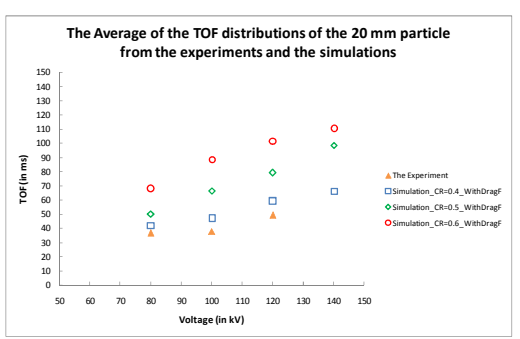
The experiments shows a good agreement with the study in [11], where the simulation based on the equation 2.14 is onlyvalid for the particles with low electric field. At the higher electric field, the micro discharges occur and disturb the particle movement.

5.3.2 Key Figures

The key figures of the TOF distributions have been compared as shown in figures 5.13 - 5.16:







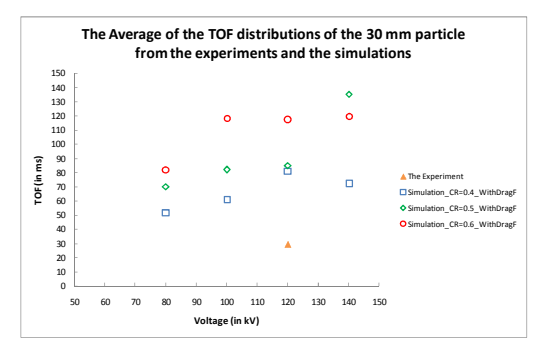
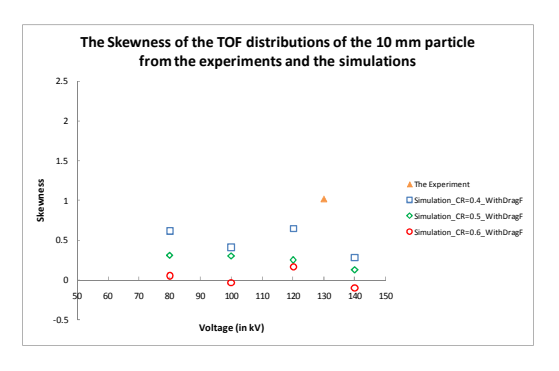
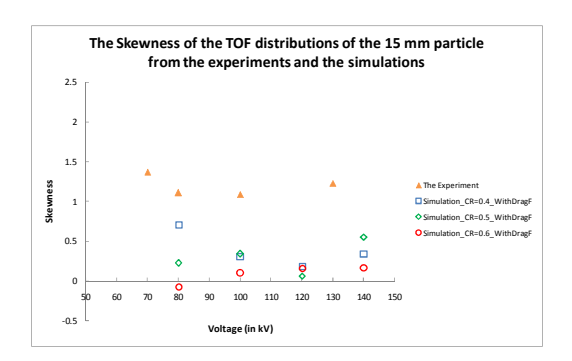
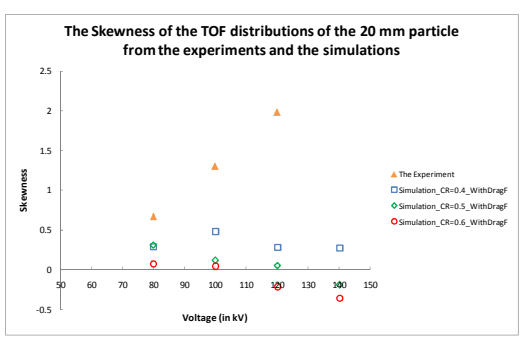


Figure 5.13 The Average of the TOF distributions of the different particles from the experiments and the simulations







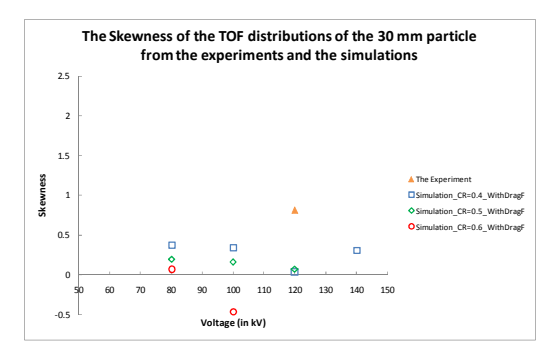
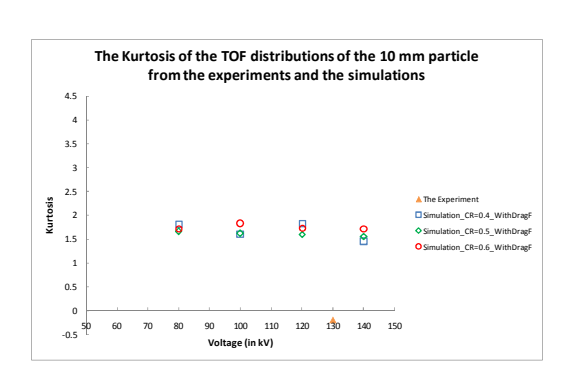
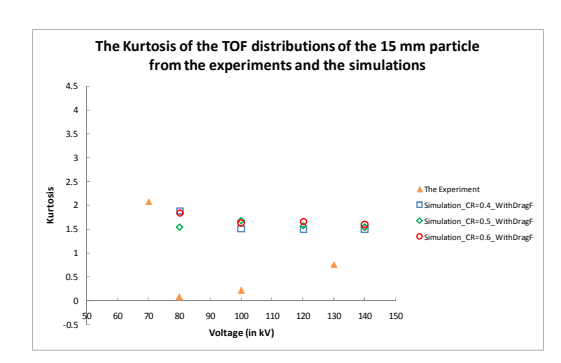
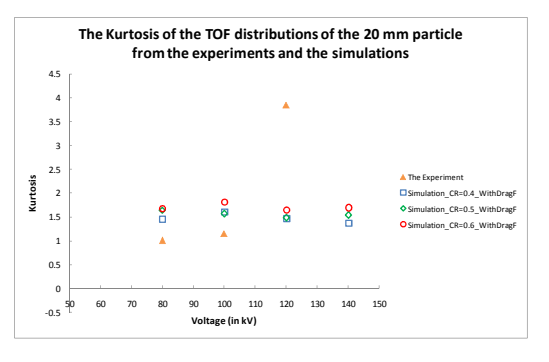


Figure 5.14 The Skewness of the TOF distributions of the different particles from the experiments and the simulations







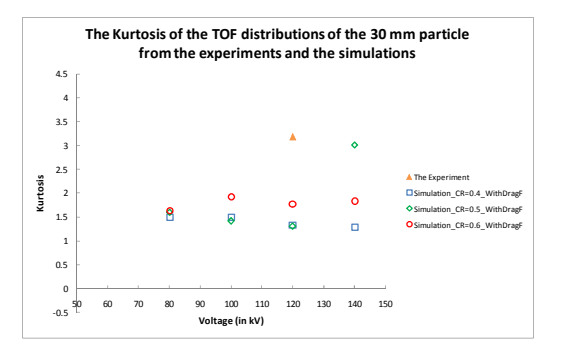
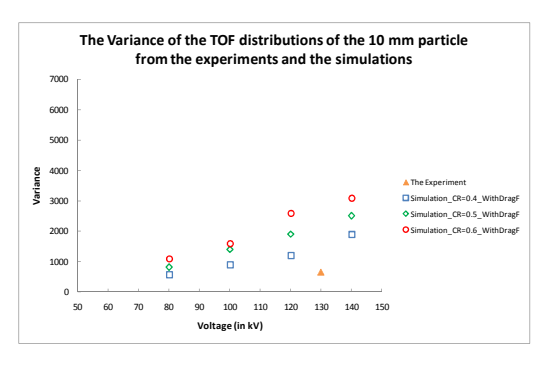
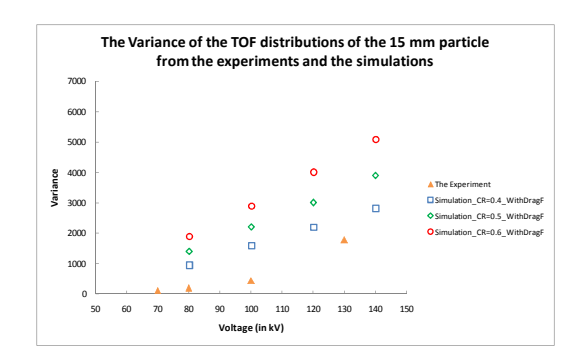
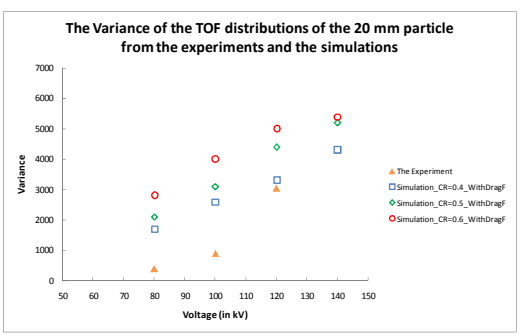


Figure 5.15 The Kurtosis of the TOF distributions of the different particles from the experiments and the simulations







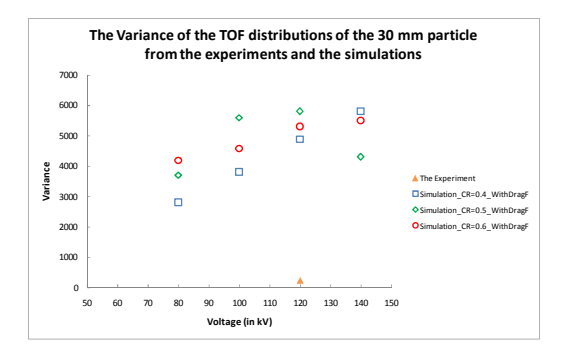


Figure 5.16 The Variance of the TOF distributions of the different particles from the experiments and the simulations

The observations on the results are the following:

- a. Except for the 30 mm particle, the TOF averages from the measurement is best fitted with the simulation with CR = 0.4
- b. The other key figures from the simulations deviate from the experiment results. This indicates the randomness of the jumping cannot be well represented by the simulation. As an example, the histogram of the 15 mm particle at 100 kV from the measurement and simulation are compared in figure 5.17:

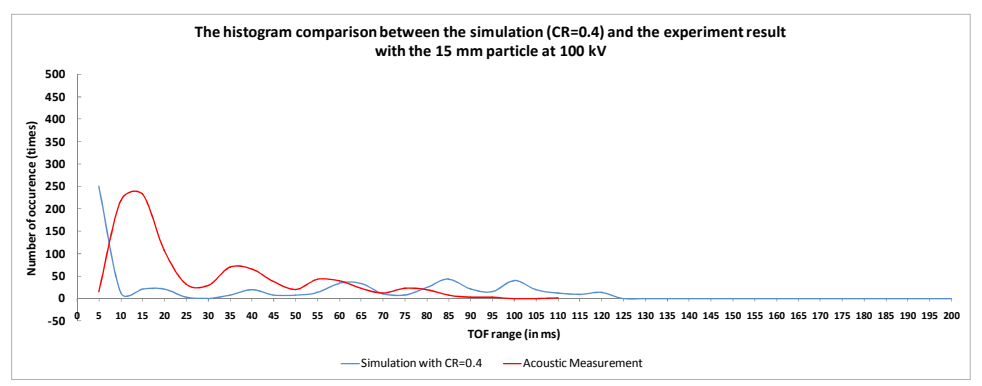


Figure 5.17The comparison of TOF histogram between the simulation and acoustic measurement for the 15 mm particle at 100 kV

In the example, the randomness difference is obvious.

5.4 Analysis

The experiment results have been reported in the previous paragraphs. The results have been compared with the parameters obtained from the simulations. Some important observations are drawn below:

1. In table 5.2, some welded particles are observed during the experiments. For the 5 mm particle, it was start jumping only for few seconds, and then it welded or if not, it fallen. A similar behavior i.e. the defect getting welded to the inner surface of the LV electrode has also been observed with the 10 mm and the 15 mm particles when the voltage was decreased below 100 kV.

The particles stopped jumping when the electrostatic force is not sufficient to overcome the adhesion between the particle and the electrode and the particle stay on vertical position as depicted in figure 5.17:



Figure 5.17 The standing particle. At 60 kV, the 15 mm particle was stop jumping and welded to the enclosure

- 2. The maximum heights can be summarized as the following:
 - a. The results with the 15 mm and the 20 mm particles give a good view of the relation between the maximum height and the applied voltage. The height increases as the voltage increases. A steep increase has been found when the applied voltage is higher than 110 kV. However, the average of the TOF distribution is showing a good correlation between the simulations and the experiments.
 - b. The result with the 30 mm particle shows a much lower height in the particle jump compared to the 15 mm and the 20 mm particles. In Chapter 2, the microdischarge is the reason for this decrease as has been explained in section 2.2.1., the charges accumulated on the particle can leave the particle through a 'leakage path' at the tips of the particle due to the field enhancement at these tips through a local discharges or partial discharge in the gas [23]

To investigate this field enhancement, the simulations with COMSOL 3.4 have been performed with the 10 mm, 15 mm, 20 mm, and 30 mm particles. Based on the previous experiment, the 30 mm particle can jump 20 mm high, which means the upper tip of this particle is at 50 mm from

the bottom enclosure. All of the particles are then simulated at this position, with previously calculated their surface charges according to the *equation 2.4*. The results are the following:

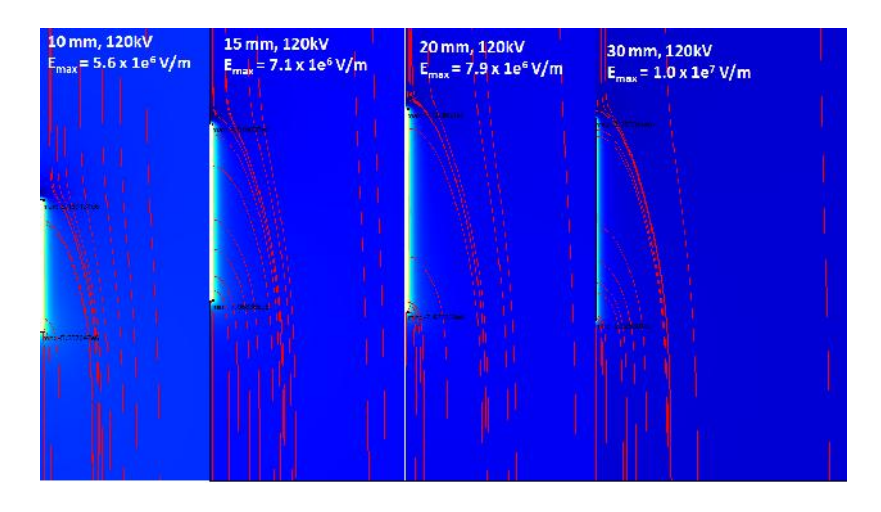


Figure 5.18The simulations of the field enhancement of different particles at distance of 50 mm from the bottom enclosure with the voltage 120 kV (the picture is presented without scaling)

In this picture, at 120 kV, the field enhancement at the 30 mm particle is 1.3 higher than the field enhancement with the 20 mm particle. The complete results are the following:

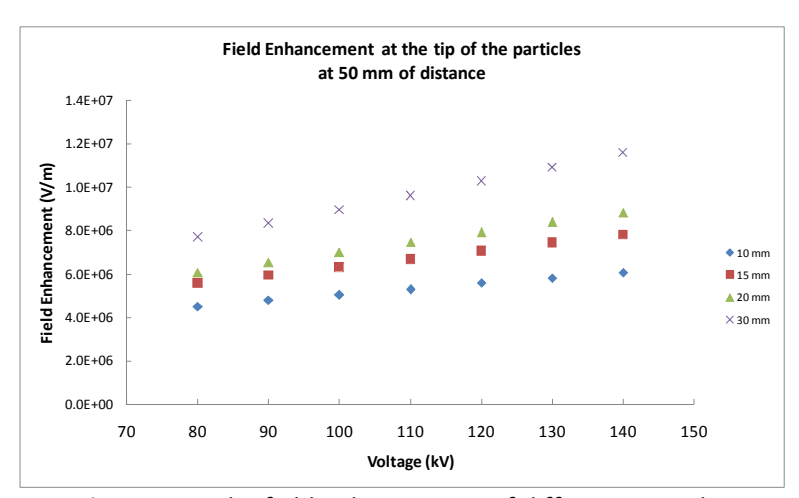


Figure 5.19The field enhancement of different particles at a distance of 50 mm from the bottom enclosure at different voltage levels

But however, the microdischarge might also occur with the shorter particles, but their net charge to the mass ratio probably still higher than the 30 mm particle. This can also be used to explain why the field enhancement can accelerate the particles according to Equation 2.6.

5.5 Conclusions

In this chapter, the results of the acoustic experiments with 10, 15, 20, and 30 mm particle lengths have been reported. The results have been analyzed and compared with the previous simulation results. Based on the results, the conclusions below are drawn:

- 1. The maximum height obtained from the measurement at avoltage below 120 kV confirms with the simulation work performed in the previous chapter. The errors obtained is about 5%.
- 2. The "Average key figure" estimated by the simulation work and the experiment results is comparable. it indicates the average altitude a defect can get during its entire movement. However, the other key figures have shown deviations due to the randomness in the particles jump.

Chapter VI

The Vibration Effects on the Metallic Particles Motion in GIS

During the laboratory experiments, it has been observed that the metallic particles were not showing any movements under AC voltage unless the external mechanical hit is given into the test object. In GIS, during a switching devices operation, such vibrations can initiate a free moving metallic particle to start moving. To simulate such situation in the laboratory, the test setup has been hit with a hammer.

In the experiment, the particles are start jumping below their lift off electric field. The calculation in *Appendix B* had shown that the voltage should at least 158.5 kV, to start the jumping, but with the mechanical hit, the particles start jumping below this voltage.

In this chapter the effect of the vibrations to start the particles jumping is discussed. In the beginning of discussions, different vibrations during the GIS operation are presented. Following, the investigation of the vibration impact by observing the relation between the vibration level (presented in G-force unit) to the partial discharges (in pC) originated from the particles motions after the hit, are performed.

Some net charges calculations with the finite element method (FEM) are presented in order to see how the net charges are changing with their position after the hits. At the end of this chapter, some conclusions are drawn including the situations that explained the particles behavior before their jump.

6.1 Vibrations in GIS

Different vibrations can be observed during the GIS operation. Most of the vibrations are too small that even cannot be recognized by the human touch. But some of them are very strong and followed with a loud noise, for example, the vibration during the circuit breaker operation.

These vibrations are summarized in table 6.1 with the frequency ranges and the G-force levels presented in figure 6.1.

Table 6.1Different Vibrations during the GIS Operation [6]

No	Source of Vibrations	Frequency range	G-force Range	Remark
1	Internal partial discharge	5 kHz - 20 kHz	10 μG - 1 mG	PD level range: 10 pC to 1000 pC
2	Electrostatic forced particles	1 kHz - 10 kHz	1 mG - 10 mG	for example: due to the bouncing particles
3	Electromagnetic oscillation parts	100 Hz - 4 kHz	1 mG - 10 mG	The presented value is according to measurement on the 77 kV potential transformer
4	Electrostatic forced part/ component	100 Hz - 200 Hz	~ 0.1 G	Originated from the vibrating conductors, shielding and metal enclosures when the resonance occurs.
5	Circuit breakers or disconnecting switches	100 Hz - 1 kHz	few G - 20 G in the neighbouring compartment is about ¼ of the opperating apparatus	
6	Short circuit or Ground fault	100 Hz - 300 Hz	10 G - 100 G	

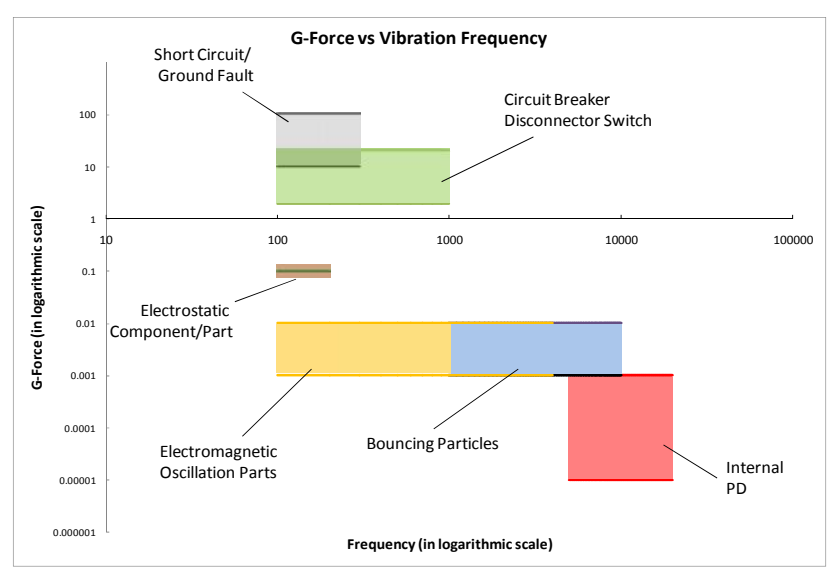


Figure 6.1Frequency and G-force Ranges of different Vibrations in GIS [6]

According to this figure, the vibration due to a short circuit has the highest G-force level among the others sources. However, fault and short circuit current are beyond the scope of this thesis. Vibrations caused by CB/ DS occur more frequent in GIS and is the subject of this chapter.

During the investigation in the laboratory, to simulate the actual situation, the vibration caused by the hammer are quantified and compare to the actual vibrations occur in the field.

6.2 Validation of the Mechanical Hit used in the Laboratory

A commercial accelerometer of Monitran 1010 with the maximum vibration range of 80 G is used to measure the frequency and the G-force of the mechanical force originated from the hammer. The signals received from the vibrations are converted into electric signals by the sensor and filtered by using a high pass filter before they viewed by the oscilloscope. Figure 6.2 shows the test setup.

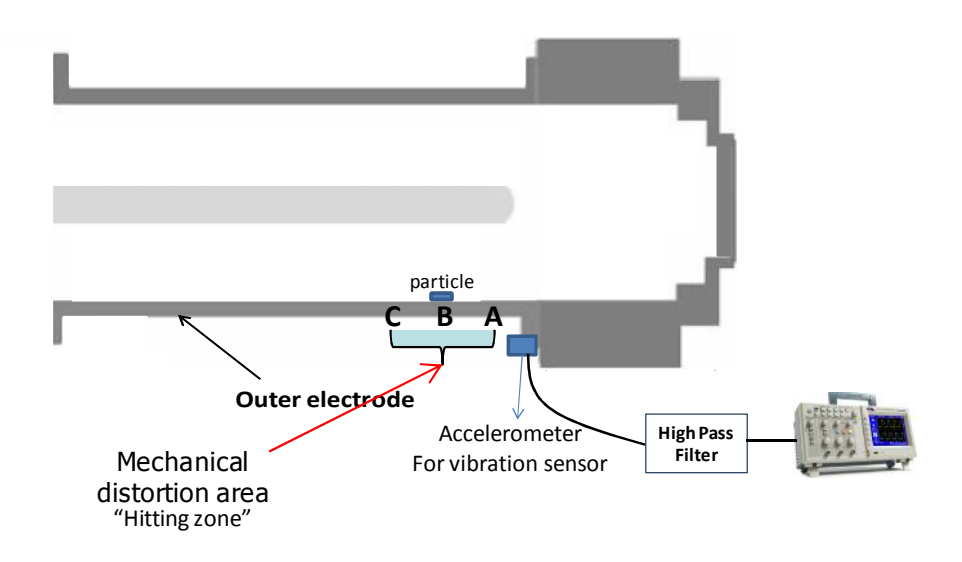


Figure 6.2Setup for measuring the vibrations

To check the repeatability of the measurements, several controlled hits were introduced into the enclosure at different points of A, B and C. These points are the area that may be hit by the hammer during the experiments. point A is positioned 5 cm to the sensor, point B and point C are positioned at 9 cm and 15 cm respectively far from the sensor. An example of the vibration signal generated by the hammer is shown in figure 6.3:

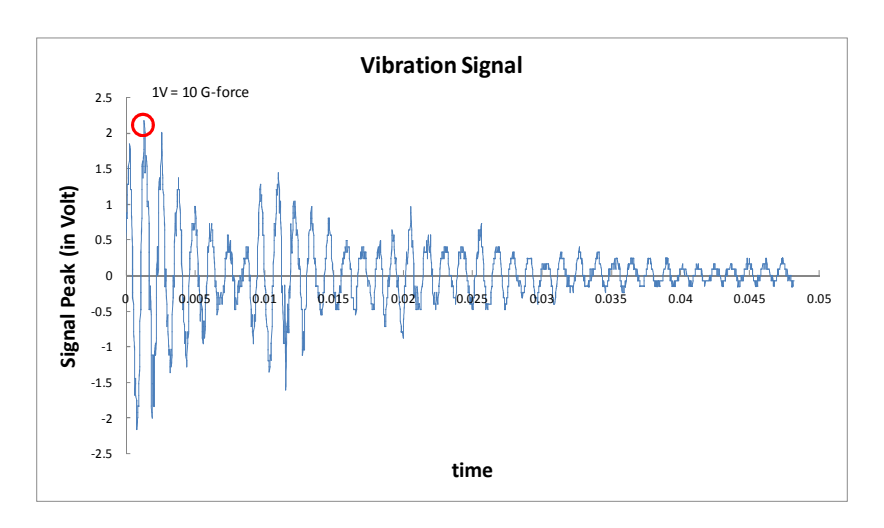


Figure 6.3An example of a vibration signal. The maximum peak of the signal is 2.16 V, which represents 21.6 G-force and the oscillation frequency is 0.8 kHz

On each of those positions, 10 consecutive hits having the same magnitude were given. 93% of the signals were found at the frequency of 0.8 kHz, while the rests are 0.7 kHz. These frequencies are agreed with the CB vibration range shown in table 6.1. The complete results are shown in figure 6.4:

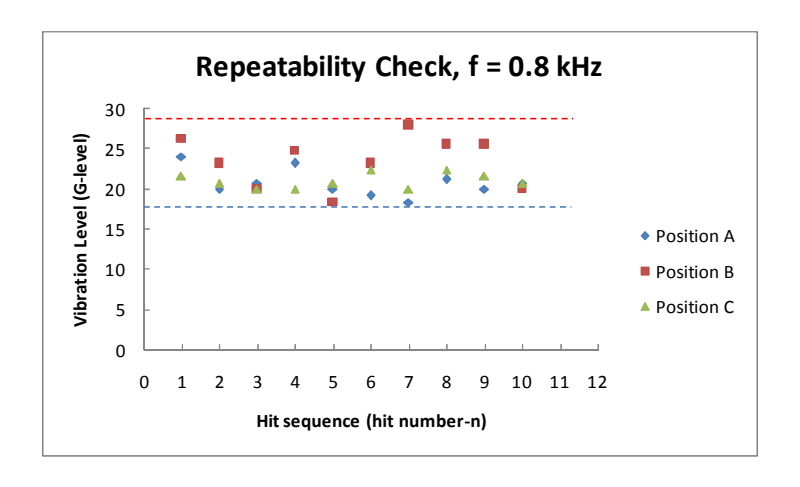


Figure 6.4Repeatability check. 10 hits were given unto position A, position B and position C at the enclosure

The average value of the 10 hits at the three different positions is calculated, the maximum difference was found in the range of 12%. The conclusions from the experiment:

1. The frequencies and the G-force levels generated by the hammer are in the range 0.8 kHz with the amplitude can be adjusted 15 G - 40 G which are in the range of CB vibration as presented in table 6.1

2. The accuracies of the G-force within the impact-area (point A to C) is close to 90%.

6.3 PD Measurements after the Hit

When particles experienced the vibrations, they received a momentum. This momentum disturbs the particle position and increases the net charges on the particle surface. If the net charges time the electric field is higher than the gravitation force, the particle start jumping.

The change of the particle position under the electric field generates the partial discharges (PD) due to the changing of the net charge on the particle surface. Therefore, the vibration impact on the particle movement can be observed by measuring the PD as well as the G-force at the time of the hammer impact as shown by figure 6.6:

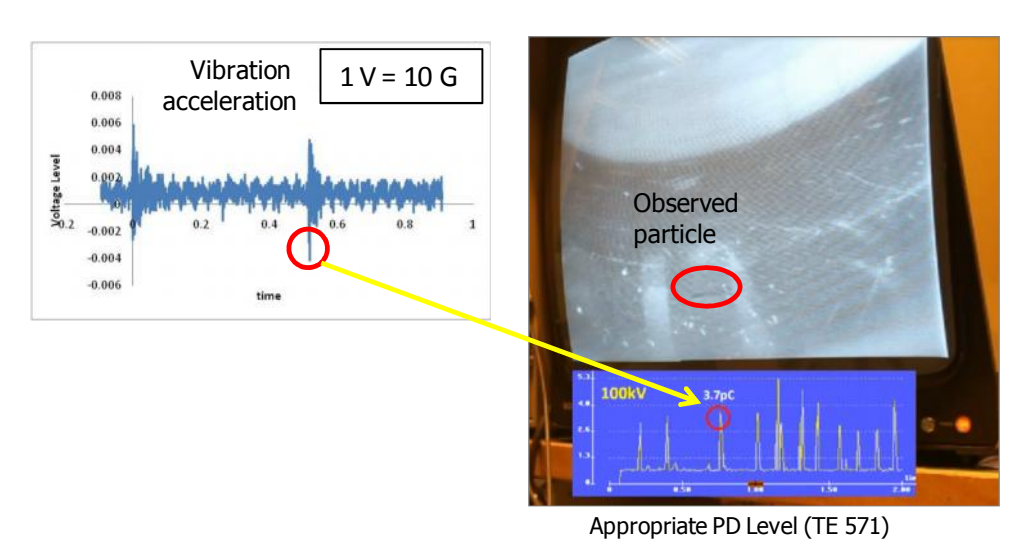


Figure 6.5An illustration of measuring the PD as soon after the hit on the compartment. The vibration is observed in the oscilloscope (left) and the generated PD is shown in the TE 571 instrument. At the same time the particle movement is also observed using a video camera (right)

The PD before the jumping are observed to see how the charges are changed before the jumping. However, the PD generated after the hits are not only due to the particles. Further investigations revealed that even without any particle, the PD impulses are still appear after the hits, with the range below 5 pC. The vibration generates small PD which possibly due to the vibrations of the conductor or any part of the test setupdue to the hit.

Consequently, the PDs below 5 pC are doubtable. But, some PDs beyond this value can be used in the study. The results with the 5, 10 and 30 mm particles at 80 kV and 100 kV are presented in the figure 6.6.

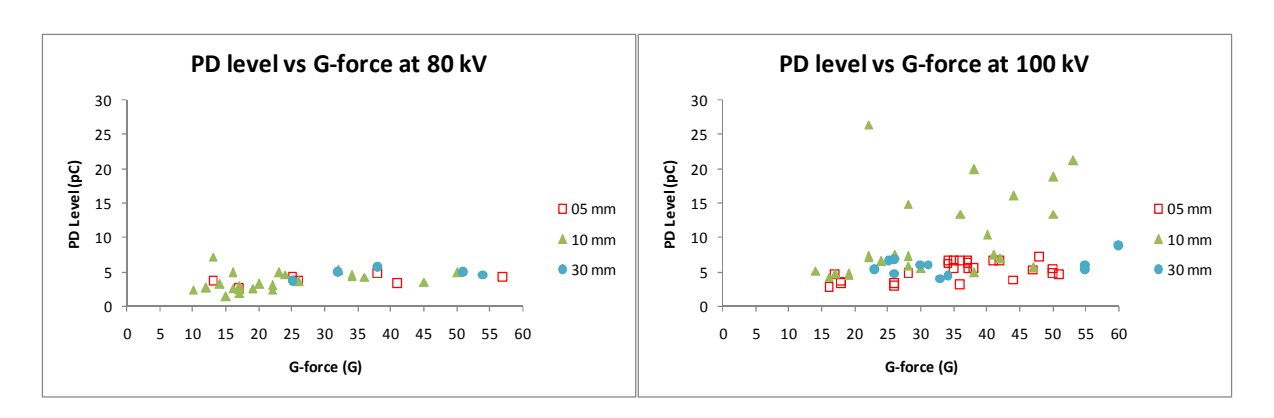


Figure 6.6PD level versus G-forces with the 5 mm, the 10 mm and the 30 mm particles at 80 kV and 100 kV

The following observations are summarized according to these results:

- 1. The increase of the G-force at 80 kV has small impact on the increase of the PD levels. But, at 100 kV, the disburse of the PD levels with the 10 mm particle is obvious. The observation by playing back the recorded video has shown that the 10 mm particle was more mobile rather than the other two particles at 100 kV after the hit.
- 2. Regarding to the explanation in point 1, the PD level correlates with the particle small movement after the hit. The term of "degree mobility" is introduced to determine the mobility of the particle at this moment. The effect of increasing the G-force to the degree mobility is more obvious at the higher electric field.
- 3. The degree mobility depends with some parameters: the momentum-per-area of the particles (mpa), the particles weight (w) and the increasing charges as soon after the hits (ch).

$$f_{mb} = f(mpa, w, ch)$$
 ... equation 6.1

The momentum-per-area (mpa) depends on the effective area of the particles that received the transferred momentum of the vibrations. This effective area is stochastic; it depends on the position of the particles at the moment of vibration. longer particles tend to distribute the momentum over their larger surface results into the relatively smaller momentum per area.

After the hits, the charges at the particles increases as long the particles are still touching the ground. The change of the particles position with a certain angle to the horizontal axis increases the net charges of the particles. The calculations of this phenomena have been discussed in the next section.

4. The three parameters in equation 6.1 are responsible to the final stage after the hits. The particles final stages are: no movement, shuffling and jumping. The new term of "transition stage" is introduced to determine the particle stage before and after the hit.

From these observations, the PD level correlates with the small discharges generate during the transition stage. The higher degree mobility of particle after the hits during the transition stage, the higher the PD observed as in the case with the 10 mm above.

The final stage of the particles after the hit depends on the three influencing parameters in equation 6.1. However, it is difficult to measure the momentum-per-area at the particles since it is a stochastic in nature. To simplify the analysis of the transition stage, the influence of the mpa-parameter is neglected, thus, only of the charges and the particle mass are considered.

6.4 Different Situations during the Transition Stage

The terms of the "transition stage" has been introduced in the previous discussion to determine the particle condition before and after the hit. Three different situations are hypothesized to explain the transition stage as shown in figure 6.7

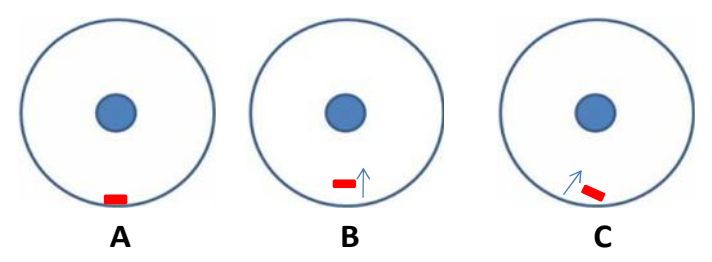


Figure 6.7Three Situations of the Transition Stages

Before the hit, the particle was resting at the bottom enclosure. The figure illustrates the situations of the particle after the hit based on the observation using the video camera:

1. A: The particle is not moving after the hit

2. B: The particle gains acceleration after the hit

3. C: The particle have an angle to the horizontal axis

Only the last two situations lead the particle to jump.

In the situation B, the particle gains an initial acceleration such that it can bridge the gravity force and therefore start moving or flying under the influence of the electric field. This can be explained by using *equation 2.7*:

$$m \cdot \vec{a} + k_a \cdot Q \cdot \vec{E} + m \cdot \vec{g} + \vec{F_d} = 0$$

Without the initial acceleration ($a_0 = 0$), the lift off electric field is defined as:

$$\vec{E} = \frac{m \cdot \vec{g}}{k_a \cdot q}$$

but, when the initial acceleration is not equal to zero. The lift off electric field becomes:

$$\vec{E} = \frac{m \cdot (\vec{g} - \vec{a})}{k_a \cdot q}$$
 ... equation 6.2

which is showing the decrease of the lift off electric field. Besides, in situation B, the particle is moving into the higher electric field region, leads into the higher electrostatic force on the particle.

However, based on the observations in the laboratory after the hit, only the 2 mm and 5 mm particles are possible to have the situation B.

In the situation C, the particle makes an angle to the horizontal axis after it has experienced the vibration but it still attached to the inner surface of the enclosure, as illustrated in figure 6.8:

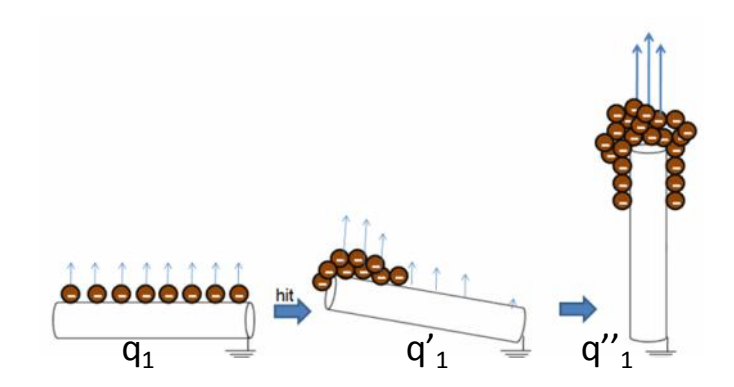


Figure 6.8The illustration of the increasing net charges at the particle surface in the Scenario C. $(q_1 < q'_1 < q''_1)$

The net charges during the transition are calculated by modeling the particle in 3D model and calculating the charges by the Finite Element Method provided by the COMSOL 3.4 software program. The particle is placed at different angles of α , in the range of 0° to 90° in steps of 10° , see figure 6.9:

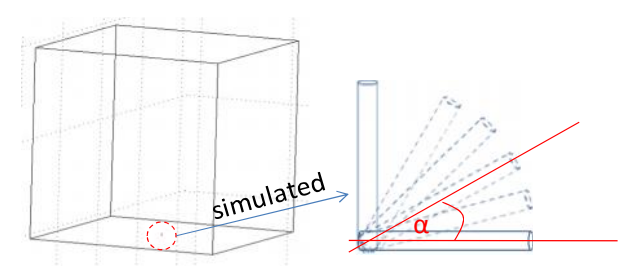
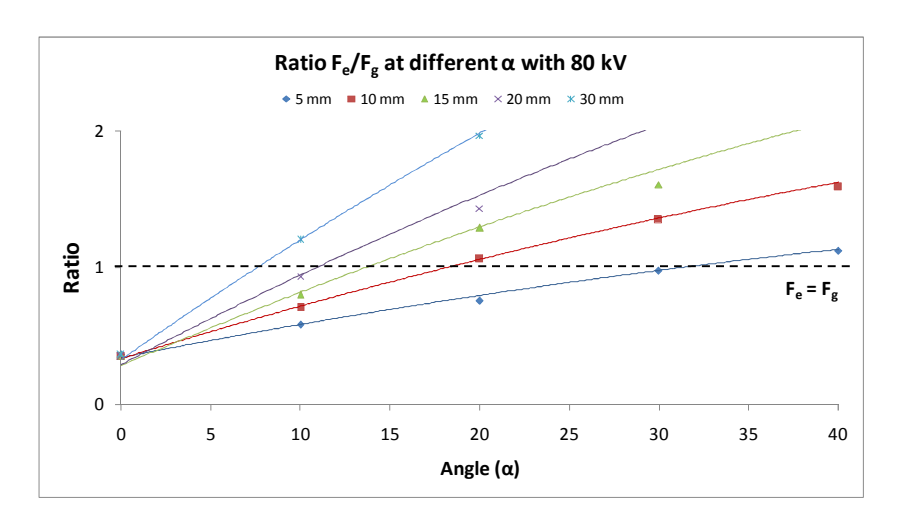
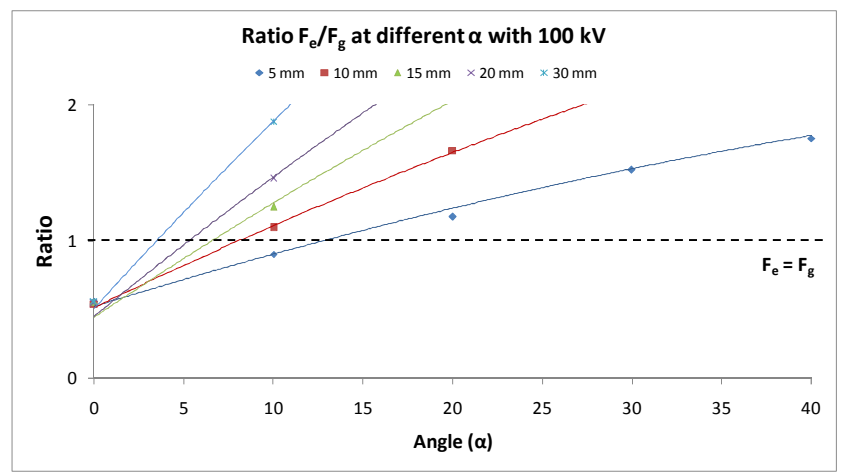


Figure 6.9The particle modeling to calculate the net charges at different angles of α

The calculations are performed at voltage levels of 80, 100 and 120 kV. The results are presented as the ratio at which the electrostatic force (F_e) and the gravitation force (F_g) as shown in figure 6.10.The stipple line determines the boundary where F_e = F_g .





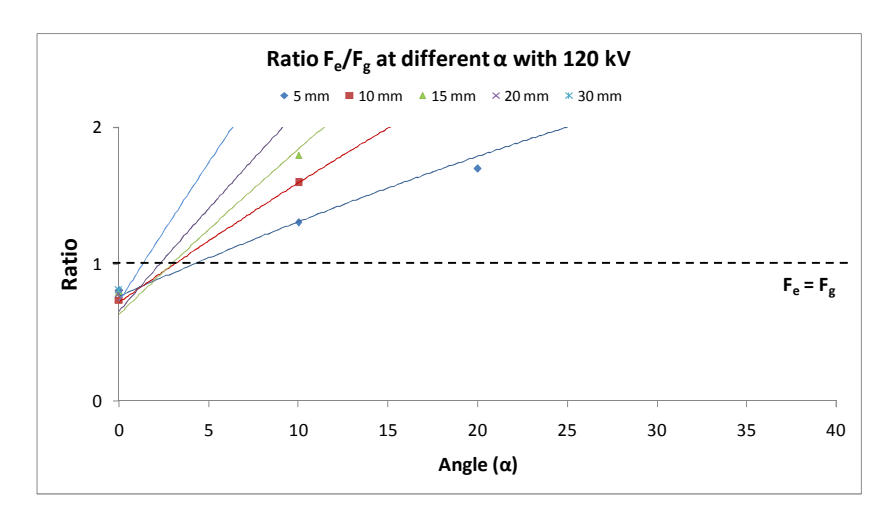


Figure 6.10The ratio of F_e/F_g of the particles at different angle of α , with the voltages of 80 kV, 100 kV and 120 kV

The following have been observed:

- 1. The ratio of the electrostatic force to the gravitation force increases as a function of the voltage, which means at the higher voltage, the particle gains more charges and having the higher possibility to start the jumping.
- 2. The ratio of the electrostatic force to the gravitation force increases as a function of the angle, α , which means the higher the angle after the vibration, the particle is easier to start the jumping.
- 3. The longer the particle, the higher the ratio because the net charges increase faster rather than the mass as a function of the particle length.

The minimum angles to make the particles jumping are summarized in this figure:

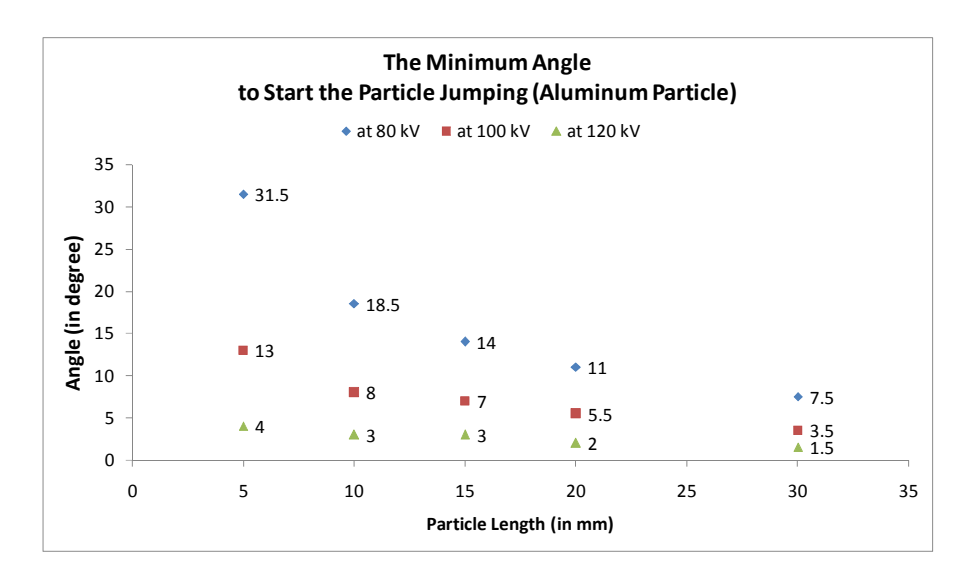


Figure 6.11. A summary of minimum angle to start the particles jumping

From this figure, the longer the particle is, the smaller the angle needed to start the jumping. But, the influence of the momentum per area (mpa) is neglected in this figure. In the real situation, the mpa also responsible to settle the particle at some particular angle. It is possibly easier to move the 20 mm particle to an angle of 11° rather than moving the 30 mm particle to an angle of 7.5°, as has been observed in the experiment under 80 kV. However, the influence of the momentum per area is excluded in this thesis.

6.5 Conclusions

In this chapter, the effects of the vibration on the particles motion have been discussed by using the simulation and the experiment results, and the following conclusions can be drawn:

- 1. The mechanical vibration initiates the particles to start jumping below their lift off electric field, due to:
 - a. The particles gain initial acceleration, and hence required a lower lift off electric field to start their movement
 - b. It is possible that a particle move with an angle with respect to the inner face of the enclosure. Such movement with an angle will increase the net charges of the particle, and therefore its electrostatic force. The increase in the electrostatic force would cause the particle to be lifted-off easily.
- 2. The vibration in the laboratory is valid to simulate the vibration originated from CB/ DS in GIS. They have a comparable frequencies and G-level.
- 3. In addition to the impact of the vibration on the particle motion, the vibration impact on PD has been investigate, however no clear relation has been founded.

Chapter VII

Free Moving Particles Detection by Means of Partial Discharge Measurements

In the last three chapters, the particles motion under the influence of the AC electric fieldhas been discussed. According to the simulations and the experiments results, particles as small as 5 mm length can move and jump under the AC operation voltage. Vibrations in GIS accelerates the particles and therefore, particles can start moving and jumping even more easily. Free moving particles in GIS have a higher probability to cause breakdown whenever they start moving. To prevent in service breakdown due to freely moving particles in GIS, suitable detection techniques are required.

Differenttechniques have been developed to detect metallic particles in GIS by the means of the partial discharge measurements. In section 2.3, these techniques have been presented and the most promising diagnostic methods are [30]:

- 1. The acoustic method,
- 2. The conventional electrical PD detection technique (based on IEC 60270 Standard), and
- 3. The unconventional method by using the VHF and UHF sensors.

During the experiments, these three methodshave been used to measure the PD activities. The objective of using the different methods is to investigate different characteristic parameters due to the particles and to see the particle detect ability within different methods. The measurements system related to each of these methods has been presented in sections 3.9.1 to 3.9.3. The measured parameters are summarized in the following table:

No.	Measurement Methods	Equipment	Signals	Measured Parameters
1	Acquetic	Transinor AS	-Mechanical Signals	-Amplitude to TOF distributions
	1 Acoustic	Transmor As	-Electric Signals	-Phase Resolved Signature pattern
2	Conventional based	Haefely TE 571,	Flactuia Cianala	-PD level in pC
2	on IEC 60270	Haefely 560	-Electric Signals	-PRPD pattern
_	\(\(\frac{1}{2}\)	UHF/VHF Sensor	Flactuie Cienale	-PD level in mV
3	VHF/ UHF	with Spectrum Analyzer	-Electric Signals	-PRPD pattern

Table 7.1 The Summary of Measurement Methods and the Measured Parameters

Different from the other two methods, the phase resolved measurement by the acoustic method is distinguished by the name Phase Resolved Signature pattern [23]. Due to the fact that not only the PD electrical signals received by the sensor but also the mechanical signals from the bouncing particle at the LV electrode.

In this investigation, the PD measurements are performedattwo different stages during the defect movement, namely:

- 1. Stage-1: No movement,
- 2. Stage-2: Jumping

In between stages, the transition stage as discussed in Chapter VI occurs after the hit and cannot be neglected to the results. The signals received from the particles in each of stage are analyzed and discussed in the following sections.

7.1 The Acoustic Measurement

The acoustic method has been introduced in Chapter V with the purpose of measuringthe jumping height of different particles. The origin of the acoustic signals has two sources:

- 1. From the PD, and
- 2. From the mechanical impact of the bouncing particle.

The PD signals have amuch smaller levels than the signals originated from the mechanical impact [29]. In this method, the signals can be represented as:

- 1. The amplitude to the time of flight (TOF), and
- 2. as the Phase Resolved signature pattern.

7.1.1 The Effect of Electric Field

The effect of the electric field and the particle length on the measurements results is analyzed. The investigation on the electric field effect to the particle activity is performed by the experiment using a 15 mm particle placed with the setup-1 and setup-2 as depicted in figure 7.1. The effect of the thread is now neglected.







Setup-2

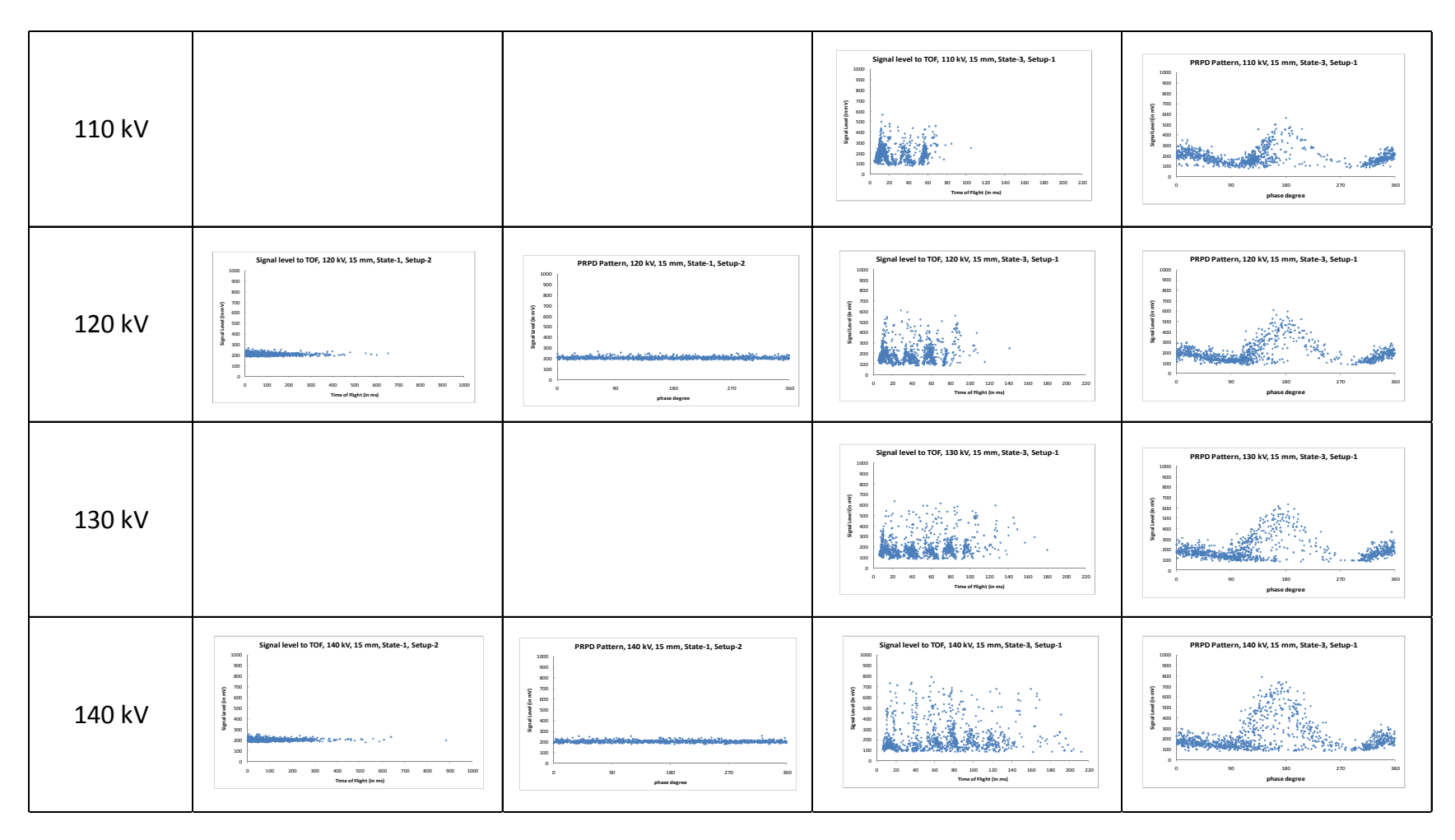
Figure 7.1 The different particles setups used in the Acoustic Measurement with the 15 mm particle

The experiment results are summarized in table 7.2:

 Table 7.2 The Summary of Acoustic Measurement with 15 mm at different voltage level

137	Particle i	n Stage-1	Particle in Stage-2		
kV	Amplitude to TOF	PR Signature Pattern	Amplitude to TOF	PR Signature Pattern	
80 kV			Signal level to TOF, 80 kV, 15 mm, State-3, Setup-1	PRPD Pattern, 80 kV, 15 mm, State-3, Setup-1 1000	
90 kV			Signal level to TOF, 90 kV, 15 mm, State-3, Setup-1	PRPD Pattern, 90 kV, 15 mm, State-3, Setup-1 1000 1000 1000 1000 1000 1000 1000	
100 kV	Signal level to TOF, 100 kV, 15 mm, State-1, Setup-2	PRPD Pattern, 100 kV, 15 mm, State-1, Setup-2 1000 10	Signal level to TOF, 100 kV, 15 mm, State-3, Setup-1	PRPD Pattern, 100 kV, 15 mm, State-3, Setup-1	

Table 7.2 The Summary of Acoustic Measurement with 15 mm at different voltage level (cont.)



According to these figures, some observations are made:

- 1. Only noise has been measured when the particle is in the Stage-1.
- 2. When the particle start jumping (Stage-2), the characteristics patterns can be found:
 - a. In the PR Signature patterns: some peaks are observed at 180° when the voltage is equal to 100 kV and above. If the voltage is decreased to 90 kV and below, the peaks, with the less amplitude, are found at 0° and 180° phase angles.
 - b. In Amplitude to TOF patterns, some parabolic groups are observed with repetition of 20 ms. The signal amplitude, and the TOF increases as the voltage increases.
- 3. The effect of the increase electric field is obvious in the patterns. As the voltage increases, the particle jumps closer to the inner conductor, therefore, signals with higher TOFs are observed at the higher voltages. The maximum amplitude of the phase resolved patterns also increases with the voltage.

7.1.2 The Effect of Particle Length

The effect of the particle length to the patterns have also been observed with the experiments with particles 10 mm, 20 mm and 30 mm. The experiments were done without the cotton thread. The results are summarized in table 7.3 - table 7.4.

Table 7.3 The Amplitude to TOF patterns of Different Particles from the Acoustic Measurement

Particle Length		Amplitud	le to TOF	
Particle Length	80 kV	100 kV	120 kV	130 kV
10 mm				Signal level to TOS, 130 NV, 10 mm, State-3, Setup-3 600 600 600 600 600 600 600 6
20 mm	Signal level to TOF, 80 kV, 20 mm, State 3, Setup-3	Signal level to TOF, 100 kV, 20 mm, State-3, Setup-3 600 600 600 600 600 600 600 6	Signal level to TOF, 120 kV, 20 mm, State-3, Setup-3 600 600 600 600 600 600 600 6	
30 mm			Signal level to TOF, 120 kV, 30 mm, State-3, Setup-3 600 600 700 800 800 800 800 800	

Table 7.4 The Phase Resolved Signature Pattern of Different Particles from the Acoustic Measurement

Particle Length	Phase Resolved Signature Pattern							
Particle Length	80 kV	100 kV	120 kV	130 kV				
10 mm				PRPD Pattern, 130 kV, 10 mm, State-3, Setup-3 600 600 600 600 600 600 600 600 600 6				
20 mm	PRPD Pattern, 80 kV, 20 mm, State-3, Setup-3	PRPD Pattern, 100 kV, 20 mm, State-3, Setup-3	PRPD Pattern, 120 kV, 20 mm, State-3, Setup-3 600 600 600 600 600 600 600 6					
30 mm			PRIO Pattern, 120 kV, 30 mm, State-3, Setup-3 000 000 000 000 000 000 000 000 000					

The observation on these figures results to the following:

- As the particle size increases, the difference of the maximum amplitude at 180° and at 0° increases. This phenomena can be explained by the corona during the travel, which is known as the corona-in flight. The discussion about the corona in flight is given in the analysis
- 2. In general, the patterns of the amplitude to the TOF are similar amongst different particles. The higher peaks are observed with the longer particles since they generates larger mechanical impact.

The signals with the longer particle, is more spread. It indicates the longer particle is moving more random like at the higher electric field.

From the observation on the 10 and 15 mm particles at 130 kV and with the 20 mm particle at 120 kV, the number of the parabolic-groups, are increasing as the particle size is increased.

7.1.3 Analysis of the Phase Resolved Signature Patterns

The phase resolved signature patterns can be explained as the following:

a. According to the simulation performed in Chapter IV, the particle trajectory has a parabolic shape determined by the initial condition at the lift-off. Under the AC electric field the metallic particlesmake an oscillatory movement which is in-phase with the applied voltage. Therefore the moment the particle hit back the LV electrode is not equally distributed over the positive and negative half cycles.

The positively charged particles hit the enclosure around the zero crossing from the positive to the negative (180°) as illustrated in the following figure [43]:

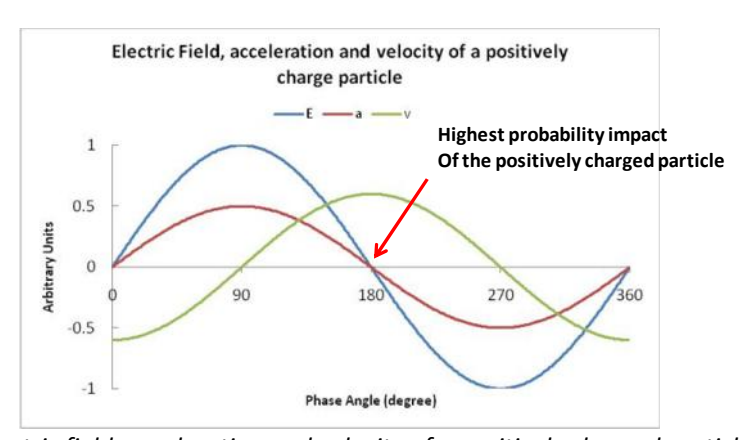


Figure 7.2Electric field, acceleration and velocity of a positively charged particle [43]

The electric field, E, is proportional to the particle acceleration, a (see equation 4.2). Integrating the acceleration yields the velocity, v. Therefore the positively charged particle gains its maximum velocity towards the enclosure at the zero crossing from positive to the negative half cycle. (at positively charged particle, when E changes to negative, F_e will be negative, and the particle accelerates toward the enclosure). This is the reason why the maximum peaks appear around the 180° and the 0° (for the negatively charged particles).

b. At voltage levels of 80 and 90 kV(see Table 7.2), the patterns during the positive and negative half cycle are symmetric because the negatively charged and the positively charged particles occur with the similar frequency [43], and when the voltage increases to 100 kV and higher, the patterns become asymmetric possibly because the "corona inflight" occur at negatively charged particle. The negative charge is removed from the particle through this process.

7.1.4 Analysis of the Amplitude to TOF Patterns

The explanations of the Amplitude to TOF patterns are the following:

The particle possibly gain its maximum charge at the voltage peak, and hit the enclosure back at the appropriate zero crossing as illustrated in figure 7.3. The distance between those two points, T, are 15 ms.

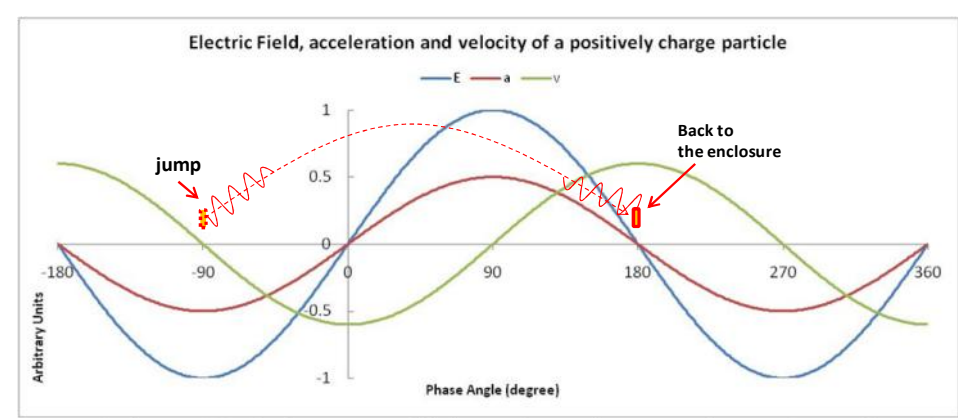


Figure 7.3The positively charge particle leave the enclosure at the maximum (negative) Electric Field and most possibly back to the enclosure 15 ms later. the distance between departure and hitting back enclosure is increasing with the electric field

At longer flight time, T increases by one or more voltage cycles [43]. This can be observed in figure 7.4:

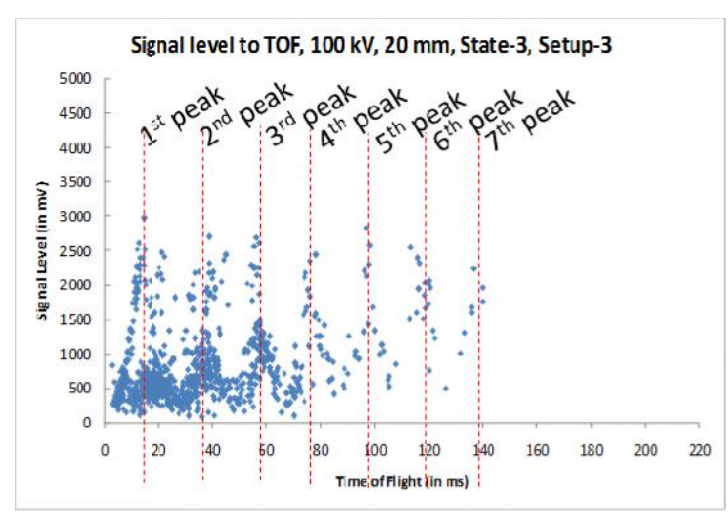


Figure 7.4An example of the signal level to the TOF pattern. The first peak appeared at 15 ms, with the following peaks groups appeared in the distance of 20 ms later.

The increasing of the electric field results into the increasing number of parabolic groups in the pattern. This conforms with the fact that the particle is jump higher with the higher electric field.

7.2 The PD Measurement Based on the IEC 60270 Standard Method

The conventional PD detection measures the apparent charge by using a coupling capacitor and a measuring impedance based on the IEC 60270. The setup has been discussed in section 2.6 and the schematic diagram is redrawn in figure 7.5. The parameters that can be obtained from this measurement are the following:

- 1. PD Inception Voltage (PDIV)
- 2. Apparent PD level (in pC)
- 3. PRPD pattern

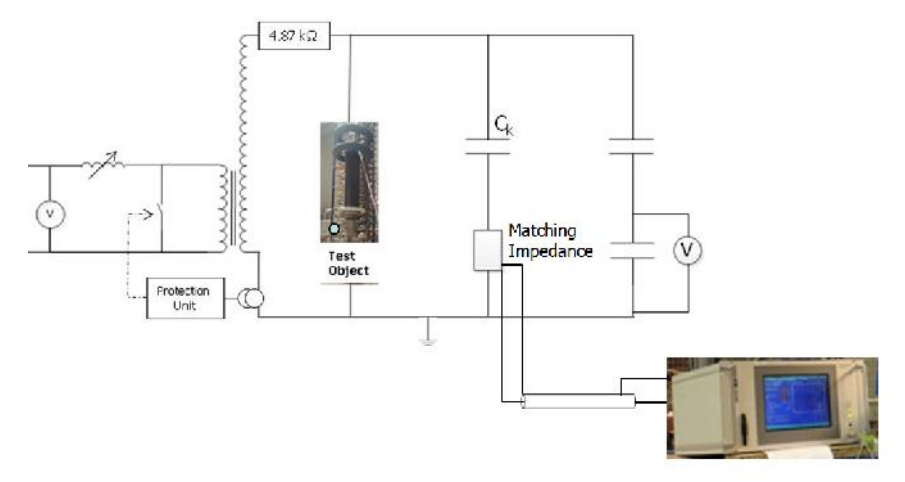


Figure 7.5Schematic diagram of Conventional PD measurement method. A coupling capacitor is installed (Ck) and the matching impedance to measure the apparent PD

The main objective in this section is to evaluate the PD behavior (apparent charge) and the PRPD pattern as a function of the particle size and the electric field. Before running the experiment, the accuracy of the measurement has been checked with the capacitor standard and has shown the error of 10%-20%. The accuracy check is given in *Appendix C*.

Particles of sized 2 mm up to 30 mm with the Stage-1 and Stage-2 have been observed.

7.2.1 The Effect of Electric Field

The effect of the increasing electric field is discussed by presenting the results from the experiment with the 15 mm particle installed with the setup-2 (see figure 7.1). The results are summarized in table 7.5 and figure 7.6:

Table 7.5The Phase Resolved PD Pattern of 15 mm Aluminum Particle tested at Different Voltages. The particle was installed with setup-2 and the measurement was perform during the jumping

kV	PRPD Pattern	Maximum PD Level (pC)			
50 kV		53	kV	PRPD Pattern	Maximum PD Level (pC)
60 kV		64	100 kV		116
	o de		110 kV		124
70 kV	10 10 00 00 7 d	78	120 kV		128
80 kV		93	130 kV		132
90 kV		104	140 kV		172

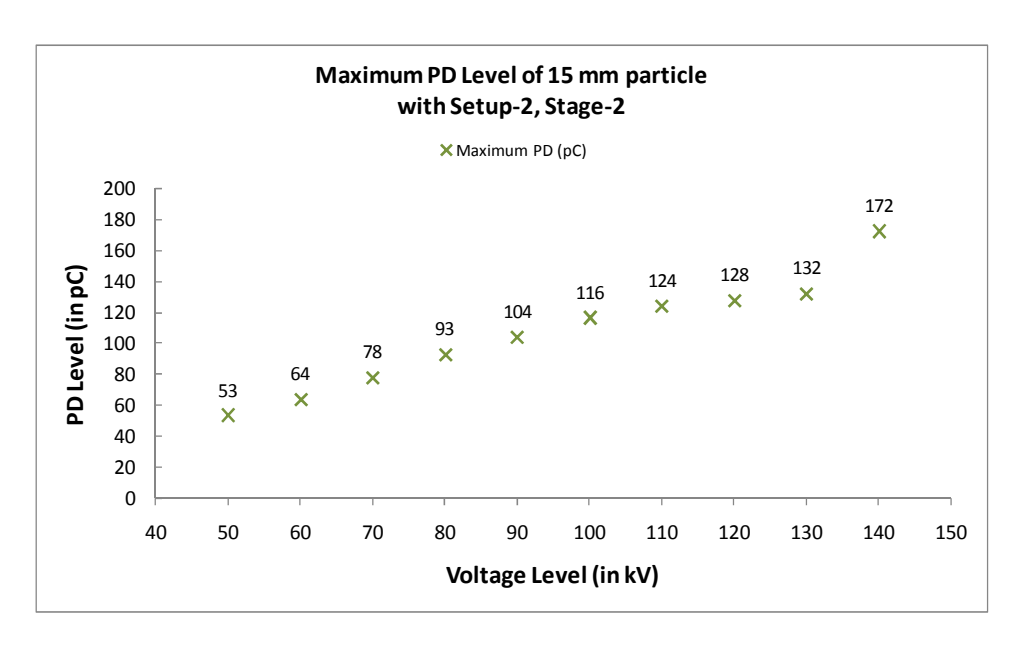


Figure 7.6The summary of the maximum PD level observed from the experiment with the 15 mm particle.

Observation:

- 1. All the PRPD patterns were recorded during the jumping. In general, the shape of the patterns are following the sinusoid of the voltage source. There are two sinusoids superimposed each other as shown in each of the graphs. The amplitude of each peaks represents the maximum discharge situation during the jumping. The higher the jumping is, the higher the discharge level.
 - It seems the maximum height occur during the maximum voltage and most of the jumping occur not so far after the maximum voltage crest (see the more intensive points after the 90° and 270° voltage phase.
- 2. At 50 kV, the pattern is symmetric, but starting from 60 kV up to 140 kV, the negative half cycle is truncated.
 - The maximum PD is steadily increasing during the positive half cycle, but during the negative half cycle, the PD is relatively constant within the range of 70 pC 80 pC at the voltages of 80 kV up to 140 kV. The differences will be discussed in the analysis section
- 3. At 120 kV and above, the external noise is appearing in the PRPD patterns. Further investigation revealed that the PD is coming from bad connection to the external protective resistor (as shown by number 6 in figure 3.3). These additional patterns are disappear after the resistor is removed.

The effect of the cotton thread used in the previous experiment has been investigated by a comparison with the experiment without the thread. The PRPD patterns in the following experiment thread are presented in figure 7.7:

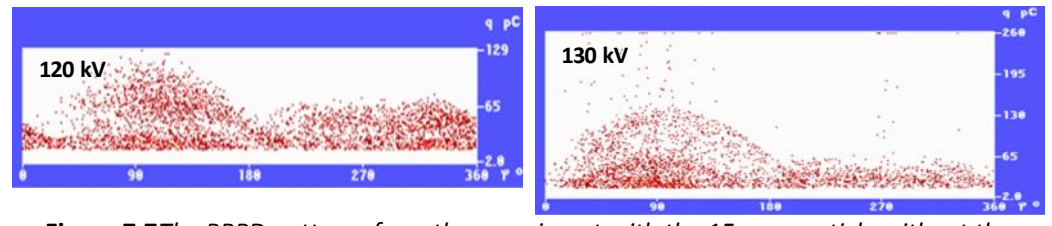


Figure 7.7The PRPD patterns from the experiment with the 15 mm particle without the thread after the removal of the protective resistor. Test voltage= 120 kV and 130 kV.

Observation:

1. In comparison with the previous result shown in table 7.5, the maximum of the sinusoid peaks at the sinusoid patterns are closely similar as shown in table 7.6.

Table 7.6The maximum PD Level observed on the experiment with 15 mm particle with and without the cotton thread

kV	With the thread (pC)	Without the thread (pC)
120 kV	128	129
130 kV	132	130

However, at 130 kV, some points are observed beyond of the maximum sinusoid peaks. These points appear when the particle is reached (or getting closer) to the inner

conductor. The result supports the fact that the cotton thread used in the previous setup limits the maximum jumping of the particles.

2. There is no external noise in the results. The protective resistor has been removed during the measurement.

7.2.2 The Effect of Particle Length

Particles with different lengths are investigated before and after the jumping. Before the jumping, no PD has been observed. The field enhancement due to the particle horizontally lying at the bottom electrode is too small to be detected.

The results from the experiments with different particles are summarized in the following table 7.7. In the experiments, the particles are placed without the cotton thread.

Table 7.7The Phase Resolved PD Patterns of Different Particles During their Jumping.

The Particle is placed without the Cotton Thread. The 5 mm was jumping for 15 seconds. The patterns cannot be obtained, but the PD level was observed

Particle Length	PRPD Pattern						
Particle Length	100 kV	120 kV	130 kV				
5 mm		**					
10 mm							
15 mm		4 1 6 1 1 1 1 1 1 1 1 1 1 1 1 1 1 1 1 1					
20 mm							

Observation:

- 1. The PRPD patterns are similar amongst different particles. The patterns are also truncated during the negative half cycle.
- 2. The PRPD pattern for the 5 mm particle cannot be obtained, but the maximum PD level was observed at 6.5 pC

7.2.3 Analysis

The analysis of the experiments are the following:

- 1. The asymmetric pattern is characteristic in every PRPD patterns observed in the results. The is explained by the following [45]:
 - a. At the lower electric field, the particle was jumping near to the bottom enclosure. The corona-in-flight as discussed earlier is not yet occurred. The measured charge mainly originated from the charge exchange between the particle and the ground. Therefore, the PRPD pattern is symmetric during the positive and the negative half cycle.
 - b. At the higher electric field, the particle can jump into the higher electric field region, or even can reach into the inner conductor. With this situation, the charge exchange is not only occur with the bottom enclosure, but also to the inner conductor, or via micro discharges due to the corona during the excursion.

The corona onset depends with the provision of the initial electron at the particle tip. This initiation is easier during the half negative voltage cycle, since during this period, the electron emission provides electron with higher efficiency rather than the detachment process during the positive half cycle [45]. Therefore, the corona tends to occur during the negative half cycle. This corona is responsible with the particle's loss net charge during the excursion, and results into the asymmetric characteristic patterns.

2. The summary of the maximum PD level of different particles during their jumping are summarized in figure 7.8:

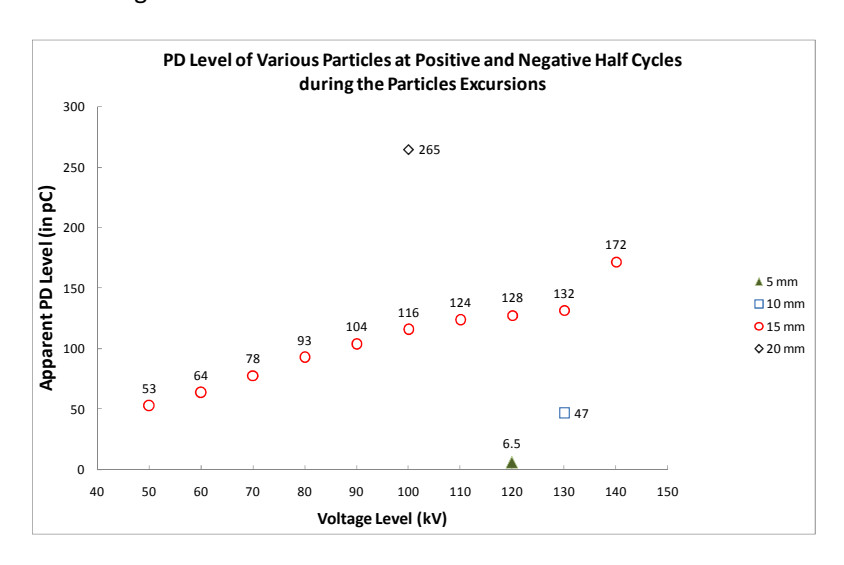


Figure 7.8The maximum PD level of various particles during their jumping

It can be seen that the maximum PD is increasing as the particle size is increased. The longer the particle and the closer the particle to the inner conductor generates higher discharges.

In the experiment, the jumping particle as small as 5 mm can be detected by using this method with the apparent PD 6.5 pC. This conforms with the critical length and the

critical apparent charge of typical defects mentioned in the CIGRE document, where the critical particle length is in the range 2 - 5 mm with the apparent charge of 2 .. 10 pC [46].

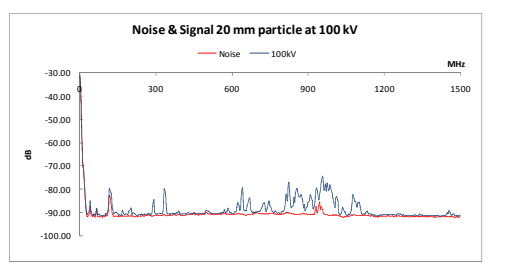
3. Before the jumping, there was no PD.

7.3 The PD Measurement by using UHF/ VHF Method

The other method to detect the free particles is by measuring the generated PD by using the UHF/ VHF method. An internal UHF/VHF sensor is placed inside the compartment as shown in figure 3.14. For the investigation of free particles, the investigated frequency is in the range of 100 - 900 MHz [16]. The main objective in the thesis work is to see the PRPD patterns generated by different particles.

In doing the measurement, a "full span" of background noise and PD pulses from the particles are compared. The voltage is increased gradually from 60 kV up to 140 kV. The measurements are presented either in the frequency-domain (frequency spectra), or in the time/phase domain (PRPD pattern)

Figure 7.9 presents the full spectra from the experiment with 20 mm particle at 100 kV before and after the particle jumping. These spectra were obtained by making the average of 20 sweeps frequency spectrum from 0 MHz to 1.5 GHz of noise and PD signals.



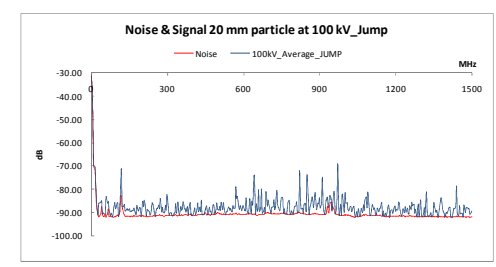


Figure 7.9Frequency spectra measured for a 20 mm free particle at 100 kV before and after the particle jumping

In the left figure, there was no PD activity, since the particle was still in Stage-1, a number of frequency peaks are observed mostly beyond the 800 MHz. In the right figure, when the particle start jumping, the peaks are more distributed in all frequency range.

In the following discussions, the PRPD pattern in the phase domain are obtained with choosing the center frequency 641.25 MHz.

- S. Meijer [16, 48, 49] had distinguished the frequency spectra for the free particles into three different stages:
- 1. No movement
- 2. Moving/Shuffling
- 3. Jumping

However, as earlier mentioned, in this thesis work only the situation in Stage-1 and Stage-3 can be observed with intermediary situation after the hit ("transition stage", see section 6.3). The PRPD patterns presented in this section obtained when the particle was in "transition stage" or when it start jumping.

7.3.1 The PRPD Results

The PRPD patterns of different particles are presented in table 7.8:

Table 7.8The PRPD Patterns of Different Particles at Different Voltages observed during the transition stage and the jumping (*)

Dantiala Laurath	PRPD Transition Stage							
Particle Length	60 kV	80 kV	100 kV	120 kV	130 kV			
2 mm								
5 mm	implies	STATE	1 mm, 100V CF - 641,3 Mm;	7 + 04.13 M/s	Tame, 1690 V			
10 mm								
15 mm	If models of the control of the cont	Immalay CHILASIA	13 mm.2500 C = 4 t is 10 th W to st	11—_1100 07—113 10% What				
20 mm	Dimension CHR12 Min. Water 6	25 mm, BDV C5 mills 80 m W h nt	\$1 mm_188W C7 = 16.13 M/h JUPPile	22 may 22 800 22 may 22 800 33 may 22 800 34 May 1 34 May 1 3				

7.3.2 Analysis of PRPD Results

- 1. The influence of the increasing electric field can be observed in the results. As an example, the observation with the 15 mm presented in the following:
 - a. The maximum amplitude is increasing as the voltage is increased.
 - b. The peaks appear at 180° and at 360°, and they are shifted to the left as the voltage is increased. In [16, 18], such pattern represent the contact noise. This is possibly true, since the particle in the transition stage after the hit, considered as a contact noise to the test setup.
 - The voltage shift is unexpected since a phase synchronizer has been installed in the measuring circuit. It is probably due to the miss-tuned for about 20° ..
 - c. At 120 kV, the particle was jumping. The PRPD patterns is a combination of the signal during the particle in the transition stage and the jumping. The higher amplitude level can be observed when the particle starts jumping. In different setup [49], the PRPD pattern for the jumping particle is shown in figure 7.10:

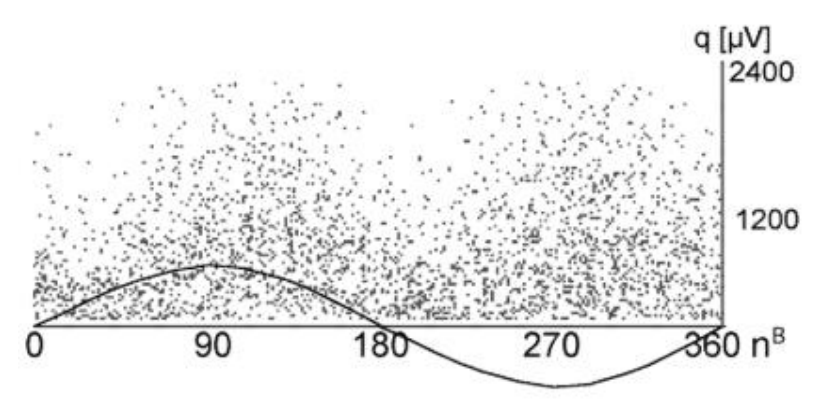


Figure 7.10A phase-resolved PD patterns measured for a free moving particle during the jumping [49]

The disburse signals beyond the red line as shown in table 7.8, seems similar with the patterns in figure 7.10. The similar situation with the 20 mm, even though the pattern is truncated at the higher PD level.

- 2. The PD levels shown in the results is not directly representative the PD generated by the particles, since the software used to present the graph is designed for cable. In order to get the correct level, the sensitivity check should be performed before the measurement by using a standard signal generator. This is not performed during the investigation, since the interest at this moment is to investigate the pattern.
 - However, the increasing PD still can be observed . The maximum amplitudes of the patterns are summarized in figure 7.11.

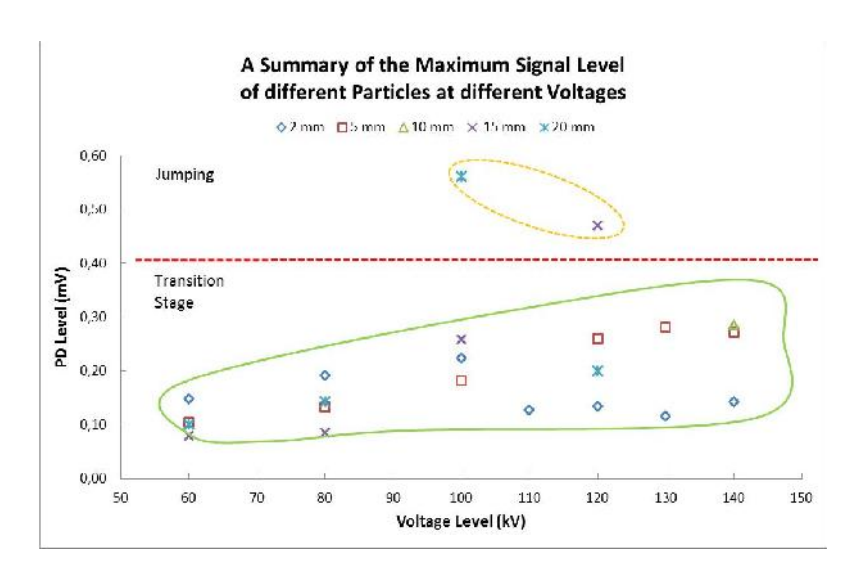


Figure 7.11A Summary of maximum PD levels of different particles at different voltage levels. Most of the particles are observed during the transition stages when the particles having a small movements after the jumping

Analysis regarding to the figure above:

- 1. The PD level is jump as the particles start jumping
- 2. In transition stage, the increasing of the maximum PD is not linear with the particle size. This is probably related to the degree mobility of the particle after the hit, as discussed in section 6.3 (see Figure 6.6)
- 3. The particle as small as 2 mm can be detected with this method when the particle in the transition stage.

7.4 PD Measurements in GIS

All the PD measurements presented in this chapter have been successfully detecting the jumping particles in GIS. They have shown the characteristic patterns that represent the PD activity due to the particles. The amplitude of the PD increases as the increase of the voltage level and particle size.

However, regarding to the real implementation in GIS, some points should be considered:

- 1. The measurement can only run with the GIS operating voltage at 1 p.u.
- 2. The limitation to perform the online measurement.
- 3. The noise from the external is more intense rather than in the laboratory.

Therefore, some analysis is given regarding to the implementation of the detection methods in GIS:

1. Acoustic

At 1 p.u., this method shows a good result in detecting the jumping particle. During the laboratory work, the 10 mm particle can be detected with a good result. In the other experiment, the particle as small as 2 mm can be detected [23,38].

However this method is only sensitive to the particle close to the sensor, therefore, for a continuous monitoring in GIS, a lot of sensor should be installed along the compartment, which is not efficient. This method is best use to localize the position of the particle.

2. Conventional PD Detection Method based on IEC 60270

At 1 p.u., this method can detect the jumping particle as shown in table 7.7. The 5 mm particle can be detected. However this method is difficult to implement during the GIS operation, since a big coupling capacitor is necessary to perform the measurement. Providing the high voltage to the capacitor is another problem. Therefore this method is not applicable in field, especially for the routine maintenance. Usually this method can only be performed in the laboratory setup with limited number of GIS segments.

3. UHF/ VHF Method

In the previous laboratory work, at 1 p.u., the particle as small as 2 mm can be detected. This method is the most promising technique to detect the partial discharges in a real time, including the free particles detection. Some sensors can be placed at different locations in GIS, as in the case of Meeden 380 kV EHV GIS Substations. These sensors can also be accessed remotely via the internet network.

According to the explanation above, the combination of UHF/ VHF method with the acoustic measurement will give the best result. Once the particle is detected by the UHF sensor inside a particular segment in GIS, the acoustic measurement can be performed to localize the position of the particle.

7.5 Conclusions

Different methods have been used to detect the movement of free particles during the GIS operation. Some conclusions can be drawn:

- 1. The PD level increases with the voltage level and the particle length.
- 2. Three methods have been used to detect the particles jump. The detectability has been summarized in table 7.9.

Table 7.9The detectability of particles under 1 p.u.

Based on the experiments. D: Detected, NP: Not Performed, NR: Not Recorded

particle length (mm)	Acoustic Method	Conventional Method	UHF/VHF Method
2	NP	NP	D
5	D,NR	D	D
10	D	D	D
15	D	D	D
20	D	D	D
30	D	D	D,NR

It was possible to detect 2 mm particle length by using UHF/ VHF method during its transition stage. The 5 mm particle length has been detected by the acoustic and the conventional methods. It should be noticed that the ability to detect 2 mm particle length by using the acoustic and conventional methods has not been performed during the experiments.

Chapter VIII

Investigation of Free Moving Particles under AC + Lightning Impulse Stresses

The investigation of free moving particles under AC electric field has been discussed in Chapter IV through Chapter VII. The maximum jumping heights of elongated aluminum particles have been simulated and measured by means of measuring the maximum Time of Flight (TOF) by using the acoustic instrument. The impact of vibrations that makes the particle start jumping below their lift-off electric field has also been discussed in chapter VI. Finally, the experiment results of different free particles detection methods have been presented in Chapter VII.

In the following discussion, the influence of free particles to the breakdown of gas insulation under AC + LI stress is discussed. According to the discussion in section 1.2, the maximum amplitude for the superimposed AC + LI used in this thesis work is 3.5 pu-peak. The interest of this study is to investigate whether the breakdown can occur during the particle jumping under AC + LI stress. The approaches are the following:

- 1. The particle is hanging at the upper enclosure to simulate the height of the particle jumping, see figure 3.11 in section 3.8.
- 2. The test is only running with the LI, instead of AC + LI. This is valid since the duration of the LI is much shorter than the AC voltage.

In the first section of this chapter, the experiment results under Lightning Impulse are given. Thereafter, the analysis of the particle possibility to have a breakdown is discussed in section VIII.2. The analysis includes the relation between the maximum jumping height and the distance in the gap that can have a breakdown.

8.1 The Experiment Results

The Lightning Impulse was generated from the surge generator with the test setup discussed in section 3.4, see figure 3.5. The LI has a standard shape of $1.2/50~\mu s$ accordingly to the IEC 60071-1. The impulse is redrawn in figure 8.1.

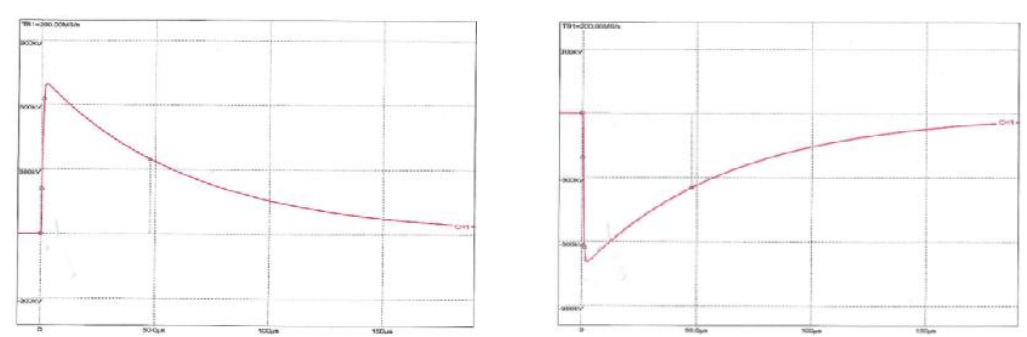


Figure 8.1Standard Lightning Impulse according to IEC 60071-1, positive polarity (left) and negative polarity (right)

In this experiment, the LI is given in step of 20 kV, starting from 250 kV-peak and increased up to 600 kV-peak (3.5 pu peak). After a breakdown, the sample should be replaced, since it degraded as shown in figure 8.2 below:

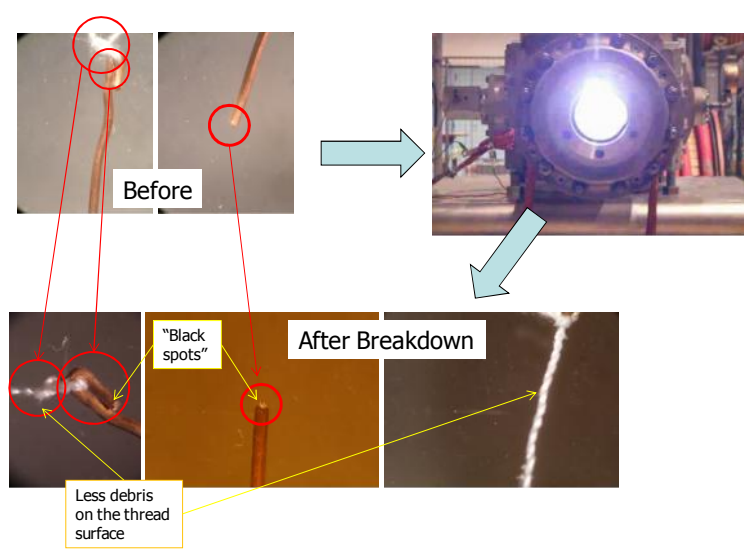


Figure 8.2The particle before and after the breakdown observed by using a microscope

The experiment results are summarized in matrixes that showing the relation between the particle size and the percentage distance from the bottom electrode. Once the breakdown is found at a certain size particle, then it is assumed the breakdown is also occur with the other longer particles. In the experiment, the breakdown under positive LI is higher than under negative LI, therefore, the breakdown observed under positive polarity covers the experiment with the negative polarity. The results are presented in the following matrixes:

(+) Polarity			Di	stance from	the bottom	electrode ([%)		
mm	10%	20%	30%	40%	50%	60%	70%	80%	90%
2									NBD
3									
4								NBD	BD 3.2pu 4.15 μs
5							NBD		
10					NBD	NBD	BD 3.1pu 1.87 μs		
15				NBD					
20		NBD		BD 2.9pu 3.39μs		BD 2.4pu 1.87 μs			
25	BD 3.5pu 3.85μs								
30		BD 2.7pu 4.01μs							

(-) Polarity			Di	stance from	the bottom	electrode ((%)		
mm	10%	20%	30%	40%	50%	60%	70%	80%	90%
2									NBD
3									
4								NBD	
5							BD 3.5pu 2.38μs		
10					NBD	BD 3.5pu 2.79μs			
15				BD 3.5pu 1.78μs					
20		BD 3.3pu 1.91μs							
25									
30									

Figure 8.3Thebreakdownmatrixes from the experiment with LI. The positive LI polarity (up) and the negative LI polarity (bottom)

The green columns determine the condition without the breakdown, while the red ones determine the breakdown, the yellow ones are at the boundary. The black columns represent the particles reach the inner conductor.

Based on these matrixes, some points can be summarized:

- 1. The breakdown under positive polarity is higher than the breakdown under the negative polarity. This characteristic is similar with the previous study with the protrusions [48].
- 2. The shorter particle needs to move closer to the inner conductor to have a breakdown. This can be seen with the 2 mm particle, where the breakdown occurred at 90% of the gap distance.
- 3. The time to breakdown and the breakdown level are decreased as the particle is moving closer into the conductor. This is based on the results from the experiment with the 20 mm particle.
- 4. At the similar distance to the inner conductor, the longer particle has the higher probability to have the breakdown. This can be observed by comparing the 10 mm particle at 50% of distance with the 20 mm particle at 40% of the distance. The reason for this is the longer particle has a shorter remaining gap to the ground, so that the surge leader is easier to make the path for a breakdown.

According to these results, the breakdown under AC + LI depends with the following parameter:

- 1. Particle size.
- 2. Distance particle to the inner conductor
- 3. The amplitude of the LI

Therefore, the height of the particle jumping also determines whether a breakdown can occur under AC + LI. This relation is discussed in the following sub chapter.

8.2 The Critical Distance to have a Breakdown

In the previous work discussed in Chapter IV and Chapter V, the maximum heights of the particles jumping have been measured and simulated. By combining those information with the distance where the breakdown is observed under LI tests, the relation between the particle size with the critical distance to have a breakdown can be derived. The results are shown in the following figures:

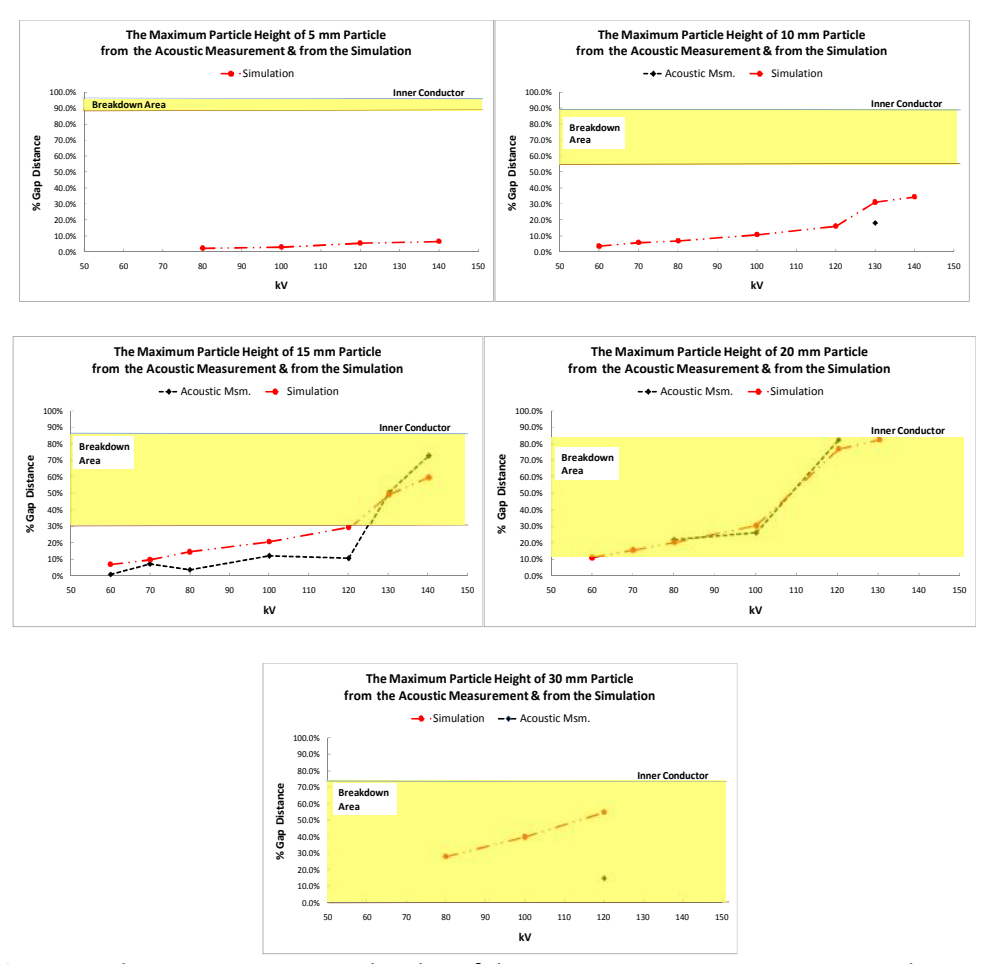


Figure 8.4The maximum jumping heights of the 5 mm, 10 mm, 15 mm, 20 mm and 30 mm particles and their breakdown area under AC + LI

The breakdown area is derived from the LI tests with the tolerance of 10%. The red line in the figures is showing the maximum particle jumping based on the simulation, while the black line/ point is showing the observed maximum jumping based on the acoustic measurement. The 2 mm particle is not included in the results, since during the experiment it never jumps.

The summarize at 1 p.u. is given in the following figure:

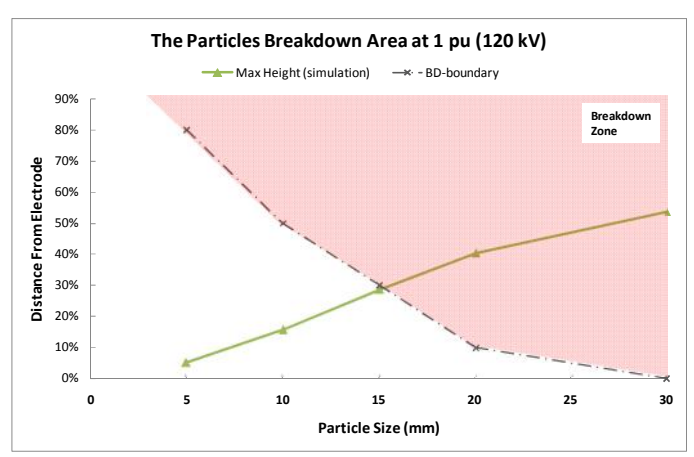


Figure 8.5The breakdown zone of different particles at 1 p.u. It can be seen that the 15 mm particle is at the boundary.

According to the results, at 1 p.u., the particle with the size 15 mm and above are dangerous to the gas insulation under AC + LI. The summary of the breakdown under 1 p.u. is given in table 8.1 below:

Table 8.1The summary of the breakdown possibility at various particles under 1 p.u.

particle length (mm)	BD
2	No
5	No
10	No
15	Yes
20	Yes
30	Yes

8.3 Conclusions

- 1. A breakdown area has been distinguished based on the experiment results under AC + LI with various particle lengths. The possibility of a particle to have a breakdown under AC + LI depends on the height of the jump.
- 2. Longer particles can jump more easy into the breakdown area.

Chapter IX

Investigation of Free Moving Particles under AC + VFTO

The other voltage stress to be investigated is the superimposed of AC voltage with the Very Fast Transient Overvoltages (AC +VFTO). During the GIS operation, the VFTO arisesdue to the operation of the disconnector switch (DS). A number of re-strikes and pre-strikes takes place due to the slow operation of the disconnector switch. The amplitude of the VFTO which can reach as high as 2.5 p.u. to 3. p.u. [51].

The generation of VFTO produces the internal and external transient overvoltages [50]. The main concern is the internal transient overvoltages which give stresses into the insulation system and possible lead into a breakdown. The external transient overvoltages give stresses to the secondary equipment and to the connected equipment such as current transformer and voltage transformer.

In this thesis work, the influence of the free particles to the breakdown under the VFTO is investigated. The investigation was taking place at the High Voltage Laboratory of Stuttgart University of Technology with the test setup redrawn in figure 9.2.

The particle was hanging as in the experiment with the LI. The picture is shown in figure 9.1. Instead of a superimposed AC + VFTO, the test was carried out only with the VFTO with assumption of additional 1 p.u. AC voltage peak.



Figure 9.1The particle placed inside of the test setup in GIS at the High Voltage Laboratory in Stuttgart

In the following section, the experiment results are presented, and thereafter section 9.2, the analysis is given to confirm the VFTO.

9.1 The Test Setup

The test setup used in Stuttgart is given in figure 9.2. The test setup is floating during the experiment. Some compartments are filled with air and some others with SF_6 gas. The summary of the gas filler is given in table 9.1. During the experiment, the gas pressure in the compartments is adjusted to get the appropriate insulation level. The determination of the gas pressure is discussed in the section preliminary experiment.

Table 9.1 The summary of the gas filler used in the compartments

, 0	
Compartment	Filler
F,A	SF6
В	SF6
G	Air
H1,H2	Air
End	Air
Compartment	ΔII

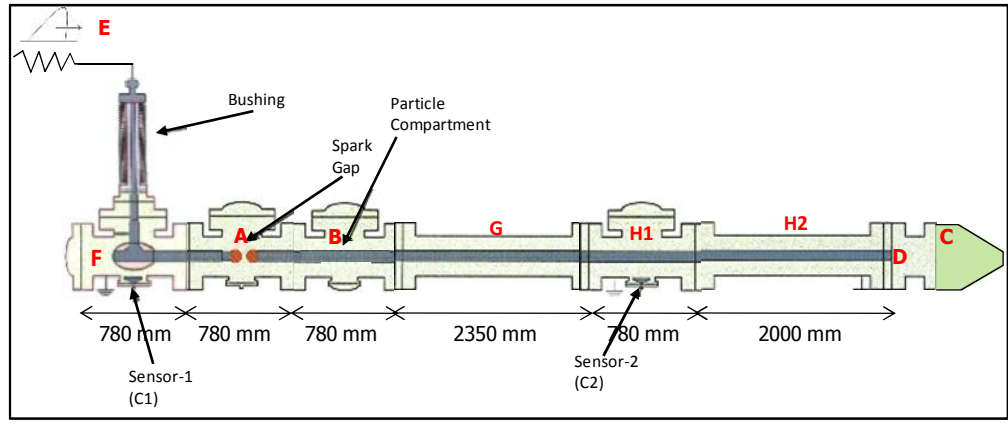


Figure 9.2Scheme diagram of the test setup Used in Stuttgart

The surge is generated from the impulse generator and it comes into the test setup via bushing (E). If the surge level between the sparking gap (A) is higher than the breakdown of the gap, the VFTO will be generated. The particle is placed in compartment B, next to the compartment with the gap. There are two options to adjust the VFTO amplitude:

- a. By changing the distance of the gap, and
- b. By increasing the pressure of compartment A

In the experiment, the second method is chosen. The gap distance was fixed at 1 cm and the gas pressure was set at 1, 3 and 5 bar. In this way, the VFTO with maximum 645 kV peak can be generated. The amplitude is limited to avoid the flashover at the bushing. Therefore, the maximum voltage used in the experiment equal to 2.1 pu.

9.2 The ExperimentResults

In the early experiment, the gas pressure in each compartments are summarized in table 9.2.

Table 9.2 The summary of the gas pressure in the test setup at the beginning of the experiment

Compartment	Filler	Pressure (bar)
F,A	SF6	3
В	SF6	4
G	Air	1
H1,H2	Air	2
End Compartment	Air	1

With this pressure combination, the breakdown has been observed at the end compartment (see point D in figure 9.2) at about 200 kV. Thus, even though the VFTO level is increased, the breakdown still occur at the similar position.

To avoid this breakdown, the insulation level of the test setup has been increased with the following steps:

- 1. An addition of a shielding shield at point D
- 2. An addition of enclosed compartment C filled with the 5 bar air
- 3. By Increasing the air pressure inside compartment G, H1 and H2 to 5 bar





Figure 9.3An additional shield at the end point (left) and the addition of an enclosed compartment filled with air at 5 bar (right)

With this improvement, the breakdown can be avoided, except at the particle in compartment B. The VFTO curve before and after the improvement are observed in figure 9.4

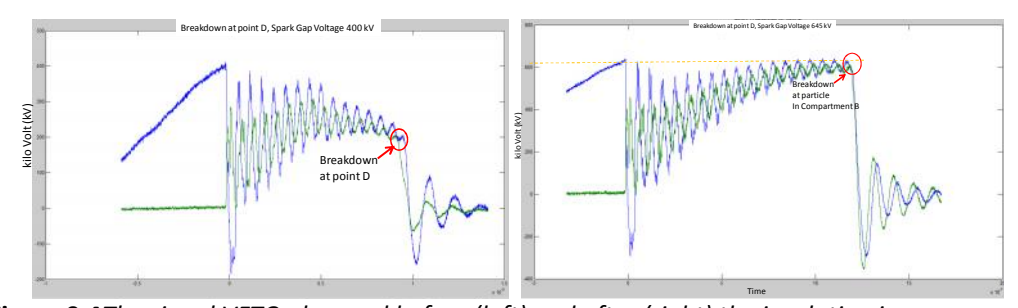


Figure 9.4The signal VFTO observed before (left) and after (right) the insulation improvement

The results of the experiment with different particles are shown in table 9.3

Table 9.3 The breakdown observed with the particle under VFTO = 2.1 p.u.

Particle Size (mm)	% gap distance	BD
15	90	No
30	70	No
30	90	Yes

The breakdown has only been observed with the 30 mm particle at 90% of the gap distance.

9.3 The Confirmation of VFTO

The VFTO readings from the sensors are confirmed by the following:

- 1. The simulation of the travelling waves in the test setup by using ATP/EMTP Program
- 2. Analysis the time rise of the VFTO waveforms

9.3.1 VFTO Simulation in the Test Setup Used in Stuttgart University

The special capacitive voltage sensors have been used to measure the VFTO. The discussions of this sensor can be found in [52,53]. The simulation by using the ATP/EMTP program has been performed as a comparison of the VFTO reading. The GIS test setup has been modeled as a distributed components as shown in figure 9.4 below. The value of each components are taken from the references [50,51] with some adjustments. The arcing is modeled by an exponentially decreasing resistance r from a very high value to zero, with the time constant, $\tau = 1$ ns [51].

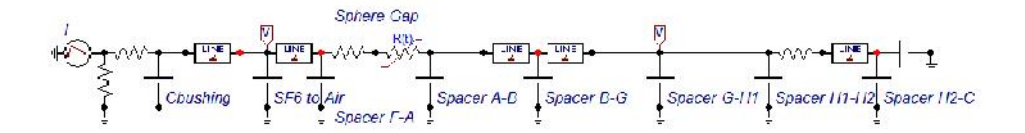


Figure 9.4Model used in the transient simulation of GIS test setup of in Stuttgart

The result of the simulation with the breakdown gap 650 kV is given in the following figure:

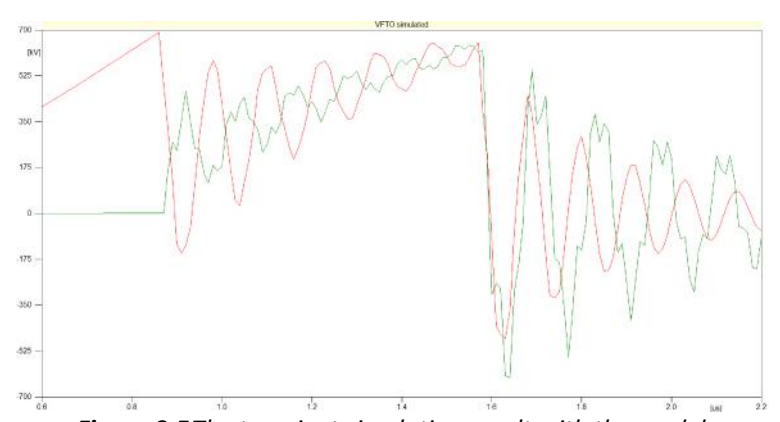


Figure 9.5The transient simulation result with the model of GIS setup in Stuttgart

The similar pattern has been observed, even though it is not identical. The difference probably due to several factors:

- 1. The simulation run with a single arcing strike.
- 2. The parameters used in the simulation are using a generic values However, the similar patterns have been observed.

9.3.2 VFTO RiseTime

Time rise time of the waveforms is shown in figure 9.6:

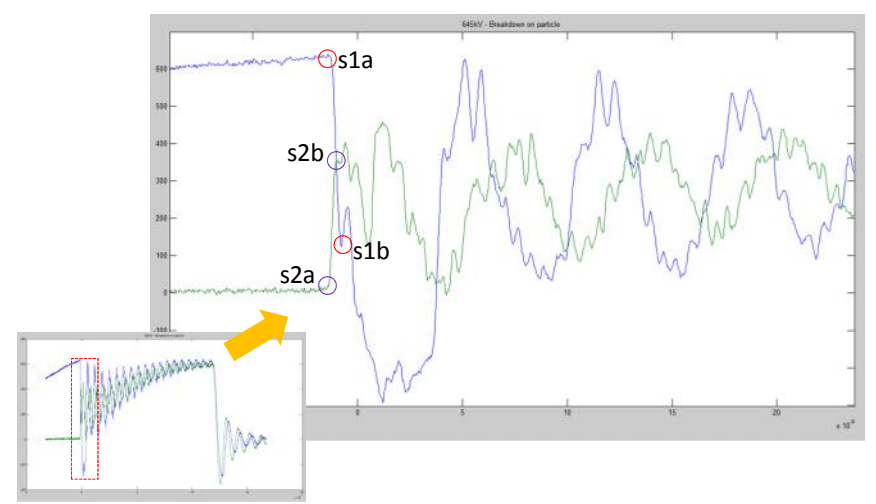


Figure 9.6The first rise time appear in the VFTO waveforms

The first rise time observed at sensor 1 (s1a to s1b) and sensor 2 (s2a to s2b) are in the range of 5.2 ns, which is confirm the rise time of the VFTO as presented in figure 1.3. The two waveforms are in opposite direction which is relevant with the opposing direction of the travelling waves sensed by the sensors.

9.4 Conclusion

The investigation with VFTO has been performed in Stuttgart. Due to the limitation of the test setup, the maximum VFTO used in the experiments limited to 2.1 p.u. At this level, the breakdown has been occurred only for 30 mm particle placed at 90% of the distance gap. No breakdown has been observed at shorter distances(from the enclosure) and by using shorter particles.

Chapter X

Conclusions and Recommendations

Conclusions:

Free moving particles can start moving under the influence of the AC electric field hence, it can cause failure in the insulation system. Beside the continuously operating AC voltage, different voltages and over voltages can occur in GIS due to, for instance, lightning impulse and switching operation. Therefore experiments in the High Voltage Laboratory has been carried out to investigate the behavior of free moving particles under AC voltage and transients namely, Lightning (LI) and Very Fast Transient Overvoltages (VFTO). The experiment with the LI has been performed with the voltage up to 3.5 p.u., and with the VFTO up to 2.1 p.u.

Particle length of 2 up to 30 mm have been subjected to those (over)voltages. The experiment results have been illustrated and discussed throughout this thesis work, and the following conclusions can be drawn. However, the conclusions have been classified in three groups based on the applied voltage as the following:

1. AC voltage:

- a. During the movement of free moving particles in GIS they make an oscillatory movement which is in phase with the applied AC voltage.
- b. The maximum jump a particle can reach under 1 p.u. AC voltage has been simulated. The results are listed in table 10.1:

Table 10.1The Maximum Particle Jump at 1 p.u. Based on the Simulation Work

Particle Size	Maximum Height (% of gap distance)		
2 mm	0%		
5 mm	5% - 14%		
10 mm	14% - 35%		
15 mm	22% - 57%		
20 mm	35% - 69%		
30 mm	55% - 100%		

The maximum jump a particle can reach increase with the particle length.

- c. A good agreement has been observed between the simulation and the acoustic measurement results at a voltage level up to 120 kV.
- d. In the laboratory work, the free moving particles have been subjected to the external vibration to simulate the vibration originated from CB/DS in GIS. The particles can start jumping below their lift off electric field after a hit, due to:
 - i. The particles gained initial acceleration, and hence required a lower lift off electric field to start their movement.

- ii. When the particles move with an angle to the inner surface of the enclosure their net charges increase, and therefore the electrostatic force increases as well.
- e. The PD activities increase with the voltage level and the particles length.
- f. It was possible to detect 2 mm particle length by using UHF/ VHF method during its transition stage. The 5 mm particle length has been detected by the acoustic and the conventional methods. It should be noticed that the ability to detect 2 mm particle length by using the acoustic and conventional methods has not been performed during the experiments

2. AC + LI Overvoltage:

- a. A breakdown area has been distinguished based on the experiment results under AC + LI with various particle lengths. The possibility of a particle to have a breakdown under AC + LI depends on the height of the jump.
- b. Longer particles can jump more easy into the breakdown area.

3. AC + VFT Overvoltage:

The investigation with VFTO has been performed in Stuttgart. Due to the limitation of the test setup, the maximum VFTO used in the experiments limited to 2.1 p.u. At this level, the breakdown has been occurred only for 30 mm particle placed at 90% of the distance gap. No breakdown has been observed at shorter distances (from the enclosure) and by using shorter particles.

Recommendations:

For future studies, some recommendations are given:

- The simulation of the jumping particles used in this report can be improved by considering the micro discharges at the higher electric fields. The confirmation of the simulation better to be performed with more than 1 GIS test setups. The effect of the coated layer to the particle movement can also be another addition to the study.
- 2. The investigation under Very Fast Transients Overvoltage(VFTO) can be developed by the following:
 - a. The modeling and simulation of the VFTO for the whole systems of GIS followed with the on-field or GIS lab model measurement.
 - b. To support the study in point a., the development of the measuring sensor in Delft University of Technology is necessary.
 - c. The investigation of the free particles under VFTO stress can be continued with the higher stress level, and different particle sizes.

References

- [1] CIGRE WG 15.03, Diagnostic Methods for GIS Insulating System, CIGRE Session 1992, Report 15/23-01.
- [2] Working Group 15.03, GIS Insulation Properties in case of VFT and DC Stress, Cigre Session 1996, Report 15-201.
- [3] The lightning flash density map on http://www.nasa.gov/.
- [4] S.Yanabu et. al., Estimation of Fast Transient Overvoltage in Gas-Insulated Substation, IEEE Transactions on Power Delivery, Vol. 5, No. 4, November 1990.
- [5] CIGRE WG 23.02, Report on the Second International Survey on High Voltage Gas Insulated Substations (GIS) Service Experience, CIGRE Brochure 150, February 2000
- [6] N.Okutsu et.al., *Pattern Recognition of Vibrations in Metal Enclosures of Gas Insulated Equipment and its Application*, IEEE Transactions on Power Apparatus and Systems, Vol. PAS-100 No. 6, June 1981.
- [7] M.Wohlmuth, *Criticality of Moving Particles in GIS*, Ninth International Symposium on High Voltage Engineering, Austria, 1995.
- [8] M.S.Naidu, Gas Insulated Substations, Departement of High Voltage Engineering, Indian Institute of Science, Bangalore, I.K.International Publishing House, 2008, ISBN 978-81-906942-9-2.
- [9] M.Morcos, H.Anis, K.Srivastava, *Particle initiated corona and breakdown in GITL systems*, IEEE Trans. On El, Vol.24, pp.561, 1989
- [10] R.E.Wootton, Investigation of High Voltage Particle Initiated Breakdown in Gas Insulated Systems, EPRI Report EL-1007, 1979.
- [11] Magnus Holmberg, Motion of Metallic Particles in Gas Insulated Systems, Ph.D Thesis, Department of Electric Power Engineering, Chalmers University, Sweden, 1997, ISBN 91-7197-533-0.
- [12] Manual book of Meeden EHV GIS Substation, belongs to TenneT, May 1993
- [13] Westinghouse Research and Development Center; "Investigation of High-Voltage Particle-Initiated Breakdown in Gas-Insulated Systems", EPRI Project 7835 Report, Pitssburgh, Pennsylvania, March, 1979.
- [14] A.H.Cookson,O.Farish,G.M.L.Sommerman, *Effect of Conducting Particles on AC Corona* and *Breakdown in Compressed SF6*, Paper 71 TP 508-PWR, IEEE Summer Meeting and International Symposium on High Power Testing, Portland, 1971.
- [15] O.Farish,M.D.Judd,B.F.Hampton,J.S.Pearson, *SF6 Insulation Systems and their monitoring*, Chapter 2 of Advances in High Voltage Engineering, Institute of Engineering and Technology, 2004.
- [16] Sander Meijer, Partial Discharge Diagnosis of High-Voltage Gas Insulated Systems, Ph.D Thesis, Delft University of Technology, Optima GrafischeCommunicatie, Rotterdam, 2001.
- [17] F.H.Kreuger, *Industrial High Voltage 1,2,3*, Delft University Press, Delft, the Netherland, 1991.
- [18] F.H.Kreuger, *Industrial High Voltage 4,5,6*, Delft University Press, Delft, the Netherland, 1991.
- [19] L.Niemeyer, L.Ulrich, N.Wiegart, *The Mechanism of Leader Breakdown in Electronegative Gases*, Transactions on Electrical Insulation, Vol. 24, No.2, April 1989.
- [20] I.D.Chalmers, I.Gallimberti, A.Gibert, O.Farish, The development of electrical leader discharges in a point-plane gap in SF6, Proc. R. Soc. Lond. A Math. Phys. Sci., 1987, 412, pp. 285-308.
- [21] I.C.Sommerville, O.Farish, D.J.Tedford, The Influence of atmospheric negative ions on the statistical time lag to spark breakdow', in L.G.Christophorou (Ed.): "Gaseous dielectric IV" (Pergamon Press, New York, 1984), pp. 137-145.

- [22] I.D.Chalmers, O.Farish, A.Gibert, J. Dupuy, *Leader development in Short point-plane gaps in compressed SF6*, IEE Proc. A, Phys. Sci. Meas. Instrum. Manage. Educ. Rev., 1984, 131, pp. 159-163.
- [23] L.E. Lundgaard, *Particles in GIS: Characterization from Acoustic Signatures*, IEEE Transactions on Dielectrics and Electrical Insulation, Vol.8 No.6, December 2001.
- [24] C.M.Cooke, R.E.Wootton, A.H.Cookson, *Influence of Particles on AC and DC Electrical Performance* of Gas Insulated Systems at Extra High Voltage, IEEE Transactions on Power Apparatus and Systems, Vol. PAS-96, no.3, May/June 1977.
- [25] W.Hauschild, W.Mosch, *High Voltage Field testing of GIS from the view point of failure mechanism*, Int. Symposium on GIS Technology and Practice, Toronto, Pergamon Press, pp. 185, 1985
- [26] N-K.Felici, Forces et charges de petit objets en contact avec une electrode affectee d'un champ electrique, Revue Generale de L'electricite, pp. 1145-1160, Octobre 1966.
- [27] O.Farish, I.D.Chalmers, X.P.Feng, *Particle-initiated breakdown in a coaxial system in SF6/air mixtures*, Proceedings of IEEE symposium on Electrical Insulation, Washington DC, 1986, pp 206-209.
- [28] O.Farish, Corona controlled breakdown in SF6 and SF6 mixtures, Proceedings of XVI International Conference on Phenomena Ionised Gases, Dusseldorf, 1983, pp. 187-196.
- [29] CIGRE Working Group 15.103, Effects of Particles on GIS Insulation and the Evaluation of Relevant Diagnostic Tools, CIGRE 1994 Session, August 28 September 3, 1994.
- [30] CIGRE WG 15.03: Diagnostic methods for GIS insulating systems, CIGRE Paris, 1992, p.15/23-01
- [31] IEC 60071: Insulation Coordination Part-1: Definitions, principles and rules, International Electrotechnical Commission, 2006.
- [32] A.Pedersen, G.Crichton, I.McAllister, *The theory and measurement of partial discharge transients,* IEEE Trans. on El, Vol.26, 1991,p.487
- [33] I.Herbst, *PD-measurements in GIS, a theoretical and experimental comparison of different electrical measurement techniques,* CIGRE Symp. Berlin, 1993, p.130-02.
- [34] A.Petit, C.Maulat, GIS monitoring by the UHF method: Effect of external perturbations and defects on solid insulators, CIGRE Symp. Berlin, 1993, p.130-07.
- [35] B.Fruth, L.Niemeyer, M.Hassig, J.Fuhr, T.Dunz, *Phase resolved partial discharge measurements and computer aided partial discharge analysis performed on different high voltage apparatus*, 6.ISH New Orleans, 1989, p.15.03.
- [36] M.Stosur, M.Szewczyk, W.Piasecki, M.Florkowski, M.Fulczyk, *GIS Disconnector Switching Operation VFTO Stud*, Modern Electric Power Systems, Poland, 2010.
- [37] TF on Very Fast Transients in IEEE Working Group on Modelling and Analysis of System Transients Using Digital Programs, *Modelling and Analysis Guidelines for Very Fast Transients*, IEEE Transactions on Power Delivery, Vol. 11, No.4, October 1996.
- [38] Lars Hofstad, User Guide-Acoustic Insulation Analyzer, Version 3.0, Norway, April 1998.
- [39] Edward Gulski, *Computer-Aided Recognition of Partial Discharges using Statistical Tools*, Ph.D Thesis, Delft University Press, The Netherlands, 1991.
- [40] F.H.Kreuger, *Partial Discharge Detection in High-Voltage Equipment,* Butterworths& Co Ltd, London, United Kingdom, 1989.
- [41] S.Burow et. al., Can Ferrite Materials or Resonant Arrangements Reduce the Amplitudes of VFTO in GIS?, XVII Internation Symposium on High Voltage Engineering, Hannover, Germany, August 22-26, 2011.
- [42] The information about momentum and impulse taken from http://wikipedia.org/.
- [43] H.D.Schlemper, K.Feser, Estimation of Mass and Length of Moving Particles in GIS by Combined Acoustical and Electrical PD Detection, IEEE Annual Report Conference on Electrical Insulation and Dielectric Phenomena, San Francisco, October 20-23, 1996.

- [44] M.Runde et.al., Risk Assessment Basis of Moving Particles in Gas Insulated Substations, IEEE Transactions on Power Delivery, Vol. 12, No. 2, April 1997.
- [45] W.Ziomek, E.Kuffel, *Activity of Moving Metallic Particles in Prebreakdown State in GIS*, IEEE Transactions on Dielectrics and Electrical Insulation, Vol. 4 No.1, February 1997.
- [46] A.Sabot, Insulation Coordination and on line Insulation Monitoring & Diagnostic Techniques for Gas Insulated Switchgear (GIS), CIGRE Session 2000, Article P1-09.
- [47] S.Meijer,P.H.F.Morshuis,J.J.Smit, *Breakdown Probability of SF6 due to Voltage Transients*, Annual Report Conference on Electrical Insulation and Dielectric Phenomena, 2004.
- [48] S.Meijer,R.G.A.Zoetmulder,J.J.Smit,A.Girodet, *Risk Assessment of Free Moving Particles in GIS using Spectral and Partial Discharge Analysis*, Conference Record of the 2002 IEEE International Symposium on Electrical Insulation, Boston, USA, April 2002.
- [49] S.Meijer, J.J.Smit, *UHF Defect Evaluation in Gas Insulated Equipment*, IEEE Transactions on Dielectric and Electrical Insulation, Vol. 12, No.2, April 2005.
- [50] J.A.Martinez et. al., *Modelling Guidelines for Very Fast Transients in Gas Insulated Substations*, Report by VFT Task Force of the IEEE WG on Modelling and Analysis of System Transients, 1999.
- [51] T.Kuczek, M.Florkowski, *Modeling of overvoltages in gas insulated substation*, ABB Corporate Research Center, Krakow, Poland, 2012, ISSN 0033-2097.
- [52] S.A.Boggs, N.Fujimoto, *Techniques and Instrumentation for Measurement of Transients in Gas-Insulated Switchgear*, IEEE Transactions on Electrical Insulation Vol. EI-19 No.2, April 1984.
- [53] V.V.Kumar, J.Thomas, *Capacitive Sensor for the Measurement of VFTO in GIS*, High Voltage Engineering Symposium, Conference Publication No.467, August 1999.
- [54] S.Meijer, E.Gulski, J.J.Smit, A.J.L.M.Kanters, Risk Assessment of Fixed Defects in GIS Under Different Voltage Wave Shapes, 18th International Conference on Electricity Distribution, Turin 2005.
- [55] S.Meijer, W.R. Rutgers and J.J.Smit, *Acquisition of partial discharges in SF6 insulation*, Conference on Electrical Insulation and Dielectric Phenomena, pp. 581-584, 1996
- [56] The information about descriptive statistic at http://wikipedia.org/

APPENDIX A

The Sensitivity Check of the Acoustic Measurement

In the measurements by using the AIA Instruments, the signals are recorded in a group of 1000 points data. An example of the AIA results is given in **figure A.1**. Three parameters are shown, these are:

- 1. The pulse interval, which is the TOF, expressed in micro second.
- 2. The pulses Level, which is the level of the acoustic signal after converted into the electric signal expressed in mV.
- 3. Synchronizer. This parameter represents the phase time used in phase measurement mode. The sinusoid voltage phase is represented in the range of 0 to 20 ms.

	of pul:		1000			
Pulse	interva	l us	Level	mV	sync u	S
11164	97	18640				
19535	83	18177				
8894	107	7073				
12364	78	19437				
79714	78	19159				
28410	102	7574				
11524	102	19099				
8507	87	7608				
19894	112	7504				
11076	83	18580				
9505	102	8087				
18998		7088				
The same of the sa	87	The state of the s				
12472	97	19561				
59274	97	18841				
9398	97	8240				
9652	97	17893				
9385	102	7280				
12308	87	19589				
27193	78	6787				
13048	112	19836				
70539	92	10383				

Figure A.1A part of the AIA report

But before running the measurements, the following methods are carried out to check the sensitivity of the AIA:

1. The sensitivity check by observing the signals in oscilloscope

By connecting an oscilloscope to the AIA Instrument, the acoustic signals that processed by the AIA at the same time appear in the oscilloscope. Some artificial impacts were introduced into the test object, and the generated signals were observed both in the oscilloscope and in the AIA report. The illustration is shown in figure A.2. The observed signals are given in Table A.1.

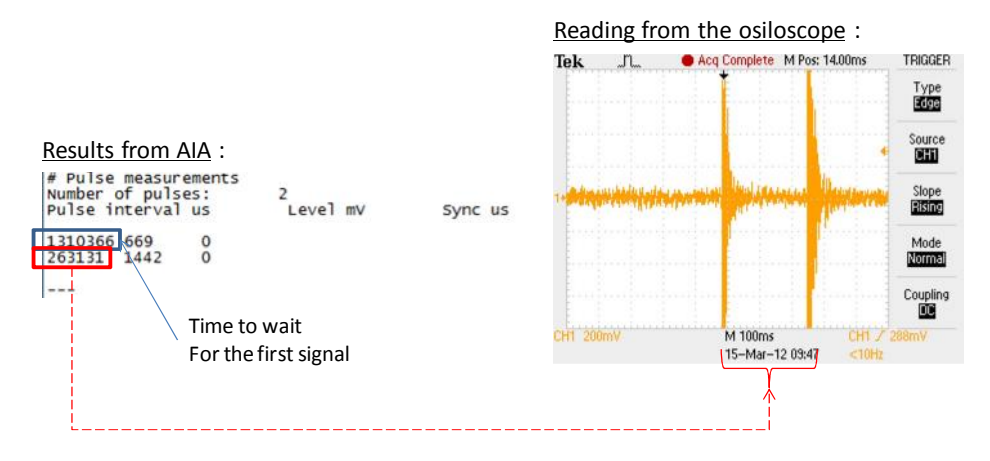


Figure A.2 The TOF readings from the AIA (left) and the signals appeared in the oscilloscope (right)

Table A.1 - The TOF readings observed in the Oscilloscope and from the AIA reports

Signal number	Oscilloscope (in ms)	AIA (in ms)	Δ%	
1	261.6	263.13	0.59%	
2	210.4	211.80	0.67%	
3	489	486.84	0.44%	
4	546	548.15	0.39%	
5	365	364.62	0.10%	
6	401	403.53	0.63%	
7	405	402.66	0.58%	
8	400	400.44	0.11%	
not triggered	10	11.62	16.24%	
not triggered	2	3.02	51.10%	
9	326	324.20	0.55%	
10	348	347.92	0.02%	
11	374	371.45	0.68%	
12	352	353.11	0.31%	
13	380	379.42	0.15%	
14	340	343.06	0.90%	

In this table, both readings are similar with accuracy of more than 99%. There are two untriggered signals also recorded into the measurement. A zoomed into the signals observed in the oscilloscope revealed into figure A.3:

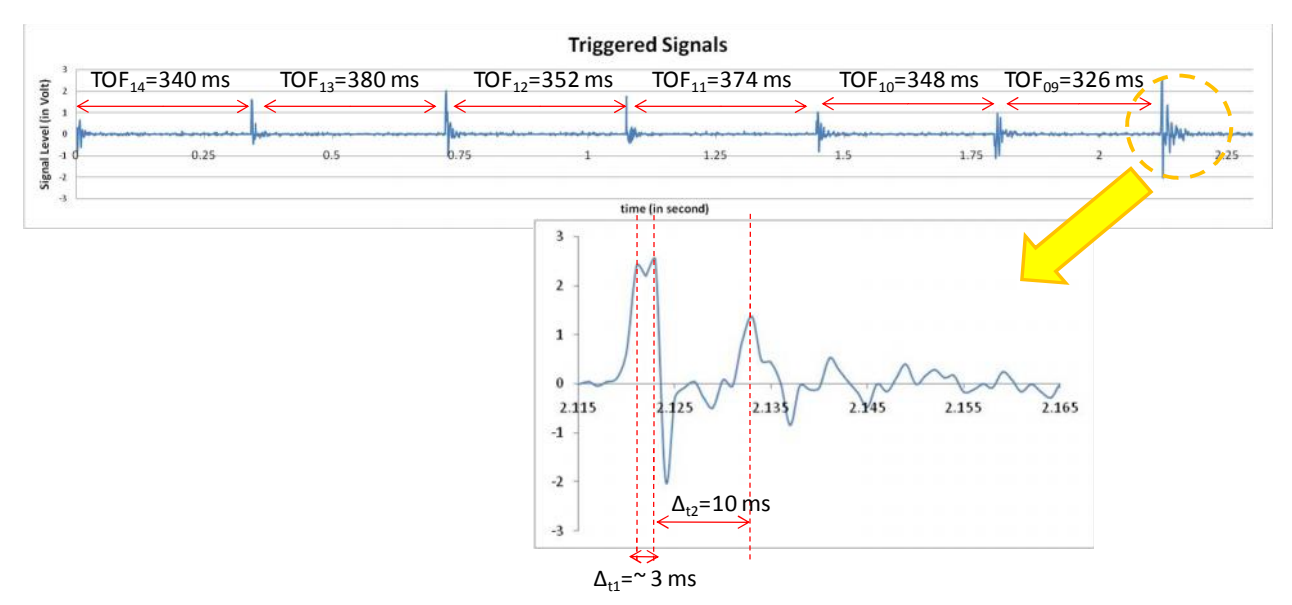


Figure A.3The artificial signals observed in the oscilloscope

From this figure, the addition of the two signals presented in Table A.1 are due to the reflections of the earlier signal. The reflected signals are above the triggered reference level so that the instrument read the signals as the new particle impacts. The pulse blocking time was 2 ms, which allowing the instrument to start recording the new signal after 2 ms.

It is necessary to put the correct setting during the measurement. The consequence of put the incorrect pulse blocking time, for example, has been shown above.

2. The Reading Confirmationwith an Accelerometer

In this method, an accelerometer is placed at the outer enclosure to compare the readings from the acoustic sensor. The signals from the accelerometer are filtered and directly connected into the oscilloscope. The same artificial impacts were given into the test object and the signals from the AIA and the accelerometer were both observed in the oscilloscope as depicted in figure A.4:

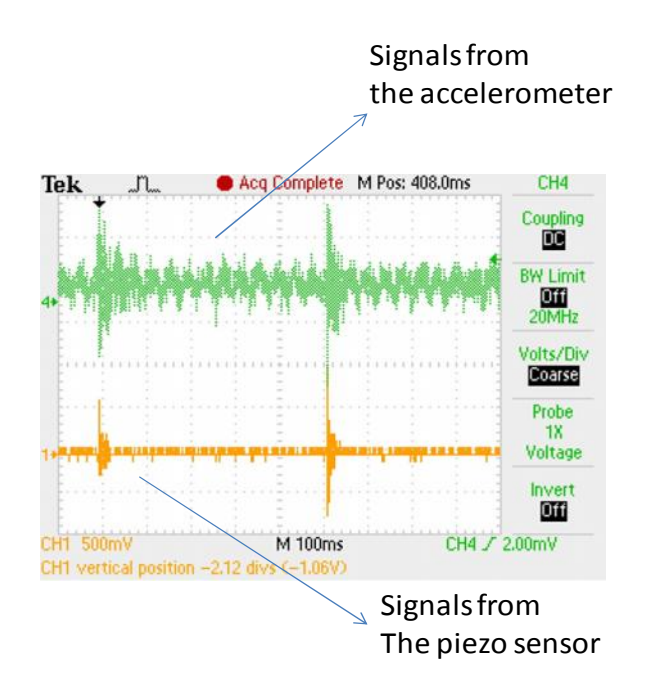


Figure A.4The acoustic signals from the accelerometer (green signal) and the signals from the AIA instrument (yellow signal)

In this figure, the signals from the AIA looks smoother than the accelerometer signals. The distance between the two peaks were calculated and compared with the result of the AIA. The result is given in Table A.2.

Table A.2 - The TOF from different readings.

(the acoustic sensors, the accelerometer and the AIA report)

Signal Number	Osiloscope-Piezo (in ms) A	Osiloscope-Accelerometer (in ms) B	AIA (in ms)	%AIA to A	%AIA to B
#1	515.2	516.4	516.31	0.21%	0.02%

According to the sensitivity checks, the AIA reading is valid with accuracy of less than 1 %.

APPENDIX B

The Lift Off Electric Field Calculation

The net charge of a horizontally lying particle can be calculated by using the formula:

$$Q = 2.\pi.\epsilon_0$$
. r. ℓ . E

The lift-off electric field is calculated by assuming the electrostatic force is equal to its gravitation force:

$$F_e = F_g$$

$$k_a.q.E = m.g$$

 $E = \rho.r.gka.2.\varepsilon0$ where:

ρ : particle mass density r : the radius of the particle

 $g\ :$ gravitation constant $k_a\! :$ constant, represent the attractive force due to image charges in the electrode

 \mathcal{E}_0 : SF6 permittivity constant, assumed to be equal with air

The equation above shows that the lift-off electric field is dependent with constant k_a . This constant represents the attractive force due to image charges in the electrode. The longer the particle is, the higher the attractive force between the particle and the bottom electrode. It has been shown that lift off electric field is slightly increase as the particle size is increased [24]. However, to simplify the calculation, the lift-off electric fields of the particles are assumed to be independent on the length [11].

In the equation above, it is important to select the correct value for k_a to obtained the appropriate lift off electric field of the horizontally lying particle. Holmberg in [11] suggested that k_a varies from about 0.71 for a horizontal cylinder to almost 1 for a long, elongated, vertical particle.

The calculated lift-off electric fields for aluminum particles with radius = 0.25 mm at different k_a are shown in figure B.1.

Some experiments under AC voltage have been carried out to estimate the correct value of k_a of the samples used in the laboratory. The experiments results have shown that none of the aluminum particles were showing any movement at the peak value of the electric field i.e. 6.6 kV/cm (at 145 kV). At this value of the electric field, the constant k_a is 0.85 and it is shown in figure B.1 by the blue line.

Because no particles were moved at this level, the k_a should below 0.85 as shown by the red colored area. The Holmberg's constant is shown with the dotted line and that value can only be reached if the voltage is increased to 158.5 kV (=7.31 kV/cm), which is beyond the capability of the voltage source. According to this experiment, an exact k_a cannot be extracted. However, a value of k_a = 0.71 seems to be suitable to be used during the investigation. The calculated lift-off electric field for the samples is 7.31 kV/cm. Therefore, the consideration of lift off electric field without the introduce of the hit in this thesis work is based on this calculation.

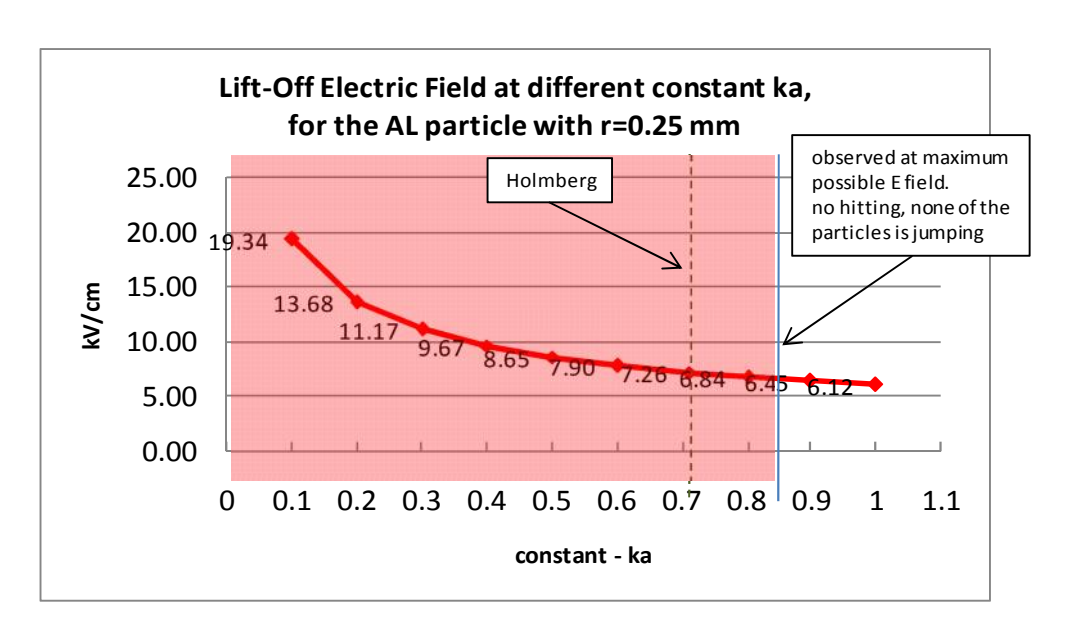


Figure B.1Lift-off Electric Fields for aluminum particle with radius 0.25 mm with different value on constant, k_a

APPENDIX C

The Sensitivity Check of the TE 571 Instrument

Before running the PD measurement by using the PD Detector TE 571, a calibration process has been performed. A capacitance standard of 100 pC was injected into the instrument and the calibration run automatically by the instrument.

With this calibration setup, various values of capacitance standard were injected into the test setup and the readings were observed in the instrument. The reading results on different pC/ division range is given in figure C.1.

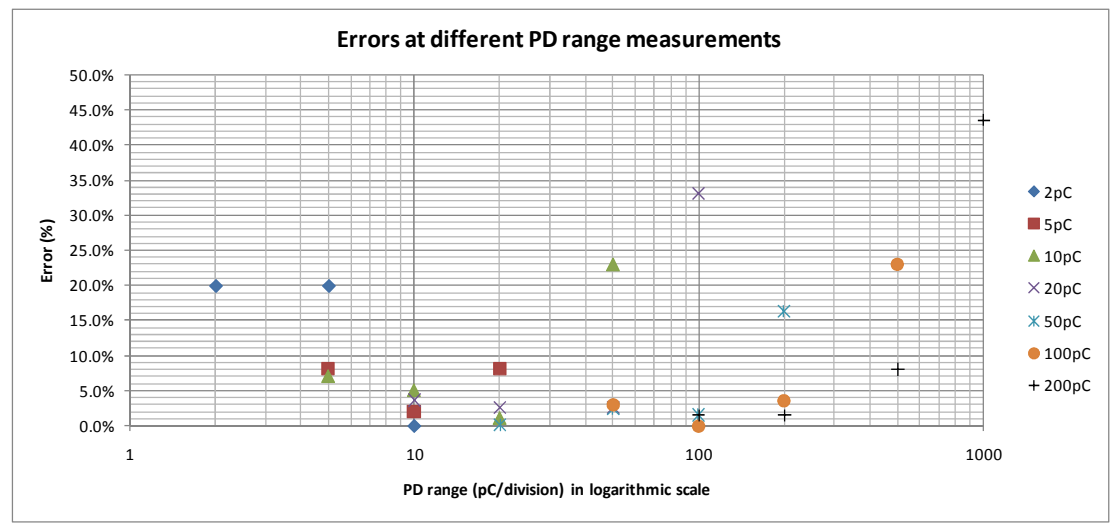


Figure C.1: The error readings of the TE 571 Instrument observed after the calibration with the capacitance standard of 100 pC

In this figure, different known capacitive standards of 2 pC up to 200 pC were injected into the instrument, and the readings at different pC/division were observed. For example, when the injected standard is equal to 10 pC (shown by the green triangle), if we use the scale of reading at 50 pC/division, then the error of the reading is about 23%.

During the thesis work, the PD level mostly observed in the range below of 5 pC (no movement on the particle) and higher than 100 pC (when the particle start jumping). Consequently, the maximum error of the measurement is in the range of 10% - 20%, depending on the chosen pC/division range.

Acknowledgments

Thanks and praise to the God Almighty who helps me throughout this thesis work. Even though this research mainly depends on the individual effort, but I owe much gratitude to many persons during the work. Firstly, I would to thank you Prof.dr.J.J. Smit for giving me the opportunity of doing my Master Thesis at High Voltage Technology and Management Group. I also send my gratitude to Dr.ir. Sander Meijer as my daily supervisor for his guidance and support. Thank you for the TU Delft HV Lab Manager, Mr. Paul van Nes, for his helps and knowledge sharing during mylaboratory works.

My special gratitude is delivered to Muhannad Al Suhaily, as my PhD mentor, for providing me with a lot of discussions during the works. The opportunity of doing the VFTO measurement in Stuttgart is very interesting to me. I also thanks to Dr.ir. Madeline Gibescu as a member of my thesis committee, for taking the effort to evaluate my report.

Thank you for all of my colleagues in HV Laboratory who helpedme during my experiments (Adrian "Johnny", Alex, Augusto), especially for Wim. The nice jokes during the tea-time are unforgettable, also the taste of homemade apple pie of Wim.

Two years in TU Delft was a great moment to me, special thanks to PLN for providing me a great opportunity to study in Delft. Thanks to Indonesian families and ISC friends who always welcome as a family, mas Senot, mbak Pungky, mbak Cisca, mas Stevie, Mia, Thomas, Jule, Irene, Yuli, Awi and also my PLN partner, Dyah. Thank you for the friendship.

To my family in Indonesia (Ibu, Bapak and Putri), thanks for your love and endless support.

"thy will be done .."

Andreas Putro Purnomoadi (Delft, 20 June 2012)